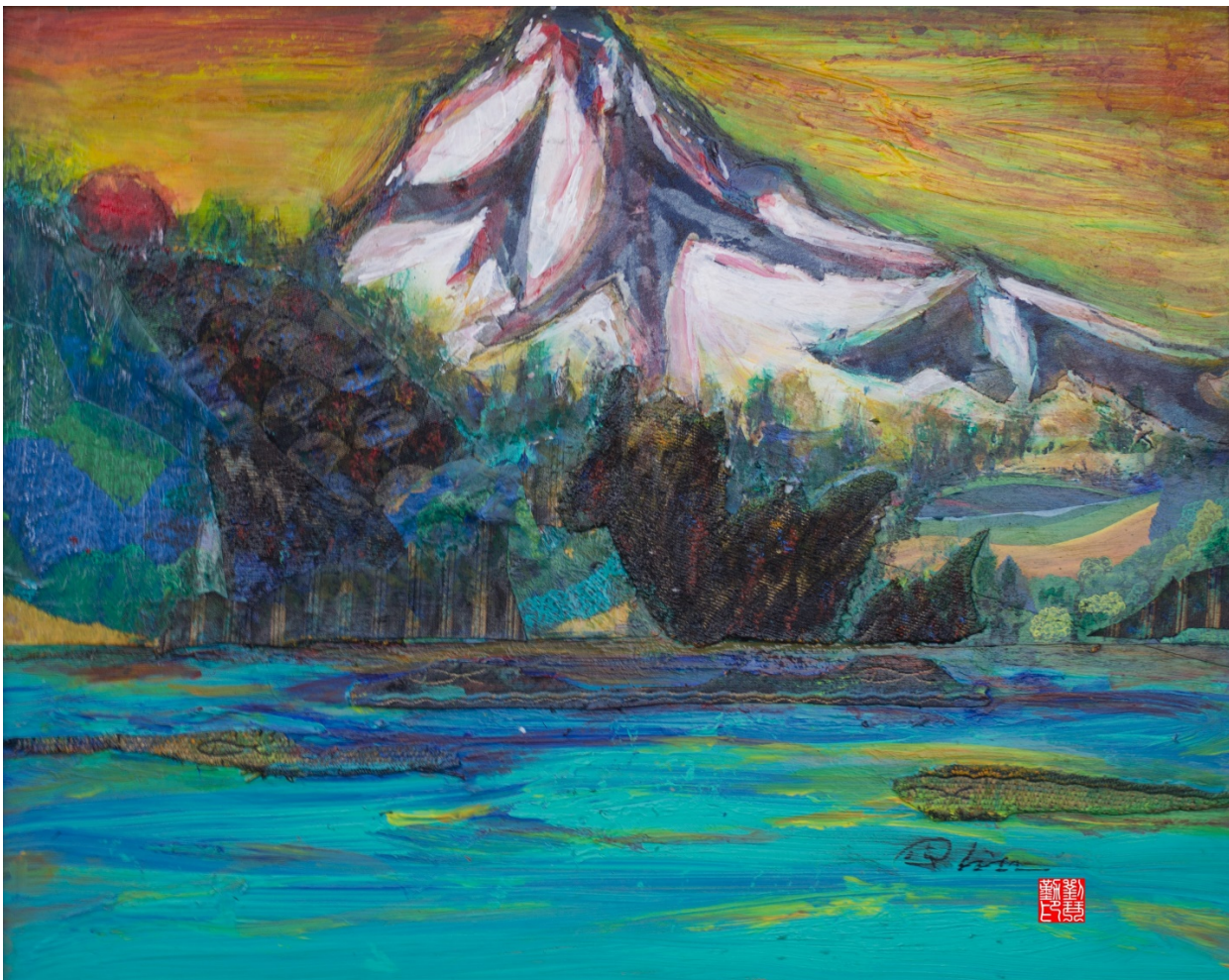




Decision Scaling Evaluation of Climate Change Driven Hydrologic Risk to the State Water Project Final Report

A Collaborative Study of the Hydrosystems Research Group, University of Massachusetts, Amherst and the California Department of Water Resources



"Snow White Mountains and Blue Watershed," Dr. Qin Qin Liu, DWR Climate Change Program, 2017

May 2019

Acknowledgments

Lead authors

Andrew Schwarz¹

Patrick Ray²

Wyatt Arnold

Contributors

Casey Brown³

Sungwook Wi⁴

Jordi Vasquez

Editors

Frank Keeley

William O'Daly

Climate Change Program Management

Elissa Lynn

John Andrew

¹ Delta Stewardship Council (formerly at California Department of Water Resources)

² University of Cincinnati (formerly at University of Massachusetts, Amherst)

³ University of Massachusetts, Amherst

⁴ University of Massachusetts, Amherst

Contents

| | |
|---|-----|
| Acknowledgements | 2 |
| Contents..... | 3 |
| Figures..... | 4 |
| Tables..... | 6 |
| Abbreviations and Acronyms..... | 7 |
| Executive Summary..... | 8 |
| Recommendations for Future Applications of Decision Scaling..... | 11 |
| Introduction | 12 |
| Climate Change in California..... | 13 |
| Observed Trends | 13 |
| Projections..... | 13 |
| Atmospheric Rivers..... | 15 |
| Drought..... | 15 |
| Relevant Studies | 16 |
| Academic Studies of Climate Change Impact on California Water Resources | 18 |
| Methodology | 21 |
| Description of Study Area..... | 23 |
| Generation of Climate Traces..... | 26 |
| Water Resources System Model | 33 |
| Model Verification..... | 48 |
| Risk Assessment Results | 51 |
| Exposure | 51 |
| Sensitivity | 51 |
| Risk | 60 |
| Vulnerability | 72 |
| Adaptive Capacity..... | 73 |
| Other Considerations and Next Steps..... | 73 |
| References | 75 |
| Annex A: GCM Likelihood Function | 82 |
| Annex B: Spatial and Temporal Climate Trends..... | 83 |
| Annex C: Resource Management Strategies Screening | 91 |
| Annex D: Adaptation Strategies – Seasonal Forecasting Skill | 92 |
| Annex E: Adaptation Strategies – Enhanced Precipitation | 94 |
| Annex F: Adaptation Strategies – Upper Watershed Management | 96 |
| Annex G: Adaptive Water Year Typing..... | 102 |
| Annex H: Groundwater Storage and Recovery | 103 |
| Annex I: Move From CalLite 3.0 to CalSim-III Operations Modeling | 106 |

Figures

| | |
|---|----|
| Figure ES1 Modeling Workflow for Climate Change Vulnerability Assessment | 9 |
| Figure 1 Mid-Century Conditional Climate Probability Density..... | 14 |
| Figure 2 Modeling Workflow for Climate Change Vulnerability Assessment..... | 22 |
| Figure 3 California Central Valley System (CVS) and Rim Subbasins | 24 |
| Figure 4 State, Federal, and Local Water Infrastructure | 25 |
| Figure 5 Sacramento 4-River Paleo Reconstructed Annual Streamflow..... | 28 |
| Figure 6 CMIP5 Ensemble of GCM Output Projecting Climate Changes by 2050 for the CVS..... | 29 |
| Figure 7 Trend Slope of Temperature With Less Than 10 Percent Missing Data in 94 Stations..... | 31 |
| Figure 8 Trend Slope of Temperature With Less Than 20 Percent Missing Data in 145 Stations..... | 31 |
| Figure 9 Seasonal Warming Patterns for Climate Projections..... | 32 |
| Figure 10 CalLite 3.0 Schematic | 35 |
| Figure 11 Maps of Three Calibration Sets For the Application of SAC-SMA-DS to the CVS..... | 39 |
| Figure 12 Input Variables With Strong Correlation to San Joaquin Water Year Type Classification — Historical Observed Data Shown | 42 |
| Figure 13 Pearson Correlation Coefficients of Two Historical Local Inflows (I_BRANANIS and I_MDOTA) With 12 Historical Rim Inflows. | 43 |
| Figure 14 Quantile Mapping Procedure Applied to Example California Sub-Basin | 45 |
| Figure 15 AD_Wilkins: Correlation With Shasta Flow..... | 46 |
| Figure 16 AD_SACAME Historical Behavior | 46 |
| Figure 17 Estimates of Sea-Level Rise by Degree C | 47 |
| Figure 18 Validation of CalLite 3.0 Stress Test Modeling Workflow for Total North of Delta Storage..... | 49 |
| Figure 19 Validation of CalLite 3.0 Stress Test Modeling Workflow for Delta Outflow..... | 50 |
| Figure 20 Validation of CalLite 3.0 Stress Test Modeling Workflow for SWP Annual Deliveries..... | 50 |
| Figure 21 Oroville End-of-April Storage System Response Surface | 53 |
| Figure 22 Oroville Carryover Storage System Response Surface..... | 54 |
| Figure 23 a-b Winter and Spring Net Delta Outflow System Response Surfaces | 56 |
| Figure 24 a-b Summer and Fall Net Delta Outflow System Response Surfaces | 57 |
| Figure 25 Average Annual SWP Deliveries System Response Surface | 58 |
| Figure 26 Average Annual System Shortages System Response Surface | 59 |
| Figure 27 Average Annual Oroville End-of-April Storage System Response Surface With CMIP5 GCM pdf at 2050 | 61 |
| Figure 28 Average Annual Oroville Carryover Storage System Response Surface With CMIP5 GCM pdf at 2050 | 61 |
| Figure 29 a-b Average Annual Winter and Spring Net Delta Outflow System Response Surface With CMIP5 GCM-Informed pdf at 2050..... | 62 |
| Figure 30 a-b Average Annual Summer and Fall Net Delta Outflow System Response Surfaces With CMIP5 GCM-Informed pdf at 2050..... | 63 |
| Figure 31 Average Annual SWP Deliveries Systems Response Surface With CMIP5 GCM-Informed pdf at 2050 | 64 |
| Figure 32 Average Annual System Shortage Response Surface With CMIP5 GCM-Informed pdf at 2050..... | 64 |
| Figure 33 a) Cumulative Distribution and b) Probability Density for April Storage in Oroville..... | 66 |
| Figure 34 a-b Cumulative Distribution and Probability Density for September 1st Storage in Oroville..... | 67 |
| Figure 35 Winter and Spring Net Delta Outflow a) Cumulative Distribution and b) Probability Density | 69 |
| Figure 36 a-b Summer and Fall Net Delta Outflow a) Cumulative Distribution and b) Probability Density | 70 |

| | |
|--|-----|
| Figure 37 a-b Cumulative Distribution and Probability Density for Annual SWP Deliveries..... | 71 |
| Figure 38 a-b Cumulative Distribution and Probability Density for Annual System Shortages | 72 |
| Figure 39 Trend Slope of Temperature With Less Than 10 Percent Missing Data in 94 Stations..... | 86 |
| Figure 40 Trend Slope of Temperature With Less Than 20 Percent Missing Data in 145 Stations..... | 86 |
| Figure 41 Seasonal Warming Patterns for Climate Projections..... | 87 |
| Figure 42 Differential Rate of Change in Precipitation Between Early Mid-20th Century (1920–1960) and Recent Past (1980–2011)..... | 88 |
| Figure 43 Weather Modification Projects in California during 2016 | 95 |
| Figure 44 Different Representations of the Central Valley..... | 104 |
| Figure 45 Representation of Stream-Aquifer Node Representation | 105 |

Tables

| | |
|---|----|
| Table ES1 Decision-Relevant Metrics..... | 9 |
| Table ES2 Probability that Mid-Century Long-Term Average Performance Will be Inferior to Current Average Performance..... | 10 |
| Table 1 Decision-Relevant metrics..... | 22 |
| Table 2 Means of Seasonal Warming Pattern..... | 30 |
| Table 3 Base Assumptions Used for Regulatory Environment in CalLite 3.0..... | 34 |
| Table 4 Twelve Major Rim Inflows to the CalLite 3.0 Model | 39 |
| Table 5 R Squared Correlations For 31 CalLite 3.0 Input Parameters With Strong Influence on Model Output | 40 |
| Table 6 Pairs of Rim Flows and Local Inflows Determined by Correlation | 44 |
| Table 7 Sea-Level Rise Discretization Within CalLite 3.0 | 48 |
| Table 8 Hydrologic Model Performance by Subbasin..... | 48 |
| Table 9 Conditional Climate Probability Density of Each Climate Change Shift, 1970–2000 to 2035–2065 | 60 |
| Table 10 Probability That Mid-Century Long-Term Average Performance Will Be Inferior to Current Average Performance..... | 65 |
| Table 11 Relationship Between Seasonal Temperatures and Elevations | 83 |
| Table 12 Relationship Between Seasonal Temperatures and Elevations, Latitudes | 84 |
| Table 13 Means of Seasonal Warming Pattern (Average Increase Per Decade) | 85 |
| Table 14 Seasonal Warming Pattern Application for Eight Increase Levels | 85 |
| Table 15 Non-Exceedance Runoff Values Given in Runoff Forecast Tables | 92 |
| Table 16 Mean and Standard Deviation of Historical Runoff Forecasts | 93 |

Abbreviations and Acronyms

| | |
|------------|--|
| AD | accretion/depletion parameters within CalLite |
| ARMA | auto-regressive moving average model |
| WARM | Wavelet ARMA model |
| CalLite | a simplified, faster version of CalSim |
| CalSim | the DWR and Reclamation California water resources simulation model |
| CALVIN | CALifornia Value Integrated Network, a hydro-economic optimization model of California's statewide water supply system |
| cdf | cumulative distribution function |
| CMIP | Coupled Model Intercomparison Project |
| CVP | Central Valley Project |
| CVS | California Central Valley Water System |
| CWP | California Water Plan |
| DWR | California Department of Water Resources |
| ENSO | El Niño Southern Oscillation |
| GCM | General Circulation Model |
| IPCC | Intergovernmental Panel on Climate Change |
| maf | million acre-feet |
| NDO | Net Delta Outflow |
| NOAA | National Oceanic and Atmospheric Administration |
| NWS | National Weather Service |
| pdf | probability density function |
| PDO | Pacific Decadal Oscillation |
| RCP | Representative Concentration Pathways |
| SAC-SMA-DS | a distributed version of the Sacramento Soil Moisture Accounting hydrologic model |
| SLW | Supercooled liquid water |
| SWE | Snow water equivalent |
| SWP | State Water Project |
| USBR | United States Bureau of Reclamation |
| WRIMS | Water Resource Integrated Modeling System |

Executive Summary

This Final Decision Scaling Vulnerability Assessment Report updates and describes a joint endeavor of the California Department of Water Resources (DWR) and the University of Massachusetts, Amherst (UMass) to improve planning for the uncertain effects of climate change on the California Central Valley Water System (CVS)¹ by integrating vulnerability-based analysis with traditional risk-based assessment methods. This report summarizes the research goals, analytical approach, workflow of modeling tools, evaluation of alternative experimental designs, refined strategy for data visualization, and assessment of the vulnerability of the CVS to climate change.

This report begins with a review of historical and projected climate change in California, which includes descriptions of several DWR-UMass team investigations of historical records, observed climate trends, and many climate projections for the CVS, specifically. The next section of this report summarizes the work previously accomplished by the academic community, the government, and the community of water resources practitioners evaluating climate change-related risks to the CVS.

With that background in place, this report explains the methodology developed for this study (illustrated in Figure ES1) and provides details on each sub-step of the process. Whereas previous studies have tested the response of some aspect of the California water system to ahistorical climate traces, the decision scaling approach adopted for this study allows systematic assessment of the vulnerability of the entire (interconnected and complex) CVS to a wide range of potential future climate conditions, and quantification of the significance of climate shift relative to natural (and climate-change-amplified) variability. The climate response function that results from the decision scaling approach depicts expected water system performance relative to historical performance across a range of climate changes. An important benefit of this approach is the ability to use a variety of climate information sources to assess the level of concern to assign to the vulnerabilities that are identified. Consequently, climate information, including climate change projections and formal probability estimates, can be used as a sensitivity factor when assessing risk, rather than the driver of the analysis. This allows discussion of risk and opportunity (each a function of impact and likelihood) in water system investment.

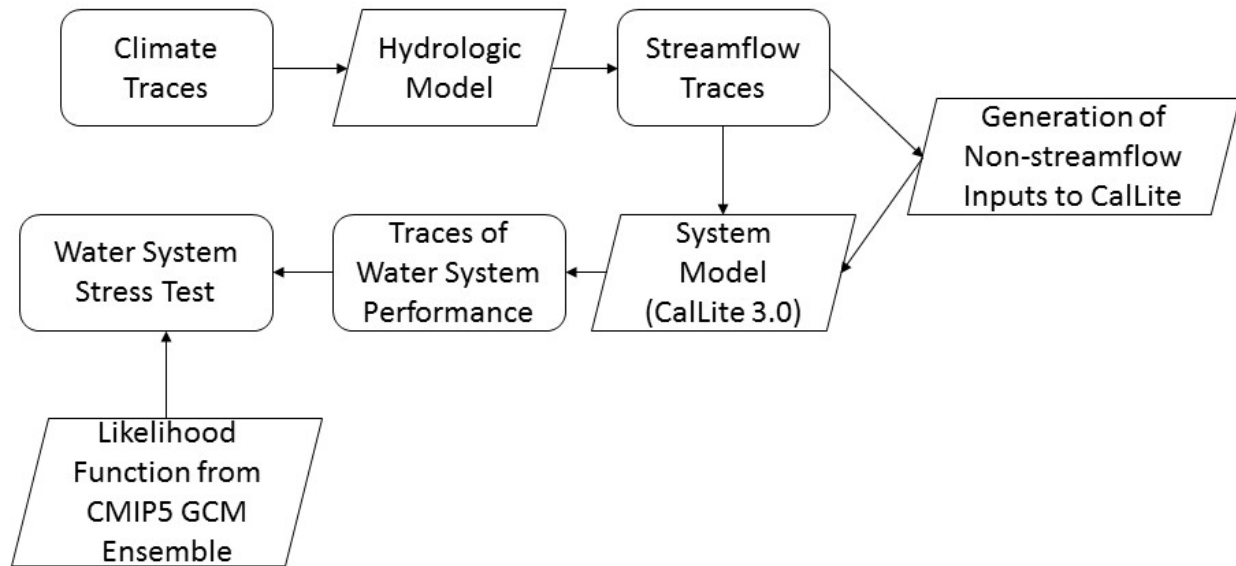
This assessment of long-term and persistent hydrologic impacts of climate change focuses on the effects to the operation of the State Water Project (SWP), including ecological conditions that dictate operating rules. DWR owns and operates the SWP for flood control, maintenance of environmental and water quality conditions, water supply, hydropower, and recreation. Consequently, analysis of SWP performance under climate-changed conditions yields an array of impact metrics across these areas of concern. The analysis focuses on persistent medium- and long-term conditions evaluated at a monthly time-step. Short-duration extreme precipitation events that cause flooding may also stress water resource management but are beyond the scope of this study.

This study has adopted CalLite 3.0 to simulate the coordinated operations of the Central Valley Project (CVP) and SWP under a wide range of climate possibilities. Climate traces are developed through coupling historical daily temperature and precipitation (1950–2013) (Livneh et al. 2013) to the paleo-dendrochronological reconstructed streamflow record of the Sacramento-4-river annual streamflow (900–2013) (Meko et al. 2014). An advanced hydrologic model, the Sacramento Soil Moisture Accounting

¹ For the purposes of this study, the CVS is considered as the interconnected system of natural river channels and man-made facilities that comprise the Central Valley Project (CVP) and the State Water Project (SWP). See Figure 3 for a map of the CVS.

distributed hydrologic model (SAC-SMA-DS), translates the hydroclimatic traces into streamflow, which are the key inputs to the water system model.

Figure ES1 Modeling Workflow for Climate Change Vulnerability Assessment



When simulated repeatedly, the resulting workflow (Figure ES1) allows the exploration of climate change impact in response to a wide range of meteorological input. Table ES1 lists the decision-relevant metrics used for the DWR climate vulnerability assessment.

Table ES1 Decision-Relevant Metrics

| | |
|----------|--------------------------------|
| 1 | Oroville Storage levels |
| | April 30 |
| | September 30 |
| 2 | Net Delta Outflow |
| | Winter (Dec, Jan, Feb) |
| | Spring (Mar, Apr, May) |
| | Summer (Jun, Jul, Aug) |
| | Fall (Sep, Oct, Nov) |
| 3 | SWP Deliveries |
| | Average Annual |
| 4 | System Shortages |
| | Average Annual |

Despite substantial uncertainty, results of the analysis show that increasing temperatures cause a significant downward shift in mid-century system performance and that the temperature increases of concern are consistent with the consensus of climate model projections. By 2050, the majority of climate outcomes that might reasonably be expected to occur lead to decreased system performance in each of the Table ES1 metrics (see Table ES2). While the results of this study are influenced by incorporation of 1,000 years of annual climate variability contained in the paleo reconstructed streamflow record, this

study does not account for projected increases in climate variability (intensification of precipitation events and extended duration of droughts) which could lead to additional performance impacts.

Table ES2 Probability that Mid-Century Long-Term Average Performance Will be Inferior to Current Average Performance

| Performance Metric | Probability that Mid-Century Performance Will be Inferior to Current Performance |
|----------------------------|--|
| Oroville April Storage | 76% |
| Oroville Carryover Storage | 95% |
| Winter Net Delta Outflow | 65% |
| Spring Net Delta Outflow | 65% |
| Summer Net Delta Outflow | 21% |
| Fall Net Delta Outflow | 56% |
| SWP Deliveries | 93% |
| System Shortages | 87% |

Improved system performance is possible if temperature increases are offset by precipitation increases, but this combination of climate changes is relatively rare across the climate projection archive, and thus considered relatively unlikely. This situation is especially acute for average Oroville September storage, SWP deliveries, and spring net Sacramento-San Joaquin Delta (Delta) outflows, in which substantial downward shifts are identified under a warmer climate.

The United States Bureau of Reclamation (Reclamation) Sacramento and San Joaquin Basin Study from 2016 provides a useful point of comparison for this study, though the climate conditions evaluated spanned a limited range of model scenarios, the possible changes were not sampled comprehensively, and the total number of evaluated changes was relatively small. Reclamation simulations showed an average decrease in 2015–2099 end-of-September reservoir storage of 9 percent relative to the Reference-No-Climate-Change scenario (where “reservoir storage” includes all system reservoirs), and an average decrease in Delta outflows of 3 percent. This study, by contrast, finds a 98 percent likelihood that September 1 Oroville storage will be lower by mid-century than it has been historically, and highlights the risk of decreases (by 25–30 percent) in Oroville storage. Regarding Net Delta Outflow (NDO), this study found a 65 percent likelihood of performance loss in spring, winter, and fall, and an 88 percent likelihood in summer. Spring NDO in low-flow years was found to decrease 25–30 percent, in median years 25–30 percent, and in high-flow years 15–20 percent. The downward shift in fall NDO was concentrated in already-at-risk low-flow years (decreasing by 25–30 percent relative to historical).

Recommendations for Future Applications of Decision Scaling

The analysis suggests that SWP performance will very likely deteriorate over the coming decades if no action is taken to adapt to climate change; however, there are opportunities for improved climate change planning. Applications of decision scaling (1-9 identified below) within three major categories are recommended for future study to support adaptation planning.

Resource Management Strategies

Among 37 resource management strategies (RMS) identified in the California Water Plan Update 2013 (Water Plan), there are several which address vulnerabilities described in this report, are technically feasible, and for which DWR has the capacity as well as the authority to implement (see Annex C: Resource Management Strategy Screening). As a next step, DWR's Climate Change Program will use the decision scaling platform built for this study to conduct a systematic evaluation of a sample of proposed climate change adaptation strategies drawn from the 37 RMS including, but not limited to:

- (1) The effect of monthly reservoir inflow forecasting ability on system operation (Annex D: Adaptation Strategies — Seasonal Forecasting).
- (2) Weather modification or “cloud-seeding” (Annex E: Adaptation Strategies – Enhanced Precipitation).
- (3) Incorporation of improved multi-objective upper watershed management (Annex F: Adaptation Strategies — Upper Watershed Management)

Supplemental Analysis

The decision scaling platform built for this study establishes a probabilistic framework and set of tools that allow evaluation of a much larger range of historical and potential future changes in inter-annual variability and drought length and severity (4). The platform, through its use of the system operations model CalLite 3.0, also reduces concerns related to accuracy of modelling regulations and institutional constraints thus enabling an exploration of the sensitivity of water indexing methods to climate change and potential ways of adapting water year typing methods to support water management decisions (5) (see Annex G: Water Year Typing). Although considered to some extent in this report, further investigation into the presence and causes of trends in seasonal and elevation-dependent warming would help prioritize adaptive strategies that are evaluated in studies using this platform (6).

Groundwater

While climate change risks to the groundwater component of water supply have not been evaluated here, DWR's Flood Managed Aquifer Recharge program (California Department of Water Resources 2018) has adopted the decision scaling platform to evaluate using flood waters to recharge groundwater aquifers (7). In addition, DWR's Climate Change Program has drafted a simplified strategy for evaluating the potential benefits of increased groundwater storage north and/or south of Delta (see Annex H: Groundwater) using CalLite 3.0 (8). If simplified modeling of groundwater in CalLite 3.0 is found infeasible, shifting the operations model used in this study from CalLite 3.0 to CalSim-III, which features a dynamic link to the California Central Valley Groundwater-Surface Water Model (C2VSIM), would enable exploration of climate change risks and adaptation strategies based on modelling of the integrated surface-groundwater system (9) (see Annex I: Move From CalLite 3.0 to CalSim-III Operations Modeling).

Introduction

Developing adaptation plans to address future climate changes is hindered by the uncertainty associated with the magnitude and character of those changes. Vulnerability-based assessments are promising for identifying where climate uncertainties are most problematic but can yield a litany of vulnerabilities with little means for prioritizing action or justifying the expenses required to address them. Given the financial constraints of the typical government water agency or municipality, vulnerabilities with unknown probabilities of occurrence can be treated as low priorities, and long-term preparedness to climate change yields to the pressing concerns of the present.

The goal of this project is to improve planning for the uncertain effects of climate change by integrating vulnerability-based analysis with traditional risk-based assessment methods. Risk-based approaches are typical for engineering water resources but are problematic under climate change because of their dependence on estimating the probability distributions of possible climate futures. The process adopted here preserves the risk-based planning framework but reserves estimation of probabilities until the assessment of adaptation alternatives, where the consequences of any assumption are quickly realized in terms of effects on decisions.

Water managers struggle to prioritize responses to the predicted hazards of climate change because of the uncertainty associated with projections of those hazards. This struggle is not without cause. At present, decision-makers face the unsavory choice of relying on trusted, traditional approaches that depend on statistics from the past, and thus may be ill-suited for the future, or adopting uncertain projections of the future known to have the least capacity for the most critical design variables (Hirsch 2011). The prevailing wisdom of “no regrets” approaches offered in response to this dilemma (Intergovernmental Panel on Climate Change 2012) is hardly a rallying cry for increasing long-term preparedness for climate change.

This effort is designed to directly address this challenge. The methodology outlined in this report enables planning for future changes that is *informed* by the best available science on climate change while not being dependent on precise prediction of future values. Instead, the process focuses on incorporating credible information on future changes within traditional risk-based planning approaches and through merging historical trends with future expectations. Those effects are delineated through a “climate stress test” that is independent of projections of future climate. Where the effects are significant compared to other factors, the concern associated with the possible occurrence of those effects is described in accordance with the best available climate science.

Previous studies that have used a robust decision-making approach (Lempert et al. 2006), including California Water Plan Update 2013 (Update 2013) (California Department of Water Resources 2013), have identified potential adaptations through stakeholder consultation and systems analysis but have not systematically assessed the alternatives. They have also not evaluated the impacts of possible changes in climate extremes such as droughts and floods. This study uses previous planning efforts, in particular Update 2013, as a foundation for illustrating the planning procedure for the climate uncertainty described here.

Climate Change in California

It has long been anticipated that anthropogenic climate change would alter the water resources of California (Gleick 1987). Recent observations indicate that changes to the hydro-climatology of California have begun and that further substantial change is likely to occur throughout this century (Pierce et al. 2018).

Observed Trends

Mean temperature has increased 0.6 to 1.1 degrees Celsius ($^{\circ}\text{C}$) since 1900 (California Department of Water Resources 2015a), and temperature change is accelerating (LaDochy et al. 2011), with the greatest rate of change occurring in temperature minimums (California Department of Water Resources 2015a). Rising temperatures in the Sierra Nevada and Northern California have triggered decreasing snowpack and earlier snowmelt (Cayan et al. 2010; Dettinger & Anderson 2015; Mote et al., 2005). Warmer temperatures also cause sea level rise, with 0.2 meters of rise recorded in San Francisco Bay in the past century (National Oceanic and Atmospheric Administration 2016). Rates of rise are now accelerating (Kopp et al. 2016), threatening the sustainability of the Sacramento-San Joaquin Delta, the heart of the California water supply system and the source of water for millions of Californians and millions of acres of farmland.

Since 1970, California has become wetter in its north and drier in its south (Killam et al., 2014), though the large historical variability of precipitation in California makes it difficult to separate trends from natural variability. Higgins et al. (2007) found that the 1976–2004 period was substantially wetter in the western U.S. than the 1948–1975 period, though the large increase in total precipitation might be partially explainable by the occurrence of the warm phase of the Pacific Decadal Oscillation (PDO). It may be that the warm phase of the PDO during the last quarter of the 20th century was an exceptional period (as suggested by the 1000-year tree-ring record [Swetnam & Betancourt 1998]) and that the last 15 years marks a return to normal, pre-1977 conditions (Pavia et al. 2016). Regionally, the central and northern regions show increases in both annual totals and number of rainfall days, while southern regions show either no significant trend or some decreases since the early 1900s. A shift from light rains to heavy rains has occurred in Northern California regions (Killam et al. 2014).

It is not yet clear that the trend observed in the past century will continue into the coming century, nor is the behavior of the PDO well-enough understood that confident forecasts can be made of its oscillations far into the future. The global climate models do not indicate a clearly wetter or drier expectation for the region (discussed later). Caution should be exercised when looking for conclusions attached to expectations of future precipitation in the region.

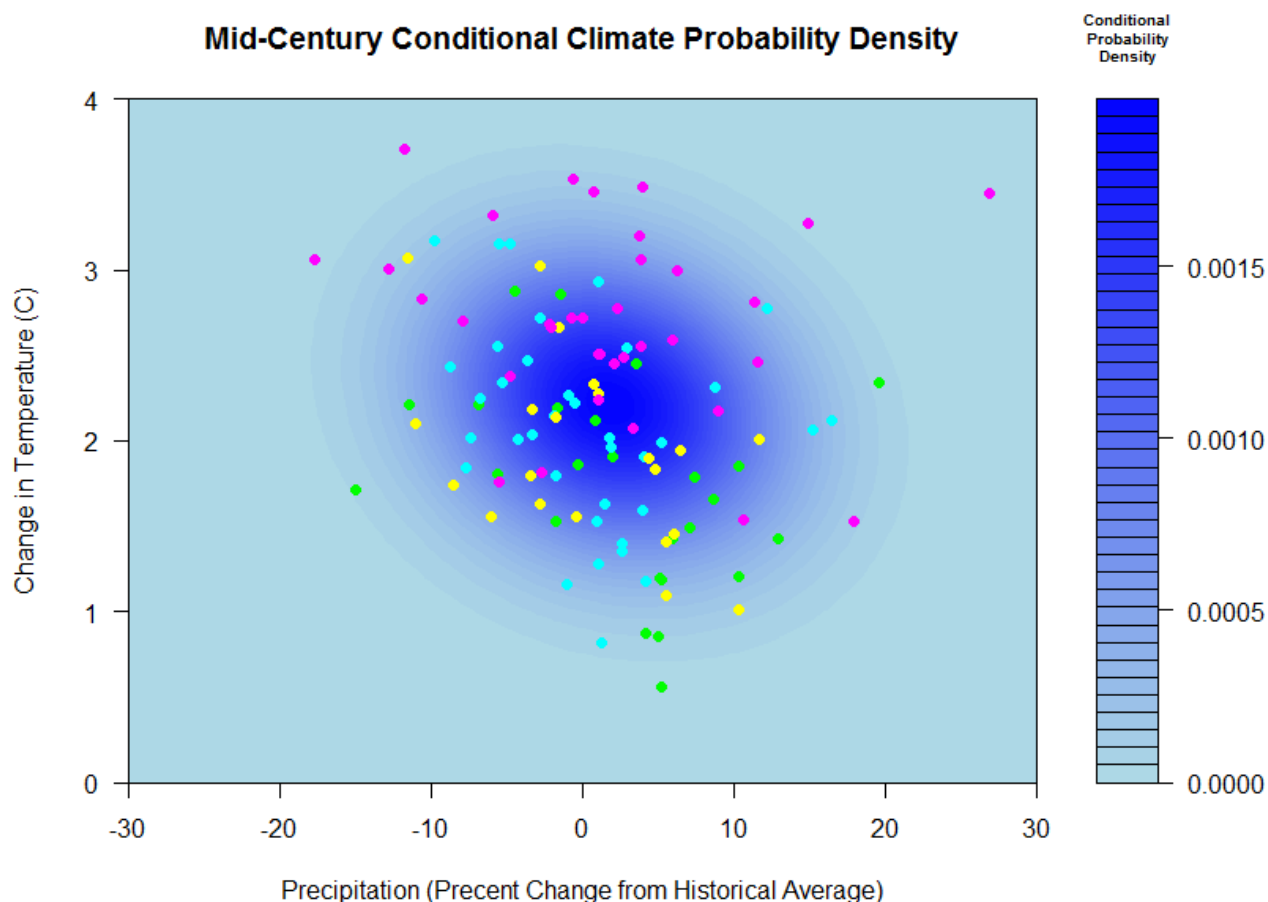
Projections

Figure 1 shows the shift in average annual precipitation and temperature for the ensemble of general circulation models (GCMs) driven with Intergovernmental Panel on Climate Change (IPCC) Representative Concentration Pathways (RCP) scenarios 2.6, 4.5, 6.0, and 8.5 (van Vuuren et al. 2011) in the region contributing flow to the Central Valley Water System (CVS)² for the 2036–2065 period relative to the 1971–2000 period. The probability density cloud identifies the bivariate normal distribution

² The CVS is considered as the interconnected system of natural river channels and man-made facilities that comprise the Central Valley Project (CVP) and the State Water Project (SWP). See Figure 3 for a map of CVS.

on the full ensemble of the Fifth Coupled Model Intercomparison Project (CMIP5) GCMs (see Annex A: GCM Likelihood Function for detailed steps on GCM probability density function). As can be seen, there is no agreement on the direction of precipitation change (positive or negative), with some GCM runs indicating increases in precipitation of over 20 percent and some indicating decreases in precipitation of over 20 percent. Temperature increases range from almost 1°C to almost 4°C.

Figure 1 Mid-Century Conditional Climate Probability Density



Note: Cyan dots represent GCMs run with RCP 8.5; yellow dots represent GCMs runs with RCP 6.0; turquoise dots represent GCMs run with RCP 4.5; Green dots represent GCMs runs with RCP 2.5.

The projected changes in California weather patterns could exacerbate both drought and flood risks and increase challenges for water supply management. Projections of future temperatures across California suggest greater increases in summer temperatures than in winter temperatures (California Department of Water Resources 2015a) and intensification of hot extremes (Diffenbaugh & Ashfaq 2010). By the end of this century, the Sierra snowpack is projected to experience a 48–65 percent loss relative to the historical April 1st average on which water supply throughout the summer and fall depends (D Cayan et al. 2013; California Department of Water Resources 2015a).

Most climate model precipitation projections for the state anticipate drier conditions in Southern California, heavier and warmer winter precipitation in Northern California, and greater proportions of

winter precipitation falling as rain instead of snow (Yoon et al. 2015). Decrease in snowpack storage and the concentration of streamflow in winter months would increase dry season deficits during periods of high irrigation-water demand.

Atmospheric Rivers

The effect of climate change on atmospheric rivers, the source of 30–50 percent of all precipitation for the west coast and the principal cause of winter floods (Dettinger 2014), is not yet well understood (Steinschneider & Lall 2015). Several simulation experiments using climate models have indicated that projected changes are mostly at the extremes (Dettinger 2011), with California’s atmospheric rivers becoming longer and more intense but not more frequent (Shields & Kiehl 2016) and carrying warmer water vapor more likely to precipitate as rain than snow at high altitudes (Dettinger 2011). The net effect is exacerbated winter floods but not reduced water stress, despite increases in winter mean precipitation (Warner et al. 2015). While the evaluation of the effect of potentially increasing climate variability is outside of the scope of this analysis, California’s high precipitation variability creates challenges for General Circulation Models (GCMs) and results in a particularly wide spread of projections (relative to ranges throughout the rest of the United States) of future precipitation values in the region (Zhang & Stanley 1999; Roy et al. 2010).

Drought

California’s most significant droughts of the past century (by hydrologic dryness) were: 1929–1934, 1976–1977, and 1987–1992. The 2012–2014 water years were California’s driest three consecutive years in terms of statewide precipitation, and the drought conditions (a combination of record high temperatures and near-record low precipitation) faced by California may be the worst in the last millennium (AghaKouchak et al., 2014; Griffin & Anchukaitis 2014). Even so, the impact of the 2012–2015 drought would be far worse if not for the slightly wet 2010 and significantly wet 2011 preceding the start of the drought (California Department of Water Resources 2015b).

Drought conditions in California are increasing in intensity and length (Diffenbaugh et al. 2015). Climate change is expected to amplify droughts in California, both because of rising temperatures (Cayan et al. 2010) and because of an intensification of ENSO activity, the warm/cold phases of which together with the transitions between phases modulate climate variability in California (Yoon et al. 2015). The rise in global temperatures has amplified naturally occurring drought conditions in California and has increased the chance of severe droughts in the future (Williams et al. 2015), though the main cause of intensification of California droughts so far has been natural precipitation variability, not warming (Mao et al., 2015; Seager et al., 2015). Sea-surface temperature (SST)-forcing, for example (a combination of a La Niña event in 2012/2013 and a warm west - cool east tropical Pacific SST pattern from 2012–2014), sustained a high pressure ridge over the West Coast that suppressed precipitation during the three winters from 2012–2014 (Wang & Schubert 2014; Seager et al. 2015). This recent event indicates that better understanding of the climatological causes of persistent North Pacific ridging events might be crucial in anticipating future severe drought in California (Swain et al. 2014).

California’s most recent drought began in winter 2011–2012, and intensified in winter 2013–2014, a period marked by very low winter precipitation, mountain snowpack, and spring runoff (California Department of Water Resources 2014b; U.S. Geological Survey 2014; United States Drought Monitor 2014). The drought drew down reservoir storage in the state to low levels and threatened the state’s

agricultural production, drinking water supply, and fisheries (California Department of Fish and Wildlife 2014; California Department of Water Resources 2014a; U.S. Department of Agriculture 2014). The drought has included:

1. Lowest three-year statewide precipitation total on record (2012–2014);
2. Most severe values of NOAA’s National Climatic Data Center drought indicators (D4, or exceptional drought, first noted across the Salinas Valley and western San Joaquin Valley in January 2014, and extending over almost 60 percent of the state by July 2014) (National Oceanic and Atmospheric Administration 2014);
3. Lowest calendar-year precipitation in the history of much of the state, including San Francisco, Sacramento, and Los Angeles (2013);
4. Warmest calendar-year temperatures on record (2014);
5. Warmest winter on record (2015);
6. Highest one-year (water year 2014, 9–12 percent above average) and three-year (water year 2012–2014, 7–9 percent above average³) potential evapotranspiration on record (Williams et al. 2015);
7. Lowest Palmer Modified Drought Index (PMDI) on record (July 2014, approximately -3) (Diffenbaugh et al., 2015);
8. Lowest recorded April 1st snowpack (2015, 5 percent of normal) (Dettinger & Anderson, 2015);
9. Record-low water allocations for State Water Project and federal Central Valley Project contractors (California Department of Water Resources, 2015a).

The drought was responsible for an estimated \$2.2 billion in economic loss from 2013–2014 alone (Howitt et al., 2014), and \$2.7 billion from 2014–2015 (Howitt et al., 2015), and took a heavy toll on people and ecosystems (Swain 2015). Snowpack was well below normal for each of the four years of the drought. Year 2015 snowpack was significantly less across all elevations and shifted to higher elevations. This shift is likely driven in part by the significantly warmer temperatures, which “would lead to less snowfall and more rainfall at lower elevations, and increased accumulation season melt across all elevations (with more melt at lower elevations)” (Margulis et al. 2016).

Relevant Studies

Recent global (Intergovernmental Panel on Climate Change), National (National Climate Assessment), regional (National Climate Assessment for the Southwest Region), and Statewide (4th California Climate Change Assessment) climate change assessments have all highlighted climate-change-driven impacts to water supply, water demand, increased flooding and drought, and changes to hydrologic processes. Climate change impacts on California has been the focus of many studies conducted by DWR and others, a selection of which include:

³ Potential evapotranspiration was calculated using gridded data from the Global Precipitation Climatology Centre (GPCC) (Schneider et al., 2014); for some grids, potential evapotranspiration for water year 2012–2014 was second highest behind water year 2007–2009. But it should be noted that statewide temperatures in 2015 were the second-highest on record, behind only temperatures for 2014. The year 2015 was not included in Williams (2015) and would likely result in record three-year potential evapotranspiration for the period 2013–2015.

- [Progress on Incorporating Climate Change into Management of California's Water Resources](#) (March 2008)
Published in the March 2008 special issue of Climatic Change — *California at a Crossroads: Climate Change Science Informing Policy*. This is an 18-page condensed version of the original 350-page 2006 report of the same name. Coauthored by DWR staff.
- [Managing an Uncertain Future; Climate Change Adaptation Strategies for California's Water](#) (October 2008)
Focuses discussion on the need for California's water managers to adapt to the effects of climate change, with a focus on the effects already affecting water supplies. This report proposes 10 adaptation strategies in four categories.
- [Using Future Climate Projections to Support Water Resources Decision Making in California](#) (May 2009)
Evaluates how climate change could affect the reliability of California's water supply.
- [Isolated and integrated effects of sea level rise, seasonal runoff shifts, and annual runoff volume on California's largest water supply](#) (May 2011)
A detailed analysis of climate change impacts on seasonal pattern shifts of inflow to reservoirs, annual inflow volume change, and sea level rise on water supply in the Central Valley of California.
- [Hydrological Response to climate warming: the Upper Feather River Watershed](#) (March 2012)
The hydrological response and sensitivity to climate warming of the Upper Feather River Basin, a snow-dominated watershed in Northern California, were evaluated and quantified using observed changes, detrending, and specified temperature-based sensitivity simulations.
- [Paleoclimate \(Tree-Ring\) Study](#) (February 2014)
New Hydroclimate Reconstructions have been released, using updated tree-ring chronologies for these California river basins; Klamath, San Joaquin, and Sacramento. The report, prepared by the University of Arizona, allows assessment of hydrologic variability over the course of centuries and millennia, gives historical context for assessing recent droughts, and can be used in climate change research.
- [Estimating Historical California Precipitation Phase Trends Using Gridded Precipitation, Precipitation Phase, and Elevation Data, DWR Memorandum Report](#) (July 2014)
This exploratory study develops and describes a methodology that uses readily available research data sets to produce gridded estimates of historical rainfall as a fraction of total precipitation for areas comprising the major water-supply watersheds of California. Written by Aaron Cuthbertson (DWR), Elissa Lynn (DWR), Mike Anderson (DWR, California State Climatologist), and Kelly Redmond (Western Regional Climate Center).

- [Reclamation Sacramento-San Joaquin Basin Study](#) (March 2016)
Assessment of potential climate change impacts to the basins' agriculture and urban water supplies and demands, flood control, hydroelectric power generation, recreation, fisheries, wildlife and wildlife habitats, water quality, and water-dependent ecological systems.
- [California Climate Risk: Evaluation of Climate Risks for California Department of Water Resources](#) (February 2017)
This inception report introduces a joint endeavor of DWR and the University of Massachusetts, Amherst (UMass), to improve planning for the uncertain effects of climate change on DWR's system by integrating vulnerability-based analysis with traditional risk-based assessment methods. This report summarizes the progress made during approximately two years of informal partnership during which the team defined research goals, established an experimental approach, developed and validated a workflow of modeling tools, tried and abandoned a number of alternative experimental designs, refined the strategy for data visualization, and produced preliminary assessments of the vulnerability of the CVS to climate change using the decision scaling approach.
- [Climate Change Risk Faced by The California Central Valley Water Resource System. California's Fourth Climate Change Assessment](#) (September 2018)
Released in September 2018, the Fourth Assessment includes 44 technical reports that address California-specific informational gaps about climate vulnerabilities. The technical report cited above assesses the future performance of key water resources management factors for the Central Valley water system using the same probability-based climate change risk assessment discussed here.

[Academic Studies of Climate Change Impact on California Water Resources](#)

In addition to the reports just described, an array of academic research has focused on specific aspects of climate change effects on California's water resources. Previous exercises in hydro-system modeling have provided substantial insights for policy-making and public discussion related to water resources management in California (Harou et al. 2010; Connell-Buck et al. 2011; Tanaka et al. 2011; Null et al. 2014;). Most of these studies have shown that California's water system, while not impervious, can stand up quite well to substantial climate disturbances without widespread catastrophic losses, if well managed.

Climate change impact assessment studies of the CVS using the CALifornia Value Integrated Network (CALVIN) (Tanaka et al. 2006; Medellin-Azuara et al. 2008; Harou et al. 2010; Connell-Buck et al. 2011), a hydro-economic optimization model of the water supply management of the intertied water supply system of California, "demonstrate that Delta export operations are often central for economic adaptation to climate change, and changes in hydrology lead to increased scarcity and costs as users adapt to reduced supplies and a seasonal shift in water availability" (Tanaka et al. 2011). Except for Tanaka et al. (2006), each of these studies provides estimates of the costs to adapt the California water system to no more than a few hypothesized futures that might be warmer, drier, more drought-prone, or some combination of the three. Tanaka et al. (2006) expand the set of considered climate futures to 12, including the possibility for a wetter future. Unfortunately, the snapshots of potential future conditions are limited and are provided without a sense for the relative likelihood of the occurrence of the conditions explored. Furthermore, the results from CALVIN, being optimized to maximize statewide net economic

benefits, are not constrained by administrative agreements governing water allocations in California in practice, and therefore (though of great value in imagining an improved future) are diminished in value to California water system planners who must operate within jurisdictional realities.

Reclamation (2016) used CalLite 3.0 to identify risks to water deliveries and water quality resulting primarily from seasonal shifts in runoff, sea level rise, and an altered state of the Delta requiring greater reservoir releases within an altered water delivery schedule. CalLite 3.0 is a simplified, faster version of the CalSim-II (Draper et al. 2004) water system model used by DWR and Reclamation to simulate the coordinated operations of the CVS. CalLite 3.0 represents reservoir operations, SWP and CVP operations and delivery allocation decisions, existing water-sharing agreements, and Delta salinity responses to river flow and export changes on a monthly time-step. It can also represent the effect on the water system of sea-level rise. Because it represents the mechanics of DWR and Reclamation allocation rules and water sharing agreements, the Reclamation (2016) study is better able to inform adaptation responses in water system planning and management than studies using CALVIN. But in the interest of computational efficiency, the Reclamation (2016) study evaluated only a limited set of five “representative” climate futures taken from the Intergovernmental Panel on Climate Change’s (IPCC’s) Coupled Model Intercomparison Project Phase 5 (CMIP5) ensemble of GCM runs (Taylor et al. 2012), plus an additional set of twelve GCM-simulated climate scenarios taken from the California Climate Change Technical Advisory Group (CCTAG). Though the evaluated range spanned a reasonably wide range of potential future climate conditions (1.5–5°C warming, and -15 percent to +35 percent average annual precipitation by 2100), the possible changes were not sampled comprehensively, and the total number of evaluated changes was relatively small.

Other water system modeling studies have indicated that the effects of climate change on water resources management in California may result in the need to: (1) increase electricity imports to the Sacramento region during hot, dry spells, when scarce water most constrains local power production (especially hydropower) (Dale et al. 2015); (2) carefully control hydropower generation and local electricity demand in an ongoing effort to balance the dual objectives of stabilizing reservoir levels and the reduction of greenhouse gas emissions (thermal power plants being used when hydropower is unavailable) (Tarroja et al. 2014); (3) give greater consideration to stream temperatures in order to protect fish habitat when developing reservoir operating rules (Null et al. 2013; Rheinheimer et al. 2015); and (4) improve conveyance between existing surface and groundwater storage (Null 2016). These studies provide important insights, but none use more than four climate change possibilities, and none use water system models that can holistically inform the vulnerability of the CVS water system to climate change.

Two studies have explored a wider range of possible climate futures on water system domains similar to those considered in this work: (1) Willis et al. (2011), a flood impact study showing the relative effects of temperature and precipitation changes on flood risk in the Sacramento River Basin (and the utility of dynamic reservoir rule curves to absorb flood flows); and (2) Groves and Bloom (2013), an analysis of water resource-management response packages for California’s Central Valley showing the reduction in system vulnerabilities (and improvement in resilience) achievable through implementation of well-designed response packages. Both studies take climate input from downscaled GCMs run for selected emissions scenarios of the Coupled Model Intercomparison Project Phase 3 (CMIP3). The ensemble of GCM projections (11 GCMs in the case of Willis et al. (2011) and six in the case of Groves and Bloom (2013), each using CMIP3 scenarios A2 and B1) provides valuable perspective on a system response to a wider range of possible climate futures.

But the climate uncertainty space explored by these two studies is less than that included in either the CMIP3 or CMIP5 ensembles (themselves an underestimate of climate change uncertainty [Stainforth et al. 2007; DR Cayan et al. 2010; Steinschneider et al. 2015; Stouffer et al. 2017]), and is not investigated in a comprehensive, systematic fashion. Willis et al. (2011) consider temperature ranges of only 0.4–1.4°C and precipitation ranges of only -6.6 percent to 16.8 percent relative to the historical. The downscaled GCM runs used by Groves and Bloom (2013) spanned a “hot and dry” extreme marked by approximately 2–2.5°C warming and -5–10 percent average annual precipitation to a “cool and wet” extreme marked by approximately 0.5°C warming and +5 percent annual average precipitation. Only 12 discrete samples were taken, and almost no samples were taken representing “hot and wet” or “cool and dry,” though those conditions are present in the CMIP5 ensemble of projections for California. Groves and Bloom (2013) identified conditions under which the Central Valley system and tributary watersheds consistently performed poorly, but the highlighted composite scenario (hot [$\Delta T > 0.67^\circ\text{C}$ increase relative to historical] and dry [$\Delta P > 25$ percent decrease]) addressed questions of climate change likelihood only subjectively, limiting the applicability of the results to risk-informed decision-making.

The findings of each of these studies, including the 2016 Reclamation study discussed earlier, are conditional on the fidelity of a downscaled set of GCM projections. These are likely not representative of the parameters of local climate variability most relevant to water management (Brown & Wilby 2012) and cannot present a direct comparison to historical performance. In terms of utility to decision-making at DWR, the Willis et al. (2011) study assesses flood risk, not water supply risk, and the Groves and Bloom (2013) study uses a Water Evaluation and Planning (WEAP) model that is a coarse approximation of Delta dynamics, which likely over-simplifies simulation of Delta water quality conditions essential to water system allocations in practice (Joyce et al. 2010).

In summary, despite a large number of studies that have evaluated the effects of climate change on the California water system, significant questions remain, such as:

- How much climate change can the system withstand?
- What are the critical thresholds of climate change which cause the system to fail to meet expectations?
- What are the specific climate changes that are problematic, and are they likely to occur?

No previous study was found presenting sensitivity of the water system to changes in climate in a comprehensive way and in connection with a quantitative assessment of the relative likelihood of possible climate change outcomes. For example, Reclamation (2016) calculated the future unmet demand that would occur in five selected climate change scenarios but provided no means by which to interpret the relative likelihoods of those five possible scenarios, limiting any meaningful quantification of risk based on the results. In response, this study presents a decision scaling (Brown et al., 2012) approach that allows systematic climate vulnerability assessment across a range of potential future climate conditions spanning a climate change uncertainty domain inclusive of (and extended beyond) the full CMIP5 ensemble, including quantification of the relative likelihood of potential future performance levels.

Methodology

DWR's vulnerability assessment for long-term and persistent hydrologic effects of climate change focuses on impacts to the operation of the State Water Project (SWP), including ecological conditions that dictate operating rules. DWR owns and operates the SWP for flood control, maintenance of environmental and water quality conditions, water supply, hydropower, and recreation. Consequently, analysis of SWP performance under climate-changed conditions yields an array of impact metrics across these areas of concern.

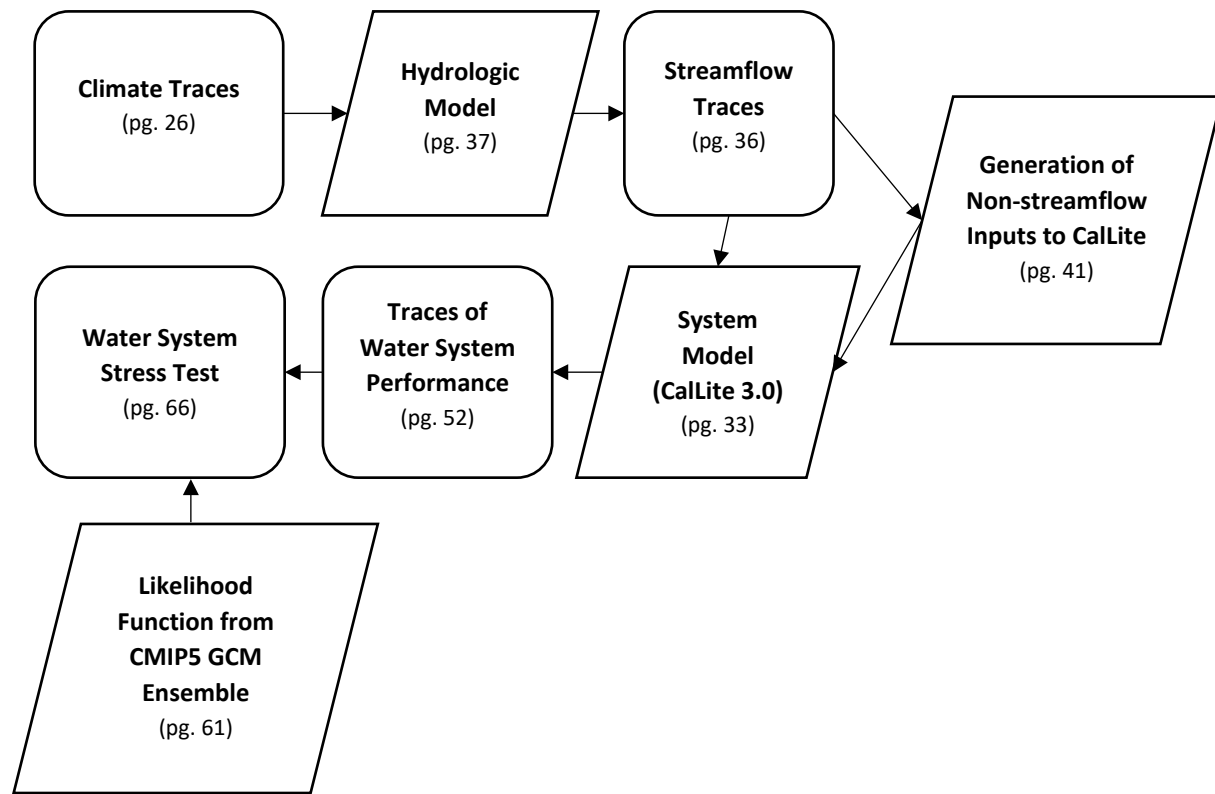
Water resources system models are essential tools for exploring the risks to water system performance of potential future hydro-climatological and socio-economic conditions (Brown et al. 2015). This section presents an overview of the modeling approach developed for this study, introducing the model workflow and key terms and concepts depicted in Figure 2. Each element of Figure 2 is explained in detail in its own dedicated section later in this report. The analysis focuses on persistent medium- and long-term conditions evaluated at a monthly time-step. Short-duration extreme precipitation events that cause flooding may also stress water resource management but are beyond the scope of this study.

To conduct a stress test that can meaningfully inform the vulnerability of the multifaceted CVS, a water system model that can rapidly simulate the coordinated operations of the Central Valley Project (CVP) and SWP is needed. This study has adopted CalLite 3.0, a simplified, faster version of the CalSim-II water system model used by DWR. DWR estimates that the trade-off for the faster speed of CalLite 3.0 is an approximate error of 1 percent when compared with a corresponding run of CalSim-II (Islam et al. 2014). CalLite 3.0 is loaded with all system-wide relational data, such as reservoir area-elevation-capacity, wetness-index dependent flow standards, and monthly flood control requirements. For each month of the simulation period, CalLite 3.0 employs a mixed integer program to maximize water deliveries and/or storage per specified priorities and system constraints. Output includes water supply indicators, environmental indicators, and water-use metrics (Draper et al. 2004; California Department of Water Resources & United States Bureau of Reclamation 2011).

CalLite 3.0 receives time series of streamflow as input; however, to inform the likelihood of climate-change-related water-system vulnerabilities, it is necessary to begin with the most fundamental factors available — those describing conditions of meteorological drought, i.e., precipitation and temperature. This study uses a paleo-dendrochronology reconstructed streamflow record (Meko et al. 2014) coupled with historical daily temperature and precipitation to develop 1,100-year climate traces of plausible alternative precipitation and temperature. A hydrologic model (SAC-SMA) translates descriptors of fundamental meteorological drought into measures of available water at Earth's surface. The estimates of available water from the hydrologic model become the key inputs to a water system model (CalLite 3.0) which simulates the complex interactions of water supply, water demand, regulatory compliance, and operational choices, producing metrics of water system performance such as water deliveries, reservoir storage, and river flow volume.

Figure 2 Modeling Workflow for Climate Change Vulnerability Assessment

Note: Page number indicates the location in this report where the description of the workflow element can be found.



Structured, repeated simulation of the resulting workflow (Figure 2) – a “water system stress test” – allows the systematic exploration of climate change impact on the water system in response to a wide range of meteorological input. Table 1 lists the CVS metrics evaluated using this approach. The response of each performance metric to a systematically-explored climate space is presented relative to a performance threshold (in this case, historical performance).

Table 1 Decision-Relevant metrics

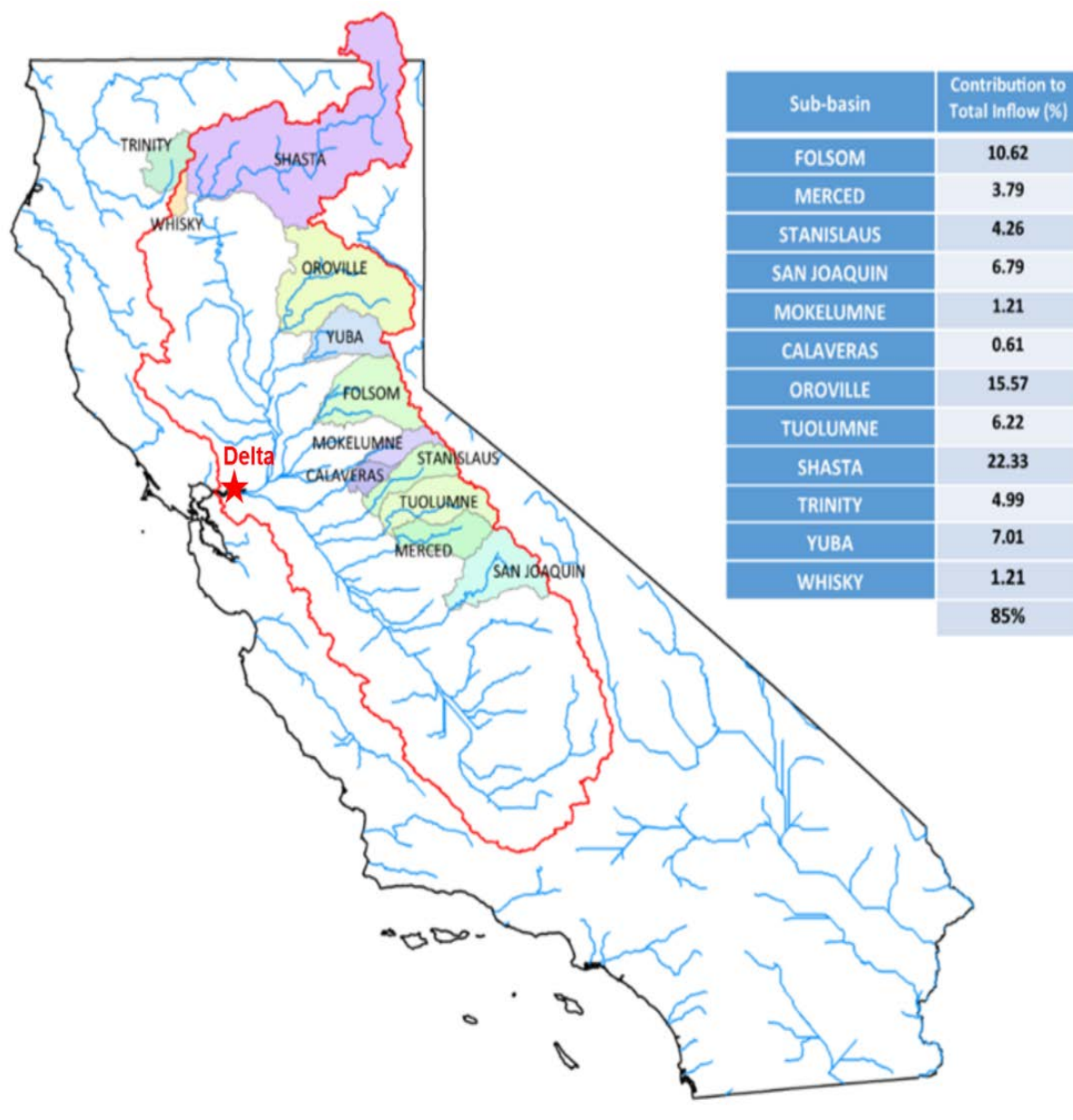
| | |
|----------|--------------------------------|
| 1 | Oroville Storage levels |
| | April 30 |
| | September 30 |
| 2 | Net Delta Outflow |
| | Winter (Dec, Jan, Feb) |
| | Spring (Mar, Apr, May) |
| | Summer (Jun, Jul, Aug) |
| | Fall (Sep, Oct, Nov) |
| 3 | SWP Deliveries |
| | Average Annual |
| 4 | System Shortages |
| | Average Annual |

Description of Study Area

The catchment area of the Sacramento and San Joaquin rivers (Figure 3) provides at least a portion of the water supply for about two-thirds of California's population. About half of California's average annual streamflow flows toward the Sacramento-San Joaquin Delta, and most of California's farmland depends on water tributary to it (Lund et al. 2010). The Delta is a web of channels and reclaimed islands at the confluence of the Sacramento and San Joaquin rivers. It forms the eastern portion of the wider San Francisco Estuary, which includes the San Francisco, San Pablo, and Suisun bays, and collects water from California's largest watershed, which encompasses roughly 45 percent of the state's surface area (Lund et al., 2010). The Delta is also a center for important components of California's civil infrastructure, such as electricity transmission lines, gas transmission pipes, underground storage of natural gas, and transportation lines, and provides crucial habitat for many California fish species that live in or migrate through it (especially four fish that are listed as "Endangered" or "Threatened" pursuant to the federal Endangered Species Act [Mount & Twiss 2005]). Not inconsequentially, the Delta is valued for its agricultural production, aesthetic appeal, and support of recreational activities (Lund et al. 2010). The usable water resources for the CVS can be approximated as the quantity of streamflow flowing into the Central Valley from the north-east upgradient regions. These regions are comprised of twelve large subbasins, referred to as the *rim subbasins* (Figure 3).

DWR and Reclamation oversee the operation of the Central Valley water systems that store and manage water supplies that flow through the Delta (see Figure 4). The California Central Valley Water System (CVS) is therefore defined as *the interconnected system of natural river channels and man-made facilities that comprise the CVP, owned and operated by the United States Bureau of Reclamation and the SWP, owned and operated by DWR*. The CVP includes more than 13 million acre-feet of storage capacity in 20 reservoirs. The CVP provides water to about 3,000,000 acres of irrigated agricultural fields, for municipal water uses, and for river and wetland water releases used to meet State and federal ecological standards. The SWP includes more than 30 storage facilities, namely reservoirs and lakes, and about 700 miles of open canals and pipelines that distribute water to approximately 25 million Californians and about 750,000 acres of irrigated farmland. The SWP is not the exclusive water supplier for those it serves, as many of its customers supplement the water provided by SWP with local or other imported sources. The SWP is designed to bolster local supplies and ensure greater supply reliability. Thus, demands on the project vary year to year.

Figure 3 California Central Valley System (CVS) and Rim Subbasins



Note: Table inset shows percent contribution of each of the 12 rim inflows to the total Delta outflow. Fifteen percent of the total Delta outflow is contributed by unshaded areas within the red outline.

Figure 4 State, Federal, and Local Water Infrastructure



Note: From Volume 3, Page 7-6 of the California Water Plan, Update 2013 (2013).

Generation of Climate Traces

In the original experimental design of this study (California Department of Water Resources 2017), a weather generator (Steinschneider and Brown 2013) produced 5000 unique climate realizations using a Wavelet Auto-Regressive Model (WARM) designed to maintain the 15-year low frequency variability of the precipitation signal visible in the latter half of the paleo record (Dettinger and Cayan 2014; Meko et al 2014). The initial sampling strategy required the establishment of a specific metric upon which to gauge the severity of the simulation (e.g., five-year precipitation). While this sampling strategy allowed exploration of system sensitivity to specific types of climatic characteristics of concern, the sampling of baseline traces was limited to within ± 1 percent of the long-term mean to maintain fidelity to the historical observed interannual climate variability. This sampling strategy resulted in the omissions of traces with extended wet or dry periods. For this reason, the current iteration of this study has adopted an approach that utilizes the paleo-dendrochronological record to generate climate traces that are informed by a larger range of interannual variability than contained in the instrumental record alone.

The paleo-dendrochronology reconstructed record of Sacramento 4-river annual streamflow (900–2013) (Meko et al. 2014) was coupled with historical daily temperature and precipitation from 1950–2013 (Livneh et al. 2013) to generate a 1,100-year climate trace. The reconstructed Sacramento 4-river annual flow provides information about long-term inter-annual variability through a 1,100-year record of the wet and dry cycles that the CVS has endured. The daily temperature and precipitation provide information about the spatiotemporal distribution of weather that produced such annual streamflow. While not evaluated in this study, the 1,100-year record of wet and dry periods provides additional data to be used for the evaluation of future drought risk, which will be the focus of a future study.

The Sacramento 4-river annual streamflow is the aggregate annual water-year (October 1–September 30) streamflow of the Sacramento River at Bend Bridge, the American River inflow to Folsom Reservoir, the Yuba River at Smartsville, and Feather River inflow to Oroville Reservoir. The Sacramento 4-river annual streamflow covers the major inflow points to the CVS. Additional flows into the CVS not covered by the Sacramento 4-river annual streamflow are highly correlated to the Sacramento 4-river flow (Meko et. al. 2014).

The following steps were taken to link the 50-year daily temperature record to the 1,100-year paleo-dendrochronological record:

Step 1: Prior to using the historical observed temperature data, it was necessary to remove the linear warming trend in the data. Temperature detrending was achieved by applying a linear trend to the data so that the detrended temperature time series had a trend line of slope zero and an average value equal to the average temperature from 1981 through 2010. This procedure was applied to each grid cell across the CVS watershed. The detrended historical temperature allows reference to current and recent historical conditions when developing the stress test as opposed to a more abstract reference to mid-20th-century temperatures at the mean of the historical time series. Furthermore, detrending was necessary to ensure the same average temperature reference is maintained across the 1,100-year coupled sequence. The observed historical precipitation data showed no trend, thus required no detrending.

Step 2: Using the historical (1950–2003) detrended temperature and precipitation data as input, the Sacramento Soil Moisture Accounting distributed hydrologic model (SAC-SMA-DS) was used to simulate streamflows in the Sacramento, Feather, Yuba, and American rivers of the Sacramento basin to generate the Sacramento 4-river annual streamflow.

Step 3: For each paleo-dendrochronology reconstructed Sacramento 4-river annual streamflow from 900 through 1949, the closest historical observed (1950–2003) analog flow was associated with it.

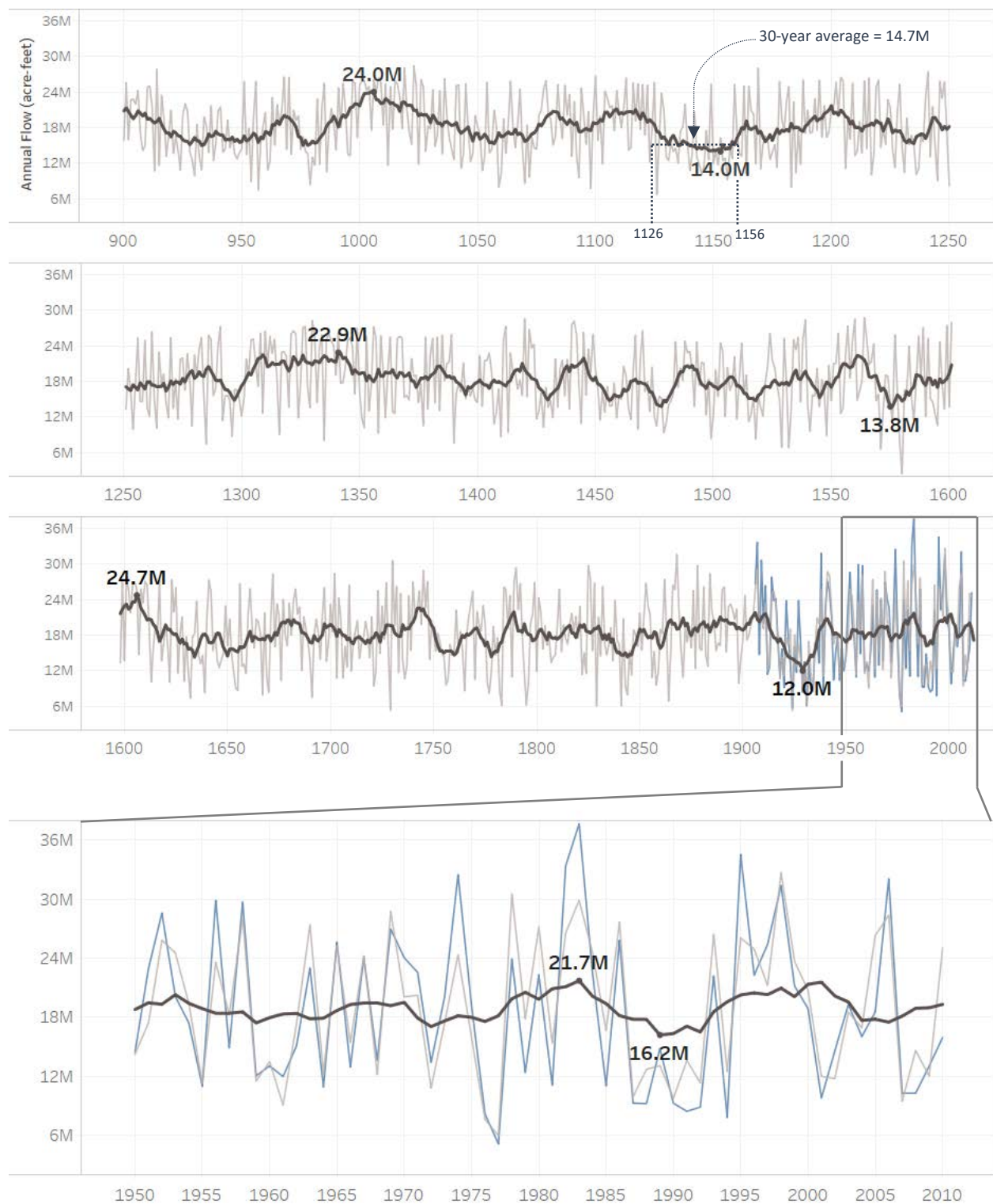
Step 4: The historical (1950–2003) detrended temperature and precipitation data for the water year of the analog historical observed flow was then copied into the historical reconstructed years.

This method of bootstrapping full years of temperature and precipitation ensures that spatial and temporal correlations are maintained and an exploration of a wider range of hydrologic inter-annual variability than is present in the observed meteorological record. There are several extended periods of below and above-average annual streamflows in the paleo reconstructed record which are greater in magnitude than found in the observed period of meteorological record (1950-2003) used in this study. For example, the maximum and minimum 10-year moving average annual streamflows calculated over the observed record are 21.7 maf (12% below the paleo maximum of 24.7 maf in the year 1606) and 16.2 maf (25% above the paleo minimum of 12.0 maf in 1929). Furthermore, periods of above and below-average flows persist for longer in the paleo record, up to 30 years (1126-1156) as shown in Figure 5.

The bootstrapped 1,100-year historical trace of daily temperature and precipitation was then perturbed systematically to explore the climate vulnerability domain of the CVS. The explored range for temperature and precipitation was informed by the range of changes projected for the CVS watershed area by the global climate models included in the Intergovernmental Panel on Climate Change's (IPCC's) Fifth Coupled Model Intercomparison Project (CMIP5) (Taylor et al. 2012). Figure 6 shows the range of average temperature and precipitation change projected (2036–2065 relative to 1981–2010) by 36 different models simulated at two different representative concentration pathways (RCP 4.5 and RCP 8.5). The scatter of the model projections indicates that the likely range of temperature and precipitation change that the CVS would experience ranges from -20 percent to +30 percent change in precipitation, and a temperature change of 0°C to +4°C (0 °F to 7.2 °F) relative to 1981-2010.

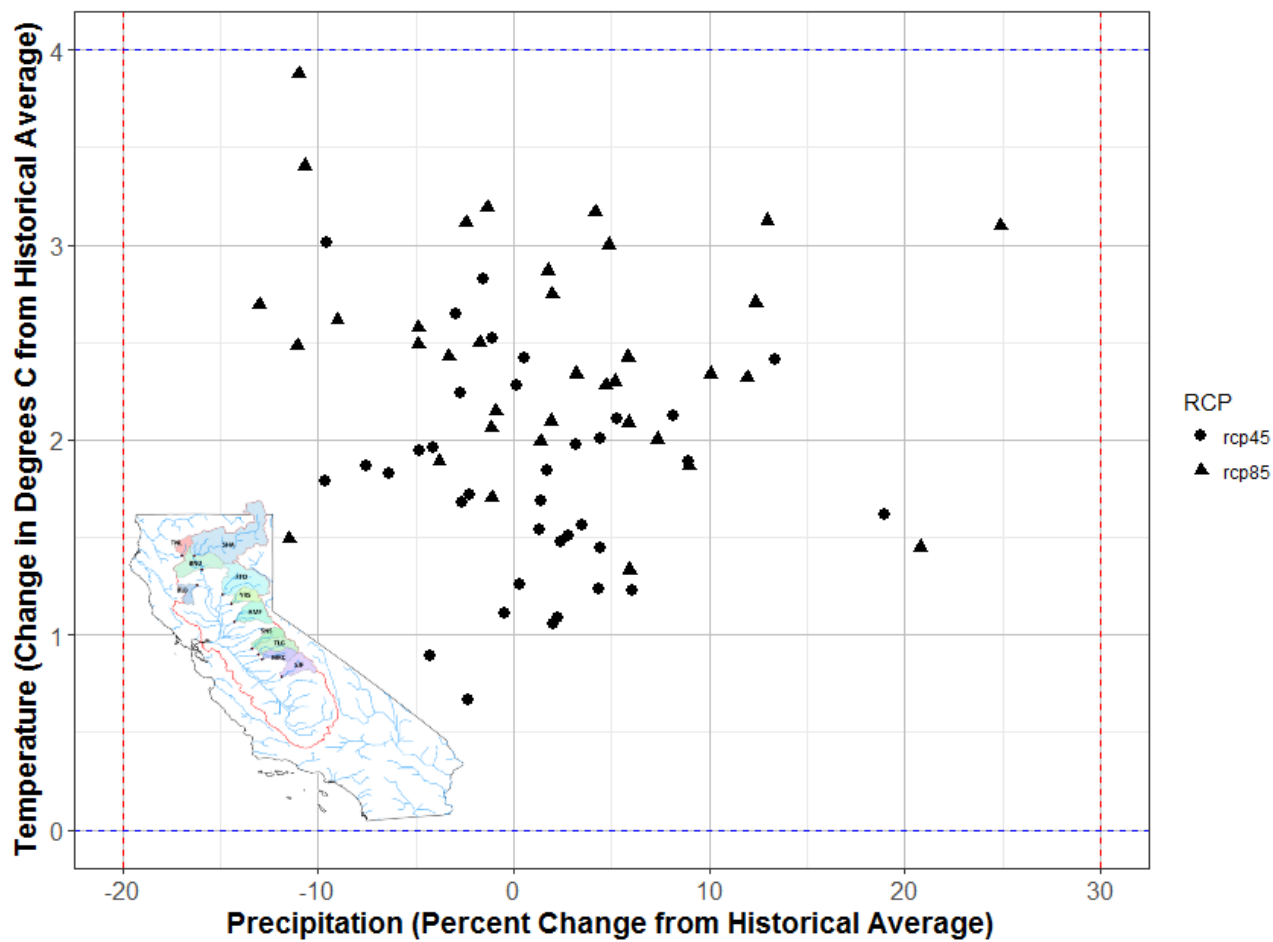
A total of 54 combinations of temperature shifts (+0°C to +4°C, by 0.5°C increments; +0 °F to +7.2 °F, by 0.9 °F increments) and precipitation shifts (-20 percent to +30 percent, by 10 percent increments) were imposed on each day of the 1,100-year historical climate record in each CVS grid cell using the Delta method described in the “Details on Approach to Climate Change Factors” section of this report. The result was 54 independent climate traces identical to the historical in internal variability but unique in average temperature and precipitation.

Figure 5 Sacramento 4-River Paleo Reconstructed Annual Streamflow



Note: The light grey line is paleo reconstructed Sacramento 4-River annual streamflow from 900 to 2010 and the blue line is observed Sacramento 4-River annual streamflow from 1906 to 2010. 10-year moving (centered) average paleo reconstructed flow is represented by the dark grey line with minimum and maximum values annotated for each time-window shown.

Figure 6 CMIP5 Ensemble of GCM Output Projecting Climate Changes by 2050 for the CVS



Note: Changes shown are average annual precipitation and temperature shifts: 2036–2065 relative to 1981–2010.

Details on Approach to Climate Change Factors

Because precipitation and temperature vary both spatially and temporally, the relationships of temperature and precipitation trends (for both observed and projected) with several geographical and timescale factors (including elevation, latitude, and season) should be investigated. In doing so, the levels of precipitation and temperature changes can be incorporated in more detail, which would help a realistic distribution of climate changes across the large study area as a function of space as well as time. This section presents an analysis conducted to analyze seasonal trends in temperature. See Annex B: Spatial and Temporal Climate Trends for further detail on spatial and seasonal trend analysis conducted for this study.

Relationship Between Temperature Trend and Season

This study uses daily climate data from the National Climate Data Center (NCDC) to identify relationships between temperature trends and season. Only the NCDC station data for which missing data rate is less than 20 percent was used. The winter dataset consists of the months of December, January, and February; spring with March, April, and May; summer with June, July, and August; and fall data with September, October, and November. Boxplots of trend slopes for five datasets (annual data, winter, spring, summer, and fall) are shown in Figure 7. The daily temperature data used to conduct this analysis went through quality checks based on two rates of missing station observations: Figure 7 results from 94

stations for which the missing data rate is less than 10 percent, while Figure 8 shows the results of trend analysis from 145 stations for which the missing rate is less than 20 percent.

In Figure 7 and Figure 8, red numbers represent medians of seasonal temperature trend, and black numbers are means of seasonal temperature trend. All trend slopes are positive, which implies that temperature tends to rise during 1950–2015. According to these box plots, seasonally distinct warming trends were observed. The seasonal warming patterns derived from this observed temperature analysis were applied to the new sequences of temperature reflecting 8 increase levels (i.e., 0.5, 1, 1.5, 2, 2.5, 3, 3.5, 4°C) as shown in Figure 9. Seasonal warming patterns define ratios among the four seasons. Then, these ratios are maintained in 8 increasing levels of temperature shift. In one season, increase levels are assumed to be the same across three months. The calculation processes are as follows:

Step 1: From the temperature data of each station during 1950–2015, Sen's slope is computed for four datasets of spring, summer, fall, and winter. Then, boxplots are calculated (Figures 7 and 8).

Step 2: From these boxplots, means of temperature trend slope (black numbers in boxplots) are attained from 94 stations (i.e., dataset with less than 10 percent missing data) and 145 stations (i.e., dataset with less than 20 percent missing data). These means are shown in Table 2 below.

Step 3: Finally, temperature increases reflecting the spring, summer, fall, and winter trends are calculated for eight scenarios (temperature increase of 0.5; 1; 1.5; 2; 2.5; 3; 3.5; 4°C). These patterns are shown in Figure 9.

Table 2 Means of Seasonal Warming Pattern

| Season (Months) | Average Temperature Increase Per Decade (°C/decade) |
|-----------------|---|
| Winter (DJF) | 0.116 |
| Spring (MAM) | 0.265 |
| Summer (JJA) | 0.1915 |
| Fall (SON) | 0.0435 |

Figure 7 Trend Slope of Temperature With Less Than 10 Percent Missing Data in 94 Stations

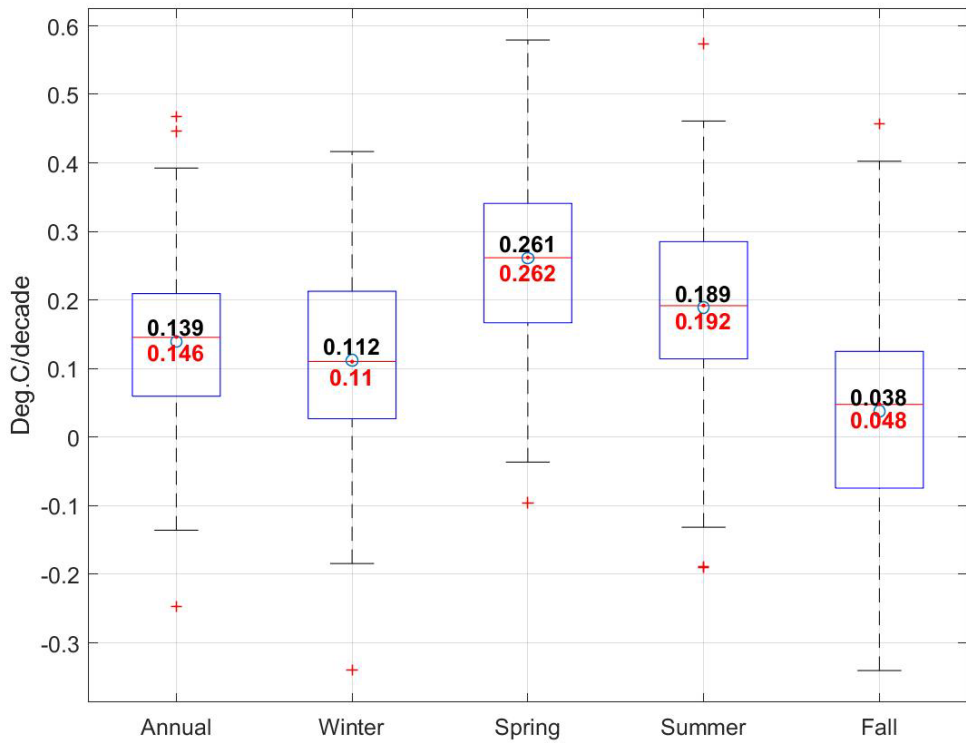


Figure 8 Trend Slope of Temperature With Less Than 20 Percent Missing Data in 145 Stations

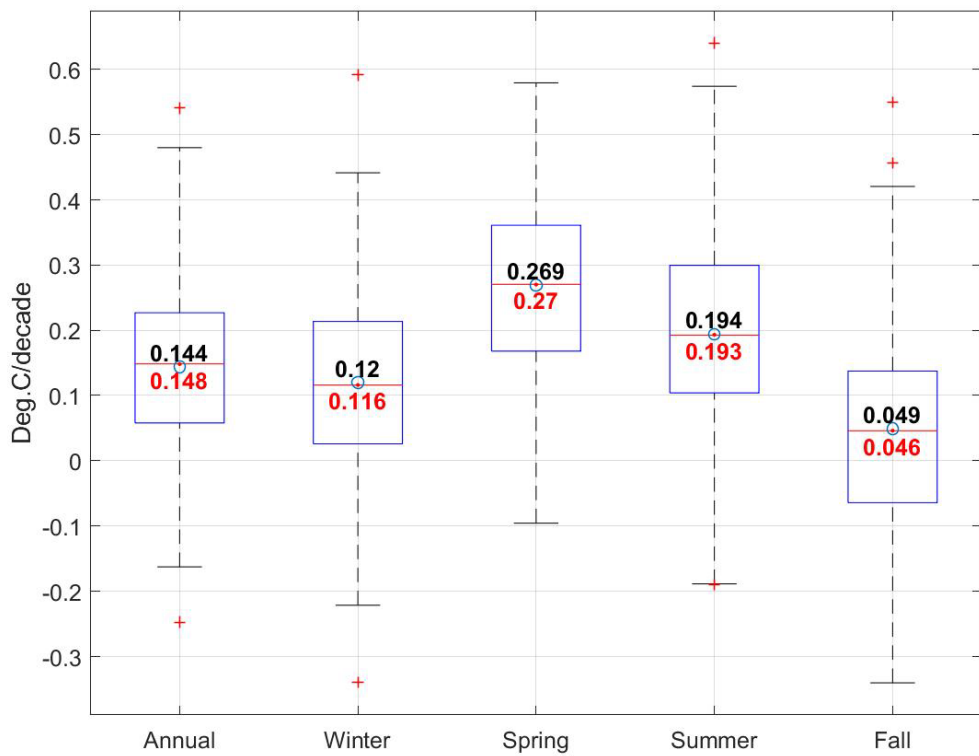


Figure 9 Seasonal Warming Patterns for Climate Projections



Conclusion

No significant correlations were found for either temperature or precipitation trends with elevation and latitude (see *Annex B: Spatial and Temporal Climate Trends* for further analysis). Consequently, mean annual precipitation changes were applied without considering season, elevation, or latitude factors. On average, temperatures in Spring and Summer were seen to warm more significantly than in Winter and Fall over the past 65 years; therefore, seasonal mean annual temperature changes were applied using the seasonal factors described above.

Although the results of this investigation enable us to account for seasonal warming effects, two major assumptions are made. First, ratios of seasonal warming to annual warming are assumed to be the same at any level of annual warming. This results in relatively large warming differentials such as at an annual warming of 4°C under which the spring is warmed to nearly 7°C compared to the winter at 3°C. Second, the seasonal warming effect is assumed to be uniform across the entire CVS area. However, as is evident in the distribution of seasonal warming trends observed in NCDC station data (see Figures 7 and 8), sub-selection of station locations in a given region of the CVS will likely result in different ratios of seasonal to annual warming. Future investigation into the presence and causes of trends in seasonal warming would improve understanding of how seasonal warming effects may persist or change in the future.

A version of this study which does not include an application of the seasonal warming effect was published in California’s Fourth Climate Change Assessment (Schwarz 2018). Although the performance metrics selected for reporting in the Fourth Assessment version of this study differ from those selected here, the Fourth Assessment study is a reference point for comparing the effect of seasonal warming at the macro, system-wide scale since both studies were completed using the modeling workflow shown in Figure 2.

Water Resources System Model

CalLite 3.0 is the water resources system model used in this study to assess impacts. It is a screening level planning tool developed by DWR and Reclamation to simulate the coordinated operations of the intertied CVS. CalLite 3.0 is the faster, streamlined version of CalSim-II⁴ (Draper et al. 2004), designed to be accessible to policy and stakeholder demands for rapid and interactive policy evaluations. CalLite’s mixed integer linear program maximizes monthly water deliveries and/or storage per specified priorities and system constraints. The system constraints and weights (fully described in Draper et al. [2004] and California DWR and Reclamation [2011]) are specified using the Water Resources Engineering Simulation Language (WRESL) (California Department of Water Resources 2000): “The objective function in the [CalLite] model is a linear combination of decision variables and their associated priority weights. In addition, slack and surplus variables added to the objective function from ‘soft’ constraints are multiplied by their associated negative penalties.”

⁴ CalSim-II, driven by the Water Resource Integrated Modeling System (WRIMS model engine or WRIMS) is “a generalized water resources modeling system for evaluating operational alternatives of large, complex river basins [that] integrates a simulation language for flexible operational criteria specification, a [mixed integer] linear programming solver for efficient water allocation decisions, and graphics capabilities for ease of use” (California Department of Water Resources & United States Bureau of Reclamation 2011). As explained by Draper et al. (2004), “for each time period, the solver maximizes the objective function to determine a solution that delivers or stores water according to the specified priorities and satisfies system constraints. The sequence of solved [Mixed Integer Programming] problems represents the simulation of the system over the period of analysis... [CalSim-II] also allows the user to specify objectives using a weighted goal-programming technique pioneered by Charnes and Cooper (1961).”

CalLite's CVS-specific design and substantial intricacy enable better fidelity to the mechanics of DWR allocation rules and water sharing agreements. That being said, the model contains many approximations of site-specific values for which historical observations are scarce, and also includes poorly-understood empirically-based relationships that pose challenges related to water system simulation under wide-ranging conditions of climate uncertainty.

CalLite 3.0, a schematic of which is shown in Figure 10, represents reservoir operations, SWP and CVP operations and delivery allocation decisions, existing water sharing agreements, and Delta salinity responses to river flow and export changes on a monthly time-step. CalLite 3.0 can also represent the effect on the water system from land use changes and sea level rise, features of particular use to this study. CalLite 3.0, released in 2014, has 796 input parameters and approximately 240 additional data tables that store all relational data, such as reservoir area-elevation-capacity data, wetness-index dependent flow standards, and monthly flood control requirements (Draper et al. 2004; California Department of Water Resources & United States Bureau of Reclamation 2011). Output includes water supply indicators, environmental indicators, and water-use metrics.

CalLite 3.0 Configuration of Regulatory Environment

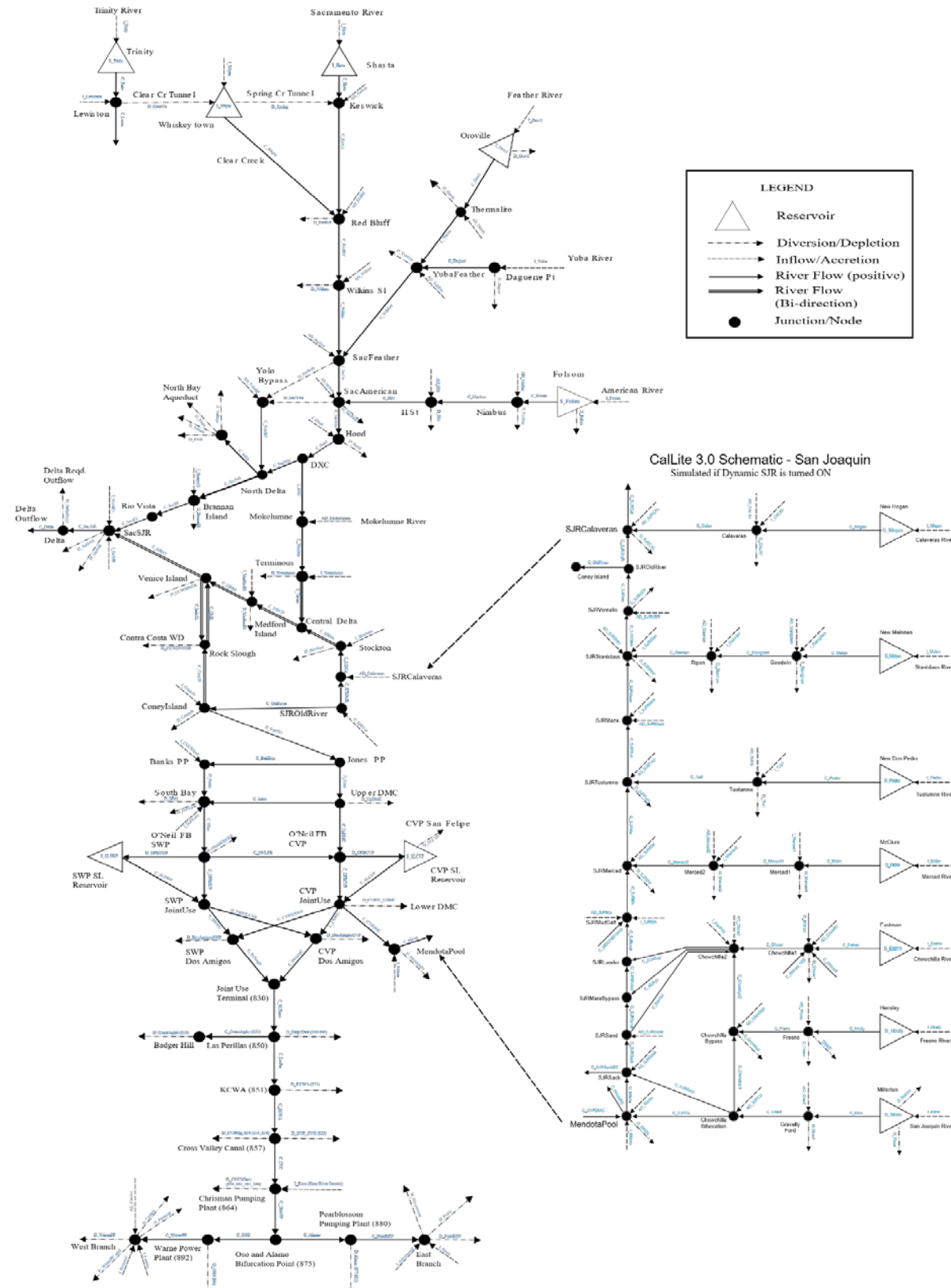
CalLite 3.0 allows users to specify and turn on or off regulatory flow requirements including various river flows, Delta outflows, export restrictions, and salinity objectives relating to the operation of the CVP and SWP. In this study, regulatory constraints are set to represent operating conditions as of the year 2015. Table 3 identifies base assumptions for the regulatory environment used in this study and contrasts it with a similar version of this study published in California's Fourth Climate Change Assessment (Schwarz et al. 2018).

Table 3 Base Assumptions Used for Regulatory Environment in CalLite 3.0

| Regulatory Standard | Configuration for this Study | Configuration for Schwarz et al. 2018 |
|--|--|--|
| Vernalis Adaptive Management Plan (VAMP) | – VAMP is turned <u>OFF</u> | – VAMP is turned <u>ON</u> |
| Delta Cross Channel | – D-1641 standard is turned <u>ON</u> – National Marine Fisheries Service Reasonable and Prudent Alternative Action 4.1.2 is turned <u>ON</u> | – Same |
| Export-Inflow Ratio | – D-1641 standard is turned <u>ON</u> – National Marine Fisheries Service Reasonable and Prudent Alternative Action 4.2.1 is turned <u>OFF</u> | – Same except Action 4.2.1 is turned <u>ON</u> |
| Delta Outflow and Rio Vista Requirements | – D-1641 standard is turned <u>ON</u> – U.S. Fish and Wildlife Service Reasonable and Prudent Alternative Action 4 X2 ^a requirement is turned <u>ON</u> – Roe Island standard is turned <u>ON</u> | – Same |
| Salinity Requirements | – Emmatton, Jersey Point, Rock Slough, and Collinsville are turned <u>ON</u> | – Same |

^a X2 = location of the 2 parts per thousand salinity contour, one meter off the bottom of the estuary, as measured in kilometers upstream from the Golden Gate Bridge

Figure 10 CalLite 3.0 Schematic



Generation of Streamflows

As illustrated in Figure 3, the coverage area of the hydrologic model includes all major tributaries to the northern CVS. The contributing flow is summarized in the Figure 3 table insert, showing the relative importance of the Shasta and Oroville subbasins. The SAC-SMA-DS hydrologic model is used to simulate streamflow at 32 locations throughout the CVS watershed. As shown in Figure 10, these 32 streamflow simulations include:

Calibration Set I: 12 rim inflows to major reservoirs throughout the CVS.

Calibration Set II: 11 gauging station streamflow points important for calculating water-year types used for regulatory constraints, management, and operational decision-making.

Calibration Set III: 9 subbasin inflows that account for a substantial portion of the rain in the system and represent “unimpaired inflows,” as they are the modeling results of estimating the runoff that would have occurred had water flow remained unaltered in rivers and streams instead of stored in reservoirs, imported, exported, or diverted (Bay-Delta Office 2007).

As shown in Figure 11, the locations of the 11 stream gages in Calibration Set II are nearly identical to the locations of the basin outlets for the 12 rim inflows in Calibration Set I. This is because the historical data for the CalLite 3.0 rim inflows are derived from the 11 physical stream gages described in Calibration Set II. To validate the workflow shown in Figure 2 relative to the baseline run of the CalLite 3.0 simulation model, the SAC-SMA-DS model was calibrated directly to the streamflow in the CalLite 3.0 package (Calibration Set I). This is different than calibrating to historical observations, as the streamflow pre-loaded in the CalLite 3.0 package is the output of previous hydrologic modeling (Variable Infiltration Capacity [VIC]) project performed for the CVS.

To evaluate the quality of the original VIC hydrologic model output used in CalLite 3.0, and to gain the confidence associated with validation relative to historical observations, it was necessary to calibrate the SAC-SMA-DS directly to the observations at the 11 physical gages of Calibration Set II. The results of Calibration Set II were not used as input to CalLite 3.0 but were used in the determination of water-year type classification as described below.

Calibration Set III was developed when it was realized that Calibration Set I and Calibration Set II failed to account for a substantial portion (especially south and west) of the total CVS basin area shown bounded in red in Figure 11. The nine unimpaired inflow basins of Calibration Set III add information on CVS subbasins that are rain-dominated (as opposed to many of the 12 rim inflows, which are largely snow-dominated), and accounts for a substantial portion of the rain that falls within the CVS system. The nine basins of Calibration Set III are referred to as “unimpaired inflows,” as they are the result of a modeling project that estimated the runoff “that would have occurred had water flow remained unaltered in rivers and streams instead of stored in reservoirs, imported, exported, or diverted” for 24 Central Valley subbasins and the Sacramento-San Joaquin Delta for October 1920 through September 2003 (Bay-Delta Office 2007). Whereas Calibration Set I was used as direct input to CalLite 3.0 and Calibration Set II was used principally as a check on Calibration Set I and in the development of water year type classification, Calibration Set III was used principally to add information to the process for generating other, minor hydrologic and non-hydrologic inputs to CalLite 3.0.

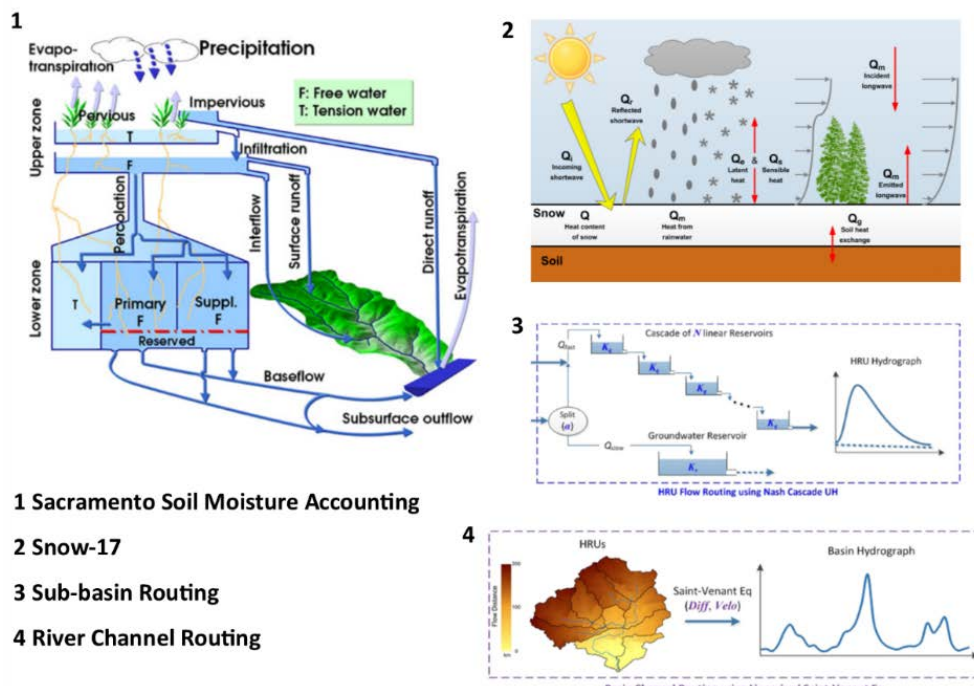
Box 1 Description of the SAC-SMA-DS Hydrologic Model

The hydrologic model is required to be extremely robust because of its essential role in the quantification of the available water on which water allocations to all water sectors are based. Hydrologic model residuals propagate through the modeling chain and contribute to a cascade of uncertainty (Wilby & Dessai 2010). This box describes the development of a distributed, physically-based hydrologic model capable of supporting subsequent phases of the climate change vulnerability assessment workflow.

The amount of usable water for the CVS can be approximated as the quantity of streamflow in the 12 largest rivers flowing from the northeast into the Central Valley. These are referred to as the *rim inflows*. To estimate those 12 streamflows, a unique version of the Sacramento Soil Moisture Accounting (SAC-SMA) model was developed.

SAC-SMA (Burnash et al. 1973), is a lumped conceptual hydrological model employed by the National Weather Service (NWS) of the National Oceanic and Atmospheric Administration (NOAA) to produce river and flash flood forecasts for the United States (Burnash 1995; McEnery et al. 2005). It was coupled with a river routing model (Lohmann et al. 1998) for application to the large, distributed CVS watershed system (consisting of approximately one thousand 1/8th degree grid cells). The coupled model is hereafter referred to as SAC-SMA-DS (Wi & Brown 2013), distinguishing it from the distributed version of SAC-SMA previously developed by NWS. SAC-SMA-DS has been applied to a number of case studies (e.g., Koren et al. 2004; Smith et al. 2004). SAC-SMA-DS (Box 1 Figure (a)) is composed of hydrologic process modules that represent soil moisture accounting, potential evapotranspiration (Hamon 1961), snow processes (Anderson 1976), and flow routing, and operates in grid formulation on a daily time-step.

(a) Distributed Hydrologic Model



Box 1 Description of the SAC-SMA-DS Hydrologic Model (continued)

The overall model structure of SAC-SMA-DS is depicted in Box 1 Figure (a) above. More details on the model components are provided in the descriptions for the modules additionally introduced to develop the distributed version of SAC-SMA.

Hamon Evapotranspiration Calculation

The potential evapotranspiration (PET) is derived based on the Hamon method (Hamon 1961), in which daily PET in millimeters (mm) is computed as a function of daily mean temperature and hours of daylight:

$$PET = \text{Coeff} \cdot 29.8 \cdot L_d \cdot \frac{0.611 \cdot \exp\left(17.27 \cdot \frac{T}{T+273.3}\right)}{T+273.3}$$

where L_d is the daylight hours per day, T is the daily mean air temperature ($^{\circ}\text{C}$), and Coeff is a bias correction factor. The hours of daylight is calculated as a function of latitude and day of year based on the daylight length estimation model suggested by Forsythe et al. (1995).

In-grid Routing: Nash-Cascade Unit Hydrograph

The within-grid routing process for direct runoff is represented by an instantaneous unit hydrograph (IUH) (Nash 1957), in which a catchment is depicted as a series of N reservoirs each having a linear relationship between storage and outflow with the storage coefficient of K_q . Mathematically, the IUH is expressed by a gamma probability distribution:

$$u(t) = \frac{K_q}{\Gamma(N)} (K_q t)^{N-1} \exp(-K_q t)$$

where Γ is the gamma function. The within-grid groundwater routing process is simplified as a lumped linear reservoir with the storage recession coefficient of K_s .

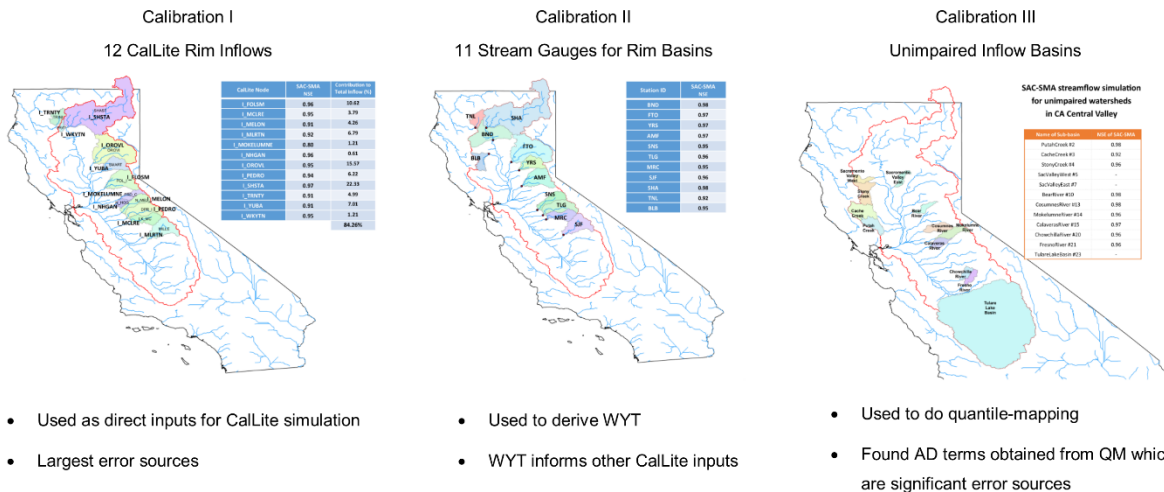
River Channel Routing: Linearized Saint-Venant Equation

The transport of water in the channel system is described using the diffusive wave approximation of the Saint-Venant equation (Lohmann et al. 1998):

$$\frac{\partial Q}{\partial t} + C \frac{\partial Q}{\partial x} - D \frac{\partial^2 Q}{\partial x^2} = 0$$

where C and D are parameters denoting wave velocity and diffusivity, respectively.

Figure 11 Maps of Three Calibration Sets For the Application of SAC-SMA-DS to the CVS



Generation of Hydrologic Inputs to CalLite 3.0

Of the 796 CalLite inputs, 39 are hydrologic inflows to the CVS. These 39 inflows consist of the 12 rim basin inflows (see Table 3), 9 “unimpaired” local inflows, and 18 “other” local inflows. Internal consistency in these hydrologic inflows can be maintained using the paleo-dendrochronology reconstructed climate traces in combination with the SAC-SMA-DS hydrologic model (see Box 1). Most of the input variables were found to have a relatively small impact on model output. Of the 796 inputs, only 20 (the 12 rim basins plus 8 of the 9 unimpaired local inflows) of the 39 inflow variables and 11 of 18 accretion/depletion (AD) terms⁵ exerted a strong influence on model output (see Table 4).

Table 4 Twelve Major Rim Inflows to the CalLite 3.0 Model

| |
|---|
| American River (into Folsom Lake) |
| Merced River (into Lake McClure) |
| Stanislaus River (into New Melones Lake) |
| San Joaquin River (into Millerton Lake) |
| Mokelumne River |
| Calaveras River (into New Hogan Lake) |
| Feather River (into Lake Oroville) |
| Tuolumne River into (New Don Pedro Reservoir) |
| Sacramento River (into Shasta Reservoir) |
| Trinity River (into Trinity Reservoir) |
| Yuba River (into New Bullards Bar) |
| Clear Creek (into Whiskeytown Reservoir) |

⁵ Accretion/depletion terms are generated in CalLite 3.0 to account for differences between CalLite 3.0 and CalSim-II resulting from a less detailed schematic. Adjustments (addition and subtraction of CalSim-II terms) are made at each CalLite 3.0 node based on CalSim II outputs.

Table 5 R Squared Correlations For 31 CalLite 3.0 Input Parameters With Strong Influence on Model Output

| CalLite 3.0 Input Parameter | Correlation Coefficient | Best Fit of Calibration Set I/II/III Outputs |
|-----------------------------|-------------------------|--|
| I_NHGAN.FLOW.INFLOW | 1 | I_NHGAN |
| I_SHSTA.FLOW.INFLOW | 1 | I_SHSTA |
| I_FOLSM.FLOW.INFLOW | 1 | I_FOLSM |
| I_OROVL.FLOW.INFLOW | 1 | I_OROVL |
| I_MCLRE.FLOW.INFLOW | 1 | I_MCLRE |
| I_WKYTN.FLOW.INFLOW | 1 | I_WKYTN |
| I_PEDRO.FLOW.INFLOW | 1 | I_PEDRO |
| I_MLRTN.FLOW.INFLOW | 1 | I_MLRTN |
| I_LEWISTON.FLOW.INFLOW | 1 | I_TRNTY |
| I_TRNTY.FLOW.INFLOW | 1 | I_TRNTY |
| I_MELON.FLOW.INFLOW | 1 | I_MELON |
| I_YUBA.FLOW.INFLOW | 1 | I_YUBA |
| I_MOKELEMNE.FLOW.INFLOW | 1 | I_MOKELEMNE |
| I_ESTMN.FLOW.INFLOW | 0.99 | ChowchillaRiver |
| I_HNSLY.FLOW.INFLOW | 0.99 | FresnoRiver |
| AD_REDDBLF.FLOW.ACCRDEPL | 0.92 | StonyCreek |
| AD_MOKELEMNE.FLOW.ACCRDEPL | 0.9 | CosumnesRiver |
| I_CALAV.FLOW.INFLOW | 0.78 | PutahCreek |
| AD_SACFEA.FLOW.ACCRDEPL | 0.77 | StonyCreek |
| AD_CALAVERAS.FLOW.ACCRDEPL | 0.75 | I_NHGAN |
| AD_YOLOBP.FLOW.ACCRDEPL | 0.7 | PutahCreek |
| AD_SJR_PULSE_V.FLOW.CHANNEL | 0.65 | I_MOKELEMNE |
| AD_SJR_V.FLOW.ACCRDEPL | 0.65 | I_MOKELEMNE |
| AD_SJR_VAMP_V.FLOW.CHANNEL | 0.64 | I_MOKELEMNE |
| AD_YUBFEA.FLOW.ACCRDEPL | 0.46 | CacheCreek |
| I_MDOTA.FLOW.INFLOW | 0.39 | I_MELON |
| I_TUOL.FLOW.INFLOW | 0.27 | CalaverasRiver |
| I_KELLYRIDGE.FLOW.INFLOW | 0.26 | SacWYT |
| I_KERN.FLOW.INFLOW | 0.25 | I_MLRTN |
| AD_WILKNS.FLOW.ACCRDEPL | 0.24 | SacWYT |
| AD_SACAME.FLOW.ACCRDEPL | 0.1 | SacWYT |

27 local inflow inputs to CalLite 3.0, which make up the remaining portion of the system's total inflows apart from the 12 rim inflows, were not directly simulated because: (1) acquisition of unimpaired natural flow for those rivers was not straightforward; and (2) the increasing computational effort was not justified by the increase in model accuracy (given the small fraction of total flow contribution). The AD terms could not be simulated using a hydrologic model because they are aggregations of hydrologic, management, and other anthropogenic behaviors that cannot be approximated as unimpaired catchment inflows.

Generation of Non-Hydrologic Inputs to CalLite 3.0

The 757 non-hydrologic CalLite 3.0 input time series' fit into one of three categories: (1) constant value, (2) time series with several discrete steps or recurring values, (3) or continuously varying time series. In both the discrete recurring value time series and continuously varying time series, the values tended to vary as a function of hydrology (wetness or dryness of month), either directly (correlated to one of the 12 rim inflows of Calibration Set I or one of the 9 additional unimpaired inflows of Calibration Set III) or by way of one of two streamflow indices developed using Calibration Set II.

To evaluate the “goodness of fit” of each CalLite 3.0 input parameter to the Sacramento and San Joaquin water-year types, 60 water-year type values were computed (5 water-year types x 12 months) for each of the Sacramento and San Joaquin water-year-type indices. The average value of each CalLite 3.0 input parameter was calculated for each month of each water-year type. To explore correlation with the water-year types, the raw time series of each input parameter was then regressed against a discrete time series (with 60 unique values) representing the water-year-type average in each month of each year of the historical record.

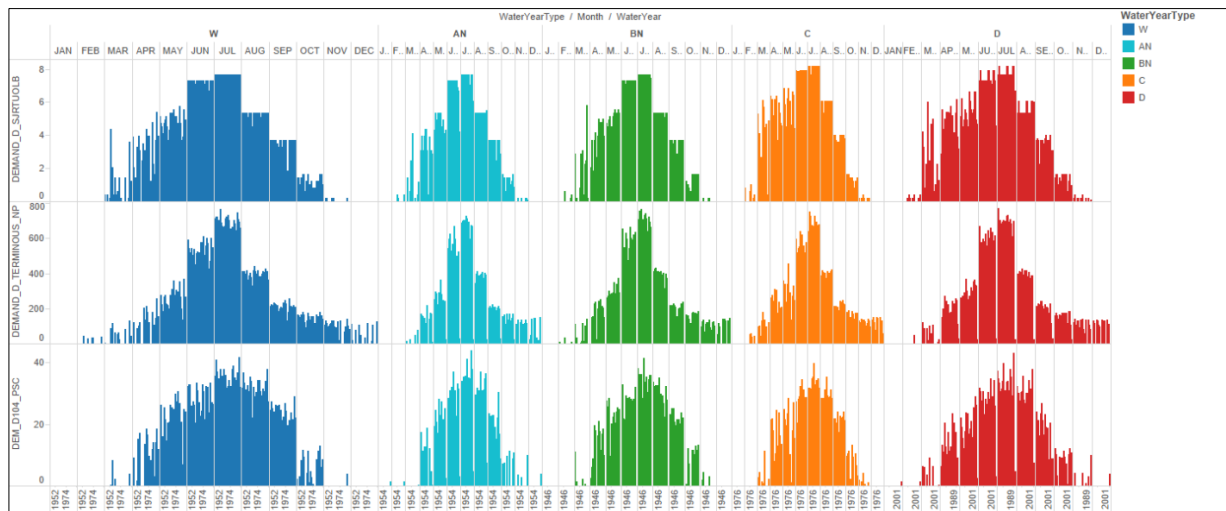
719 of the CalLite 3.0 input parameters were better correlated to a water-year-type index than they were to one of the 21 inflows of Calibration Sets I and III. Those 719 input parameters were therefore associated with one of the two water-year-type indices and varied accordingly. 63 CalLite 3.0 input parameters were associated with an inflow of Calibration Set I or III and perturbed using a quantile mapping technique. Finally, the values of two CalLite 3.0 input parameters were generated by way of special processes unique to those inputs.

Creating Synthetic Time Series by Water-Year-Type Method

For those CalLite 3.0 input parameters that correlated most closely to one of the two water-year-type classifications (Sacramento or San Joaquin), a discrete, 60-value mapping procedure was then used. The 60 values for each input variable were calculated using the historical observed dataset. The historical dataset was sorted by historical water-year-type classification and an average value for each month-water-year combination was calculated.

To generate the synthetic input time series, the water-year type was calculated based on the synthetic hydrologic input time series (Calibration Set II) using the appropriate water-year calculation methodology (<http://cdec.water.ca.gov/cgi-progs/iodir/WSIHIST>), which is a combination of rim inflows. The historically calculated 60 values were then mapped into the synthetic time-series input variable according to the water-year type and month combination. Figure 12 shows three variables that have strong correlations with the San Joaquin water-year type classification.

Figure 12 Input Variables With Strong Correlation to San Joaquin Water Year Type Classification
— Historical Observed Data Shown



Creating Synthetic Time Series by Quantile Mapping Method

Sixty-three CalLite 3.0 input parameters were synthetically generated by quantile mapping the historical unimpaired-flow time series for each of the DWR 24 unimpaired flow basins (California Department of Water Resource Bay Delta Office 2007) to the historical values of each time series in the CalLite 3.0 input file.

The CalLite 3.0 input parameters that correlated most closely with one of the rim inflows were paired with that inflow. For example, Figure 13 shows the correlation that two historical local inflows (I_BRANANIS and I_MDOTA) have with the historical inflows of the 12 rim basins, and the rim inflows of I_NHGAN and I_MOKELEMUNE are selected as the best pairs of I_BRANANIS and I_MDOTA, respectively. The pairs of local and rim inflows determined in this way are used in the quantile mapping procedure to generate new local inflows corresponding to new rim inflows. The quantile mapping procedure is described using an example in the following section. Table 5 shows pairs of local and rim inflows determined for all local inflows. Consequently, six of the rim inflows are selected based on which inflows are quantile-mapped.

Figure 13 Pearson Correlation Coefficients of Two Historical Local Inflows (I_BRANANIS and I_MDOTA) With 12 Historical Rim Inflows.

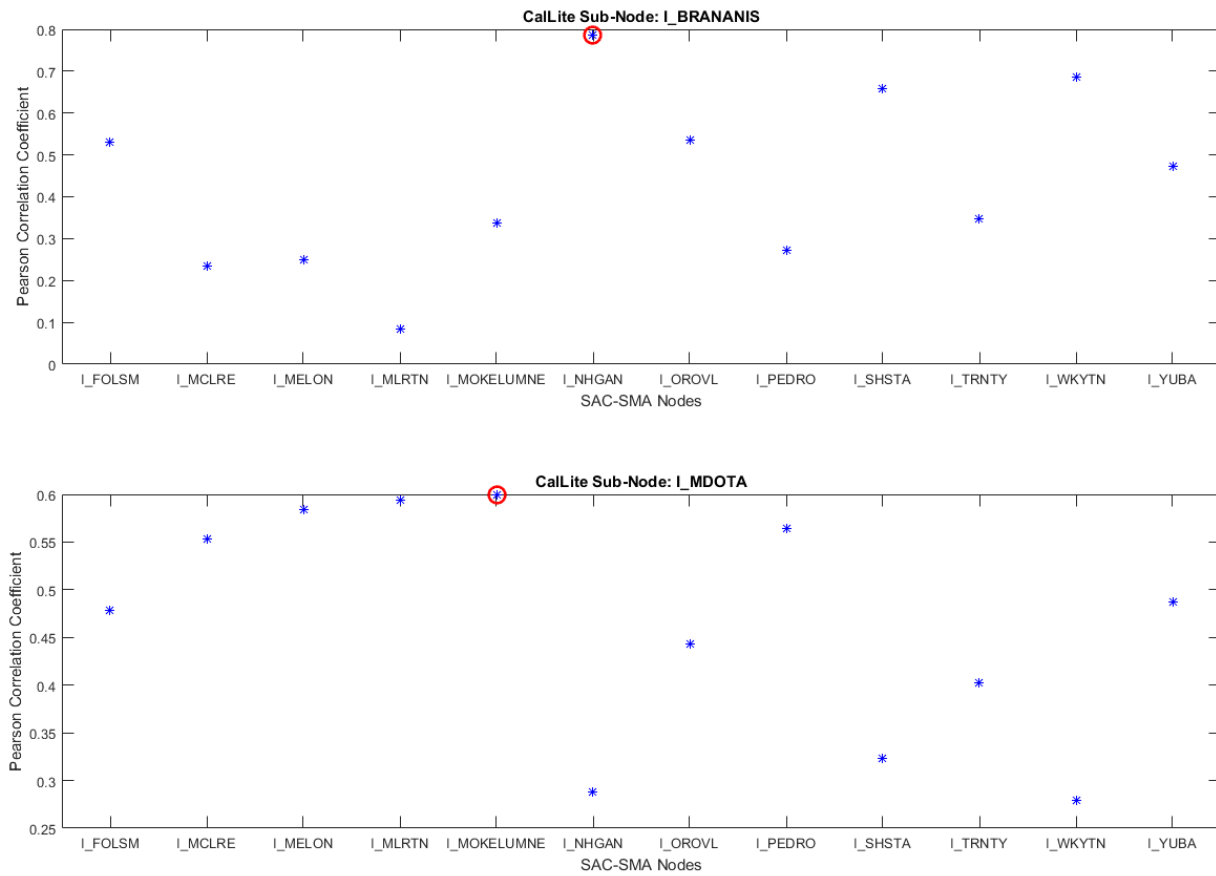


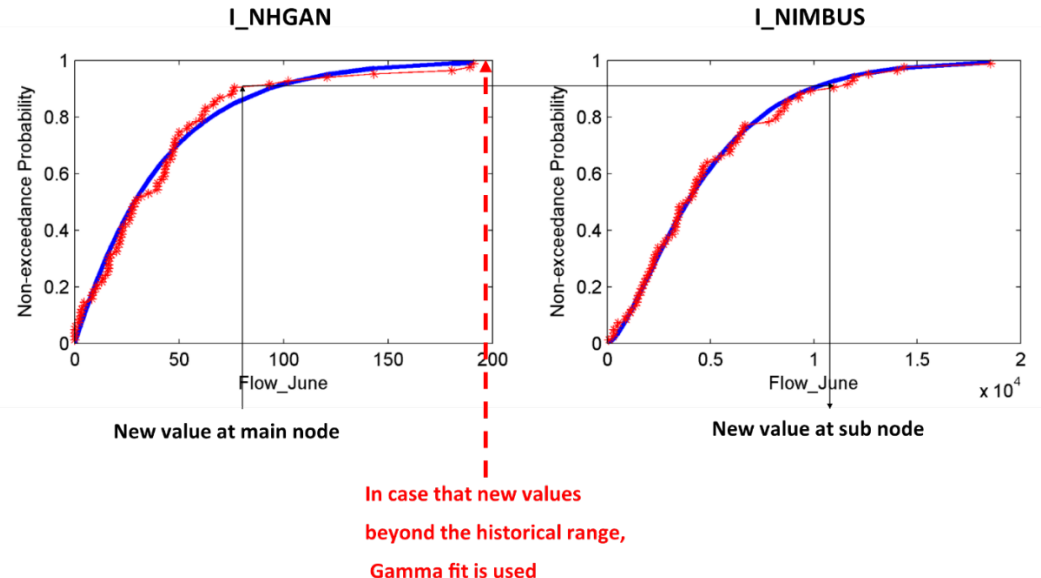
Table 6 Pairs of Rim Flows and Local Inflows Determined by Correlation

| Rim Inflow Node | Local Inflow Node | Pearson correlation coefficient | Relative contribution to total system flows |
|-----------------|-------------------|---------------------------------|---|
| I_NHGAN | I_STANGDWN | 0.99 | 0.01 percent |
| | I_NIMBUS | 0.94 | 0.03 percent |
| | I_ESTMN | 0.91 | 0.28 percent |
| | I_EASTBYP | 0.90 | 0.76 percent |
| | I_CALAV | 0.87 | 0.05 percent |
| | I_HNSLY | 0.87 | 0.33 percent |
| | I_TERMINOUS | 0.83 | 0.22 percent |
| | I_BRANANIS | 0.79 | 0.32 percent |
| | I_STOCKTON | 0.77 | 0.06 percent |
| | I_MEDFORDIS | 0.76 | 0.18 percent |
| I_MELON | I_HOOD | 0.72 | 0.05 percent |
| | I_SACSJR | 0.72 | 0.02 percent |
| | I_CONEYIS | 0.71 | 0.10 percent |
| | I_MARSHCR | 0.61 | 0.13 percent |
| | I_SJRMMS | 0.57 | 0.09 percent |
| | I_SJRMSA | 0.57 | 0.09 percent |
| | I_TUOL | 0.42 | 0.79 percent |
| | I_SJRMAZE | 0.58 | 1.45 percent |
| | I_SJRSTAN | 0.58 | 0.08 percent |
| | I_MERCED1B | 0.51 | 0.33 percent |
| I_MLRTN | I_KERN | 0.49 | 0.10 percent |
| | I_STANRIPN | 0.32 | 0.40 percent |
| I_FOLSM | I_KELLYRIDGE | 0.38 | 0.50 percent |
| I_MOKELOMNE | I_MDOTA | 0.60 | 0.58 percent |
| I_TRNTY | I_LEWISTON | 0.99 | 0.03 percent |

Here, we provide a detailed description of the quantile mapping procedure with an example for the local inflow of I_NIMBUS. For the I_NIMBUS, the rim inflow of I_NHGAN is selected as the best-correlated inflow, with the correlation coefficient of 0.94. The quantile mapping procedure starts with fitting those two inflows to specific probability distributions. In this study, we employed two types of distributions: (1) empirical probability based on the Weibull plotting position, and (2) theoretical probability based on the 2-parameter gamma distribution. How the quantile mapping works for the I_NIMBUS with selected rim inflow I_NHGAN is illustrated in Figure 14. For those two inflows, both the empirical and theoretical distribution are fitted as shown in Figure 14; the red line with asterisk dots represents the fit by the Weibull plotting position and the blue line represents the fit by the Gamma distribution. The red continuous empirical probability line is formed by doing a linear interpolation between values of asterisk

dots. As shown in the figure, the new rim inflow leads to the new local inflow value through those two quantile plots of local and rim inflows. The quantile mapping procedure is simply summarized in two steps: (1) find a quantile (i.e., non-exceedance probability) for the new rim inflow, and (2) find the value of local inflow that corresponds to the quantile of the rim inflow. In our quantile mapping procedure, empirical distributions are used as long as new inflows are within the historically observed range. In case the new inflows are beyond the historical range, gamma distribution fit is used. This quantile mapping procedure is conducted monthly to take into account the seasonal variability of inflows.

Figure 14 Quantile Mapping Procedure Applied to Example California Sub-Basin



Parameter-Specific Generation of CalLite 3.0 Input (i.e., Special Cases)

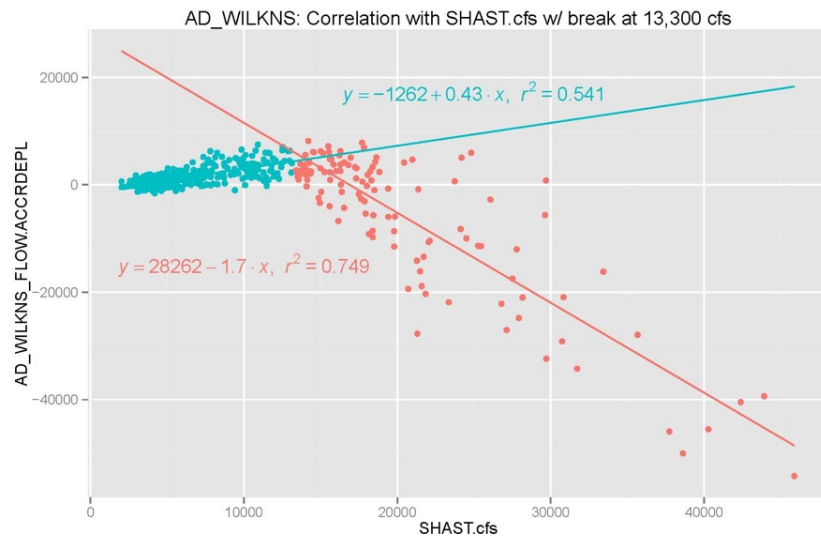
Two AD terms, AD_Wilkins and AD_SACAME, had a large impact on model performance and did not correlate well to rim unimpaired inflow or water-year-type averages. Additional efforts were made to create new versions of these time series.

AD_Wilkins

CalLite's AD_Wilkins term was developed as a mass balance of CalSim-II terms along the Sacramento River from the Red Bluff Diversion Dam to Wilkins Slough in Colusa Basin. AD_Wilkins contained very large negative values. Through visual inspection of the CalSim-II schematic represented by the single lumped AD_Wilkins term, the time series was identified as containing Tisdale weir operations in the Butte basin. The design capacity of the Tisdale weir is 38,000 cubic feet per second (cfs)⁶, which seems reasonable when compared to the largest negative values contained in the AD_Wilkins time series (Figure 15). AD_Wilkins correlated well to unimpaired flow from the Bay Delta Office's Shasta unimpaired flow basin. When flow from the Shasta Basin exceeds 13,300 cfs, it was assumed that water begins to exit the Sacramento River via a weir. Two linear equations were developed for AD_Wilkins: one for conditions in which Shasta flow is less than 13,300 cfs, and another when flow exceeds 13,300 cfs (Figure 15).

⁶http://cdec4gov.water.ca.gov/cgi-progs/products/Weir_Operations_Schematic.pdf

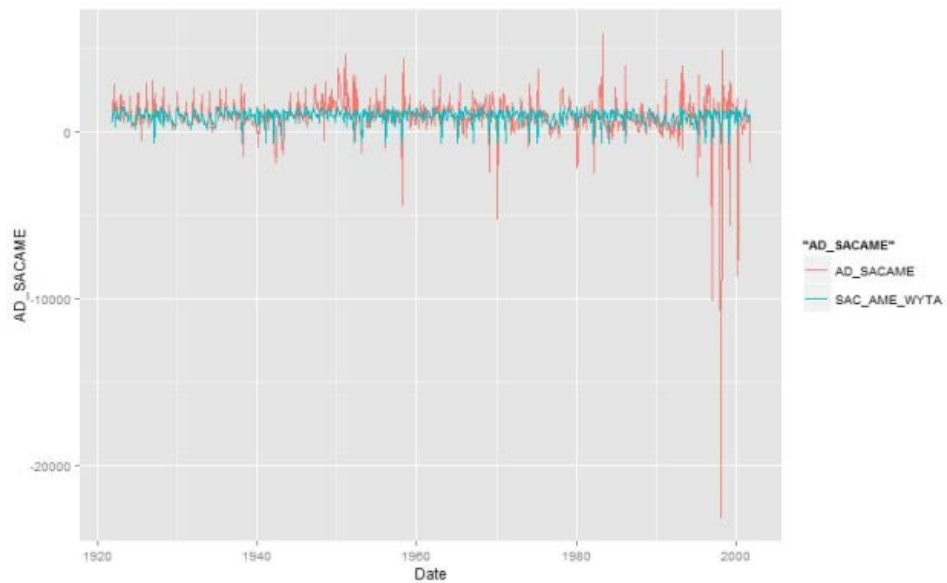
Figure 15 AD_Wilkins: Correlation With Shasta Flow



AD_SACAME

CalLite's AD_SACAME term represents the confluence of Sacramento and American rivers and was developed as a mass balance of CalSim-II terms along the Sacramento River from the Fremont Weir/Feather River confluence to Freeport. The term includes depletions in Yolo and Solano counties, agricultural and urban return flows, and water diverted from the Bear River. After an exhaustive search for a more adroit method of synthesizing the AD_SACAME variable, it was decided the best possible approximation was the Sacramento water-year-type classification average. It should be noted that the end of the AD_SACAME time series of historically observed values contains some extremely negative values (Figure 16) which call into question the assumptions used to create the CalSim-II terms on which the AD_SACAME time series is based.

Figure 16 AD_SACAME Historical Behavior



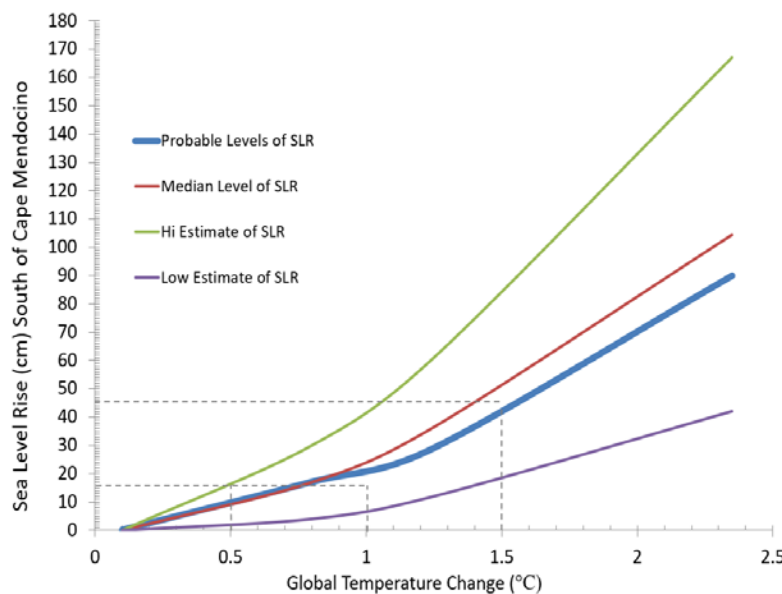
Sea Level Rise Assignment for CalLite 3.0

For operational purposes, it was important to estimate sea-level rise as a function of temperature and to associate the appropriate amount of sea-level rise with the temperature perturbation to which each CalLite 3.0 run was subjected. Sea-level rise increases saline intrusion into the Delta due to hydrostatic pressure from sea water head. During the spring and fall, DWR and Reclamation release additional water from reservoirs or reduce exports from the Delta to maintain regulatory compliance with maximum salinity limits and minimum outflow requirements.

At the start of this study, three sea-level rise scenarios were parameterized in CalLite 3.0: 0 centimeters (cm) (0 inches [in.]), 15 cm (6 in.), and 45 cm (18 in.). This coarse discretization of sea-level rise is a limitation of the model and may cause underestimation of impacts at higher temperatures (e.g., more than 2.5°C [4.5 degrees Fahrenheit (°F)], when sea-level rise would likely exceed 45 cm [18 in.]). Further, sea-level increases beyond 45 cm would likely cause significant changes in Delta hydrodynamics and would likely result in levee overtopping and additional inundation of lands that are currently protected by levees. Modeling such changes would require making assumptions about future levee investments and land uses, and those topics are beyond the scope of this project.

The National Research Council (2012) approximated the anticipated future rate of sea-level rise along the California coast, south of Cape Mendocino, for the years 2030, 2050, and 2100. These projections, in conjunction with values for projected global temperature increase by year from IPCC (2013), were used to estimate the amount of sea-level rise that should be expected along the California coast, south of Cape Mendocino, for each temperature band listed in Table 6 and shown in Figure 17. Recent guidance published by the California Ocean Protection Council Science Advisory Team Working Group projects the likely range (67% probability) of sea-level rise by 2050 to be 18.3-33.5 cm above the 1991-2009 mean (Griggs et al. 2017), placing estimates used in this study for the 2050 planning horizon within comparable limits.

Figure 17 Estimates of Sea-Level Rise by Degree C



The sea-level rise assignment for CalLite 3.0 was made according to the logic shown in Table 6, which approximates and discretizes to the three sea-level rise steps available within the model and DWR's best understanding of the level of sea-level rise that would be expected at each increment of temperature change. Each time a climate trace was run through CalLite 3.0, the degree of temperature shift it received (as described in reference to Figure 9) was noted, and the corresponding sea-level rise function within the model was set according to Table 6.

Table 7 Sea-Level Rise Discretization Within CalLite 3.0

| Temperature Change Relative to Recent Historical Average Temperature | Sea-Level Rise Relative to Recent Historical Average Sea Level |
|--|---|
| 0°C (32 °F) | 0 cm (0 in.) |
| 0.5°C – 1.0°C (0.9 °F – 1.8 °F) | 15 cm (6 in.) |
| ≥ 1.5°C (2.7 °F) | 45 cm (18 in.) |

Notes:

°C = degrees Celsius

°F = degrees Fahrenheit

cm = centimeters

in. = inches

Model Verification

Hydrologic Model Performance

To calibrate the SAC-SMA-DS, a genetic optimization algorithm (Conn et al. 1991) was used to maximize the Nash-Sutcliffe efficiency (NSE) (Nash & Sutcliffe 1970). Table 7 summarizes the performance of the simulated historical inflows of the 12 rim subbasins for calibration (1951–1980) and validation (1981–2002) periods. NSEs evaluated on the monthly simulated streamflow show values of above 0.9 for all of them except for the Mokelumne subbasin. According to Moriasi et al. (2007), model simulation can be judged as satisfactory if $NSE > 0.5$.

Table 8 Hydrologic Model Performance by Subbasin

| Subbasin | Nash Sutcliffe Efficiency | |
|-------------|----------------------------|-------------|
| | Calibration (1951–1980) | Validation |
| | | (1981–2002) |
| American | 0.96 | 0.94 |
| Merced | 0.95 | 0.93 |
| Stanislaus | 0.91 | 0.90 |
| San Joaquin | 0.92 | 0.90 |
| Mokelumne | 0.77 | 0.85 |
| Calaveras | 0.96 | 0.93 |
| Feather | 0.95 | 0.94 |
| Tuolumne | 0.94 | 0.93 |
| Sacramento | 0.97 | 0.97 |
| Trinity | 0.94 | 0.89 |
| Yuba | 0.91 | 0.95 |
| Clear Creek | 0.95 | 0.93 |

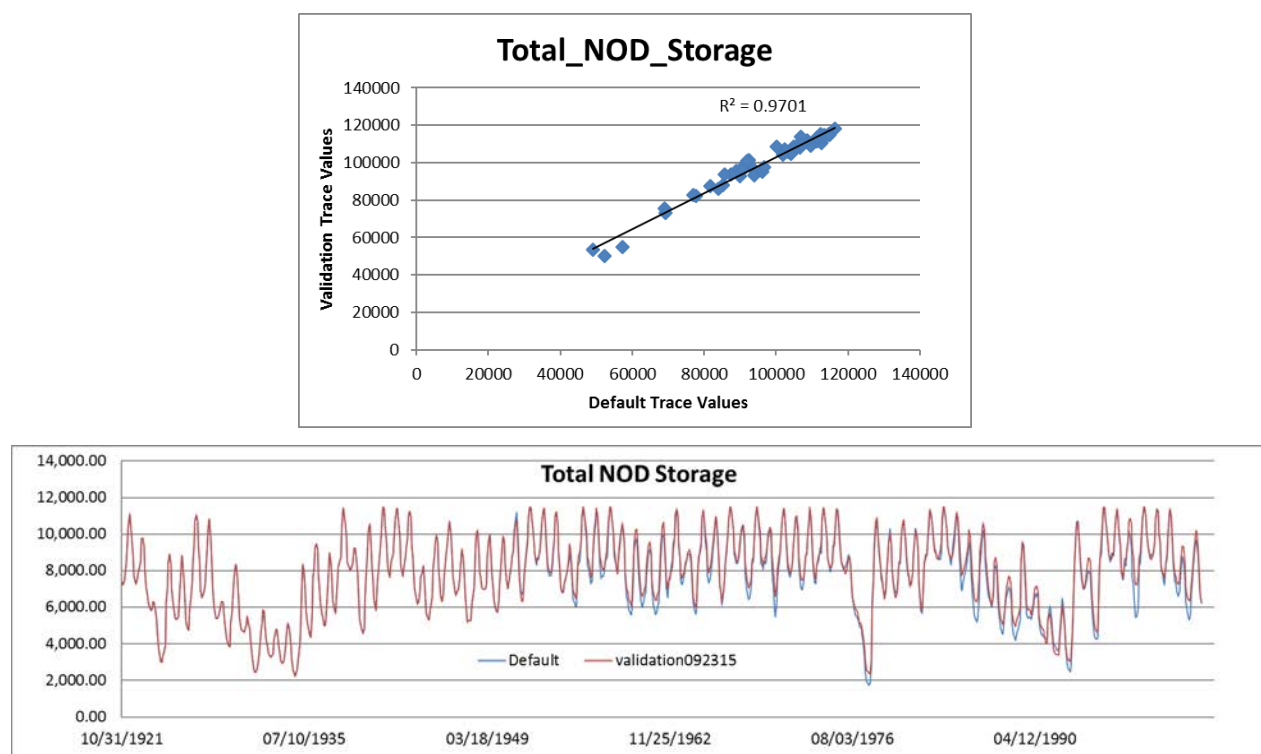
The second test of the hydrologic model concerned its ability to reproduce historical water-year type classifications based on the flow of rim-inflow rivers, using an algorithm designed to reproduce the water year classification system used by DWR. The combined hydrologic model and water-year-classification algorithm was shown to successfully match water-year type for every year of the historical record to the DWR method of water-year classification (http://cdec.water.ca.gov/cgi-progs/iodir_ss/wsihist).

System Model Performance

Figure 18 through Figure 20 show the sample output of a CalLite 3.0 validation run selected to demonstrate the ability of the model workflow (Figure 2) to reproduce historical CalLite 3.0 output for each of the decision-relevant metrics described in Table 1. Figure 18 presents the validation for Total North of Delta Storage, of which Oroville reservoir storage is a part. Figure 19 presents the validation for Delta outflow. Figure 20 presents the validation for SWP deliveries.

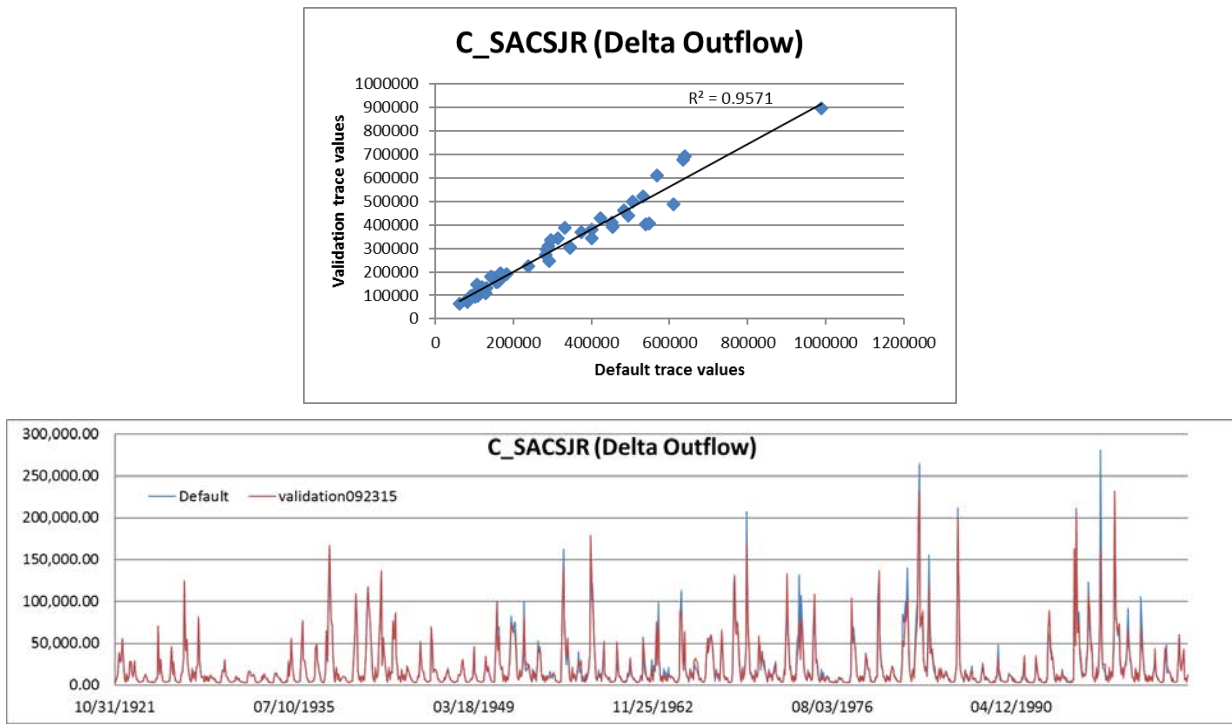
The validation is a perfect reproduction prior to 1950, as no reliable climate data were available for the development of climate traces before that time.

Figure 18 Validation of CalLite 3.0 Stress Test Modeling Workflow for Total North of Delta Storage



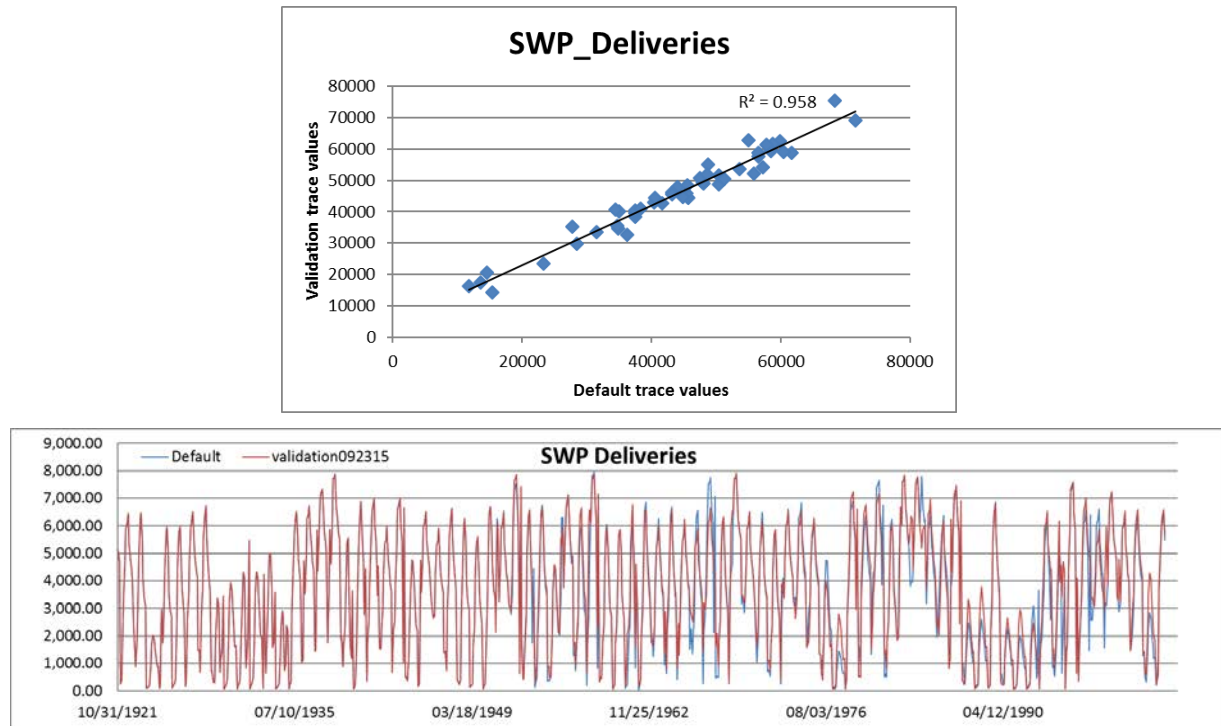
Note: Top: Scatterplot fit of annually averaged validation trace values to default trace values. Bottom: Default (blue) and validation (red) trace monthly Total North of Delta Storage showing perfect fit before 1950 and differences after 1950.

Figure 19 Validation of CalLite 3.0 Stress Test Modeling Workflow for Delta Outflow



Note: Top: Scatterplot fit of annually averaged validation trace values to default trace values. Bottom: Default (blue) and validation (red) trace monthly Delta Outflow showing perfect fit before 1950 and differences after 1950.

Figure 20 Validation of CalLite 3.0 Stress Test Modeling Workflow for SWP Annual Deliveries



Note: Top: Scatterplot fit of annually averaged validation trace values to default trace values. Bottom: Default (blue) and validation (red) trace monthly SWP deliveries showing perfect fit before 1950 and differences after 1950.

Risk Assessment Results

Exposure

DWR's operation of the SWP is exposed to climate-changed conditions throughout the state. In the watersheds from which water supplies originate, higher temperatures and changes in precipitation are expected to change the availability of water. In the Sacramento-San Joaquin Delta, water supplies interact with the Delta's complex hydrology, which is influenced by sea level, tides, and flows from several rivers. Throughout the SWP's service areas, demand for SWP water supplies will be affected by higher temperatures and changing precipitation.

Climate change exposure for these areas has been estimated using data from an ensemble of projections derived from the CMIP5 to develop probabilistic climate information. While the ensemble of models indicates a range of future outcomes in temperature and precipitation, conditional probabilities for temperature and precipitation change can be inferred by plotting the bivariate normal distribution of the projected changes of the models. Figure 1 and Table 8 present the conditional climate probability density for climate changes at 2050. By expressing the range of climate changes in the future as probabilistic possibilities, a deeper understanding of the range of potential exposures is possible. In Figure 1, deeper blue colors represent higher agreement among the GCMs about future conditions, and lighter blue colors represent future conditions that are predicted by fewer models but still considered potential future outcomes.

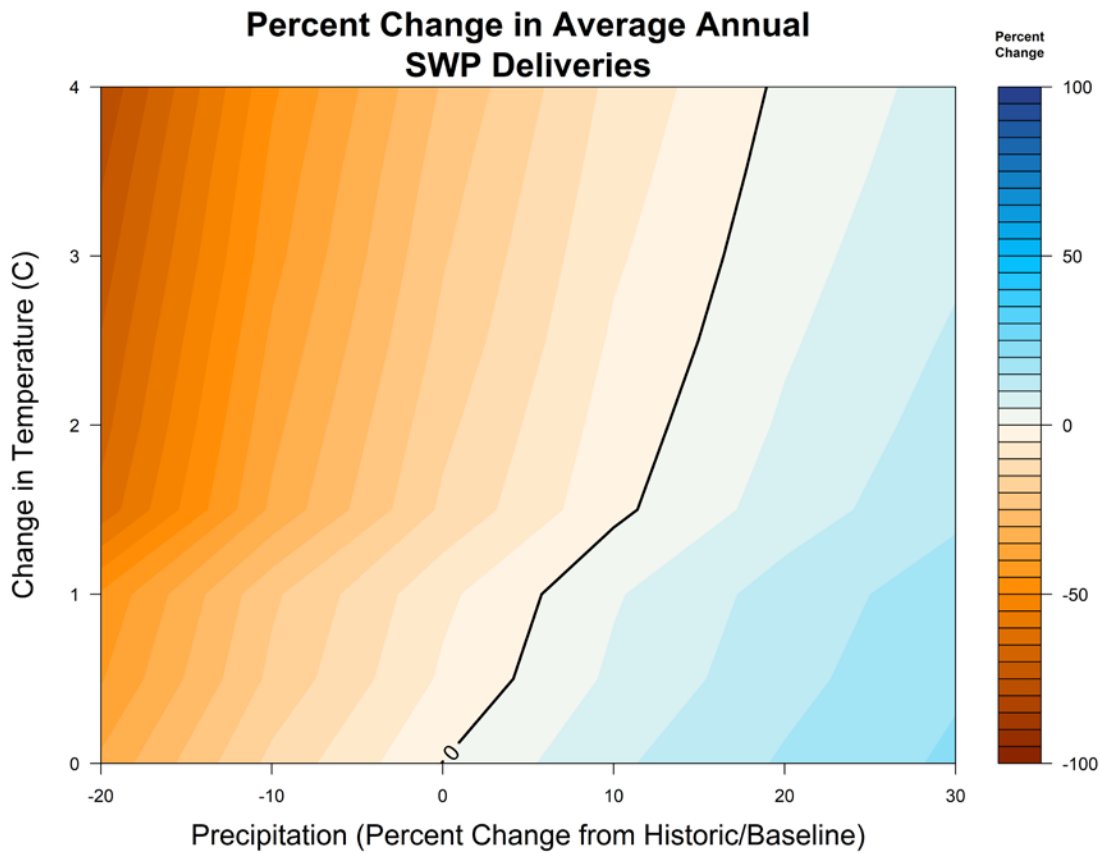
Sensitivity

The decision scaling approach described in the preceding section “Methodology” was used to explore system performance for each of the metrics listed in Table 1. The system performance response surfaces describe how the system performs over the range of temperature and precipitation changes. See Box 2, *Understanding System Response Surfaces*, for additional information on interpreting the information in these graphics.

The response surface describes the sensitivity of the SWP system to changes in climate. On the response surface, the black line represents performance at historical levels; warm colors represent performance worse than historical levels while cool colors represent performance better than historical levels. Changes in color represent sensitivity to a change in climate.

Box 2 Understanding System Response Surfaces

For each performance metric, the response surface shows the performance that would be expected for various combinations of change in precipitation, warming, and sea level. In the example below, annual SWP deliveries are shown. The value at 0 degrees warming and 0 change in precipitation essentially represents current conditions (i.e., the long-term average of annual SWP deliveries that would be expected if climate conditions remained stable at today's levels). This level of performance is referred to as the "current conditions estimate" and represents the simulated long-term average system performance over the 1,100-year hydrological sequence with no climate warming beyond what has already occurred, and no change in precipitation from historical levels, i.e., 0 percent change. A black line extends up and to the right from 0 degrees warming and 0 percent change in precipitation. This line represents system performance at the same level as the current conditions estimate. In other words, current performance levels can be maintained for the given metric at these combinations of warming and precipitation change. For example, current Average Annual SWP Deliveries could be maintained at 2°C of warming coupled with about 13 percent higher precipitation rates or 4°C warming and about 19 percent higher precipitation rates.



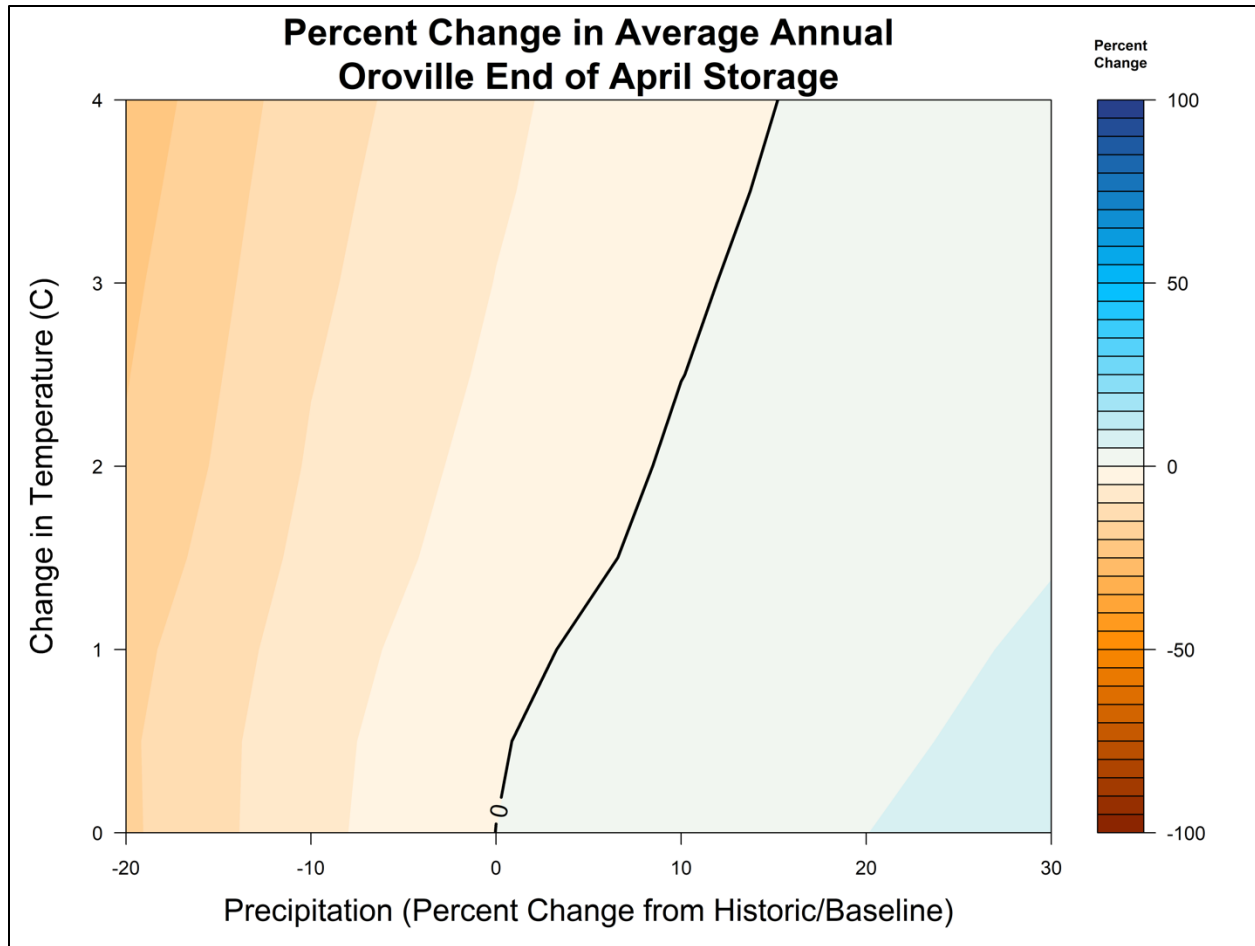
Each color band represents consistent system performance across a range of temperature and precipitation combinations. Bars that are more vertical indicate that the performance of the system is more sensitive to changes in average annual precipitation levels, while bars that are more horizontal indicate that the system performance is more sensitive to warming temperatures. Blue colors represent performance superior to current conditions and orange/red colors represent performance inferior to current conditions.

It is important to note that the response surface does not describe performance at any given time in the future. The response surface simply illustrates how the system performs, on average, over the 1,100-year hydrologic time sequence and across the range of precipitation and temperature. Also of importance is that the response surfaces presented in this report are for the current system infrastructure configuration, operations priorities, and regulations. The surfaces would change if any of these were to change in the future.

Performance Metric 1: Oroville End-of-April Storage

Historically simulated Oroville end-of-April storage levels are approximately 3.1 million acre-feet (maf). The response surface for Oroville end-of-April Storage (Figure 21) shows that this metric is moderately sensitive to changes in temperature, precipitation, and sea level. At a 2°C increase in temperature, a 10 percent increase in precipitation would be required to offset the storage losses resulting from the temperature increase. This metric is less sensitive to temperature increase than Oroville end-of-September storage (Figure 22) because it essentially measures accumulated runoff into the Oroville Reservoir during the winter rainy season. Higher temperatures are likely to result in less snowfall and faster melting rates of snow, resulting in more of the winter precipitation ending up in the reservoir and less being stored in higher watershed elevations as snow. As this additional water enters the reservoir it increases storage levels but leaves less water stored in the upper watershed to replenish the reservoir later in the season.

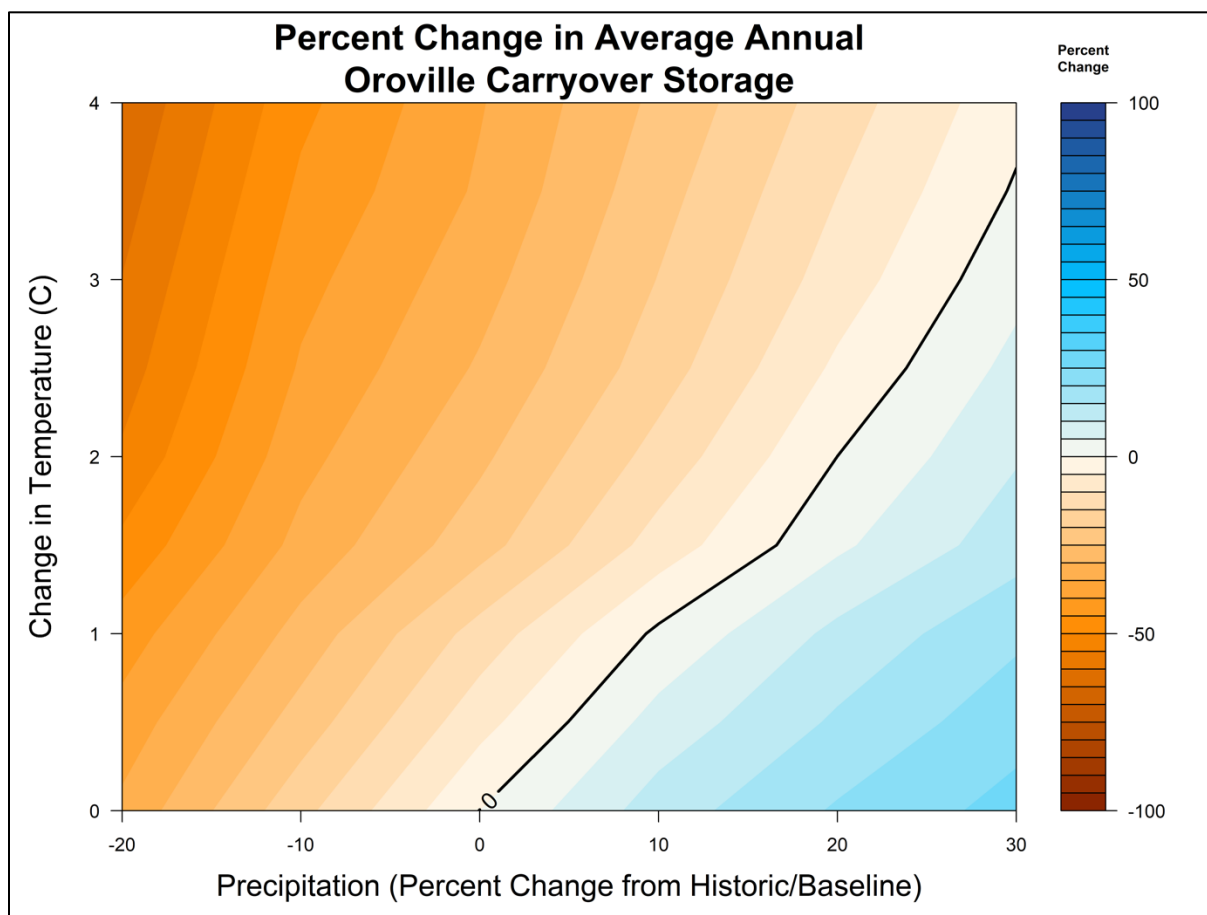
Figure 21 Oroville End-of-April Storage System Response Surface



Performance Metric 2: Oroville Carryover Storage

Historically simulated end-of-September or carryover storage levels are approximately 2 maf. The response surface for Oroville carryover storage (Figure 22) shows that this metric is highly sensitive to changes in temperature, sea level, and precipitation. At temperature increases above 2°C, a greater than 20 percent increase in average annual precipitation would be needed to offset the loss in storage from increased temperatures. As described above for the end-of-April storage metric, higher temperatures result in more winter precipitation falling as rain instead of snow and the remaining snowpack melting and running off earlier. This leaves less snow in the upper watershed for later season replenishment and culminates in much lower storage levels at the end of the summer. This system response is also related to the higher sea levels assumed at higher temperature change levels. Above 1.5°C, 45 cm of sea-level rise is assumed, thus requiring more water to be released from storage (especially during the summer months) to repel seawater intrusion and meet Delta outflow and salinity requirements.

Figure 22 Oroville Carryover Storage System Response Surface



Performance Metric 3: Seasonal Net Delta Outflow

Delta conditions dictate SWP operations in summer and fall when maintenance of ecosystem conditions and water quality for Delta agricultural diverters is a critical aspect of CVS operations. While there are a

number of regulatory standards that must be met (and those standards change from month to month), net Delta outflow (NDO) provides a reasonable aggregate metric for Delta conditions.

Upstream conditions that influence NDO change throughout the year. Winter NDO is driven primarily by rainfall events and the resulting high flows in rivers flowing into the Delta. Spring NDO is driven by snowmelt and is sensitive to temperature changes that result in changes to spring snowpack conditions. Summer and fall NDO are driven primarily by regulatory and water quality requirements. Because these regulatory requirements are given high priority in real-world water operations decisions, the water distribution algorithm used by CalLite 3.0 also assigns them a very high priority. CalLite 3.0 attempts to meet all regulatory requirements first, at the expense of other system water demands. The impacts of climate changes on summer and fall NDO conditions should be understood in this context as described in more detail below.

The climate response surfaces for each seasonal NDO condition indicate that temperature changes have little effect on winter (Figure 23a) and fall NDO (Figure 24b) and relatively weak influence on spring NDO (Figure 23b). Summer NDO exhibits unique behavior, indicating that NDO would be likely to increase under future climate conditions. In the summer NDO response surface (Figure 24a) and, to a lesser extent, in the fall NDO response surface (Figure 5-9d), discontinuities in the system performance at 0.5°C, 1.0°C, and 1.5°C (0.9 °F, 1.8 °F, and 2.7 °F) are evident. These are caused by the implementation of sea-level increases (Table 5-4). The significant discontinuity between 1.0°C and 1.5°C is the result of the shift from the 15-cm sea-level rise parameterization of CalLite 3.0 to the 45-cm sea-level rise parameterization. Sea-level rise increases the hydrostatic pressure of seawater pushing into the Delta, requiring more fresh water to be released (resulting in more NDO) to repel the sea water and maintain the required salinity conditions in the Delta. In the case of summer NDO (Figure 24a), the sea-level increase results in NDO levels that exceed historical levels.

Sea-level rise is not the only influence on summer and fall NDO. The requirements for minimum NDO (as defined by California State Water Resources Control Board Decision 1641) and minimum average monthly Delta outflow at Chipps Island (as defined by California State Water Resources Control Board Decision 1485) both scale as a function of various wetness indices in the watersheds that feed the Delta. Under wetter future climate conditions, these indices would become wetter, resulting in increases in required Delta outflows, while drier future conditions result in these indices becoming drier, resulting in relaxation or reduction of Delta outflow conditions. This effect is evident in the slight left to right tilt of the performance (color) bands on the response surface.

The changes in summer and fall NDO shown in Figure 24 are largely a reflection of how the regulatory outflow requirements change, and consequently, how the operation of the system changes to meet those regulatory requirements. The shift to greater summer NDO to repel sea-level rise and maintain currently required Delta salinity and water quality conditions means that additional water is being released to achieve this higher NDO. Water releases to meet these requirements come at the expense of other important system functions, such as carryover storage, cold-water storage for aquatic resources, water deliveries, and instream flows later in the year. At the time of this study, 45 cm (18 in.) of sea-level rise was the highest parameterization available. At a temperature increase of more than 2.5°C (4.5 °F), higher sea-levels would be expected but were not modeled here. As a result, it would be expected that higher levels of NDO would be required during the summer if sea-levels rise more than 45 cm (18 in.).

Figure 23 a-b Winter and Spring Net Delta Outflow System Response Surfaces

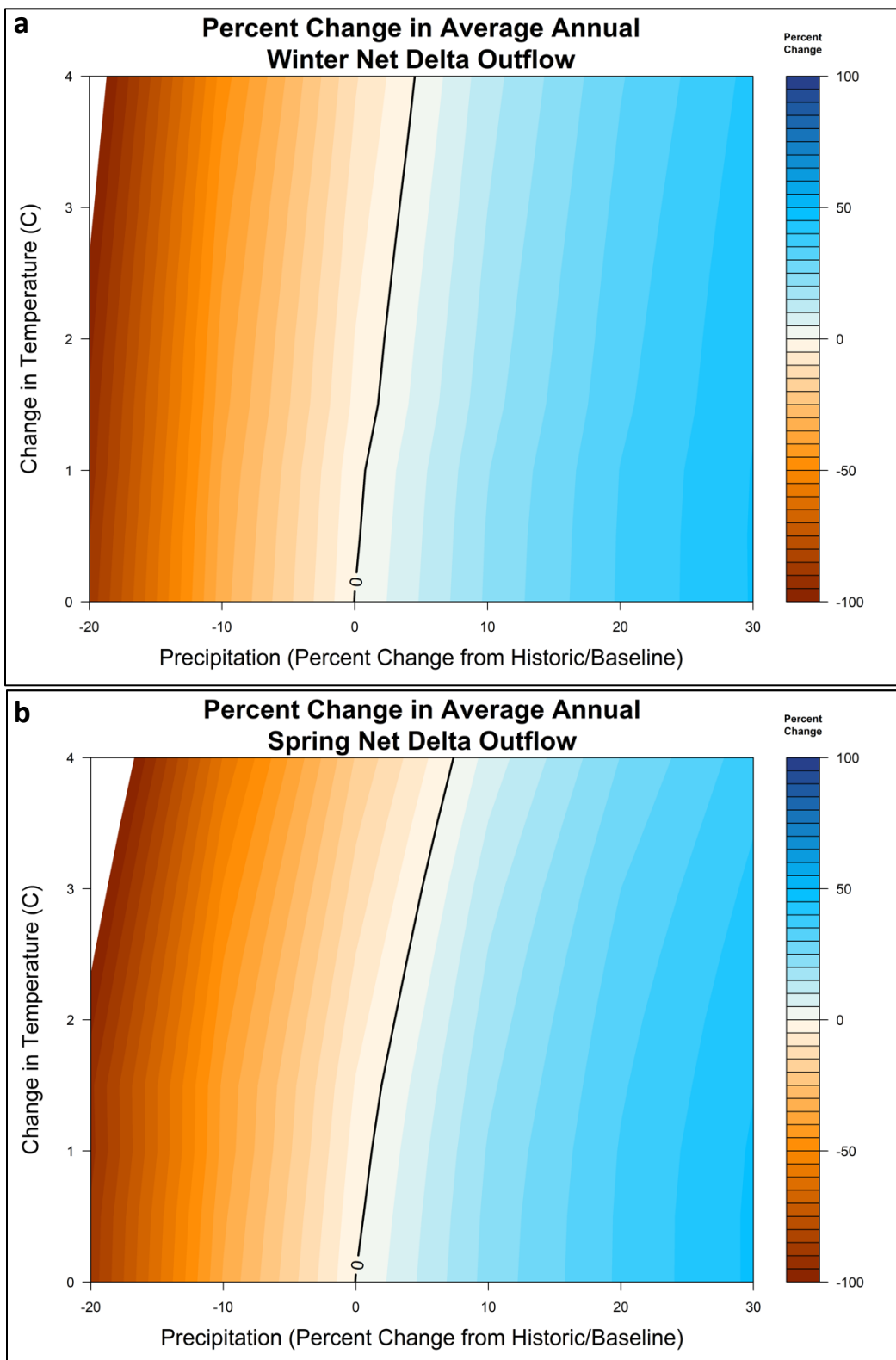
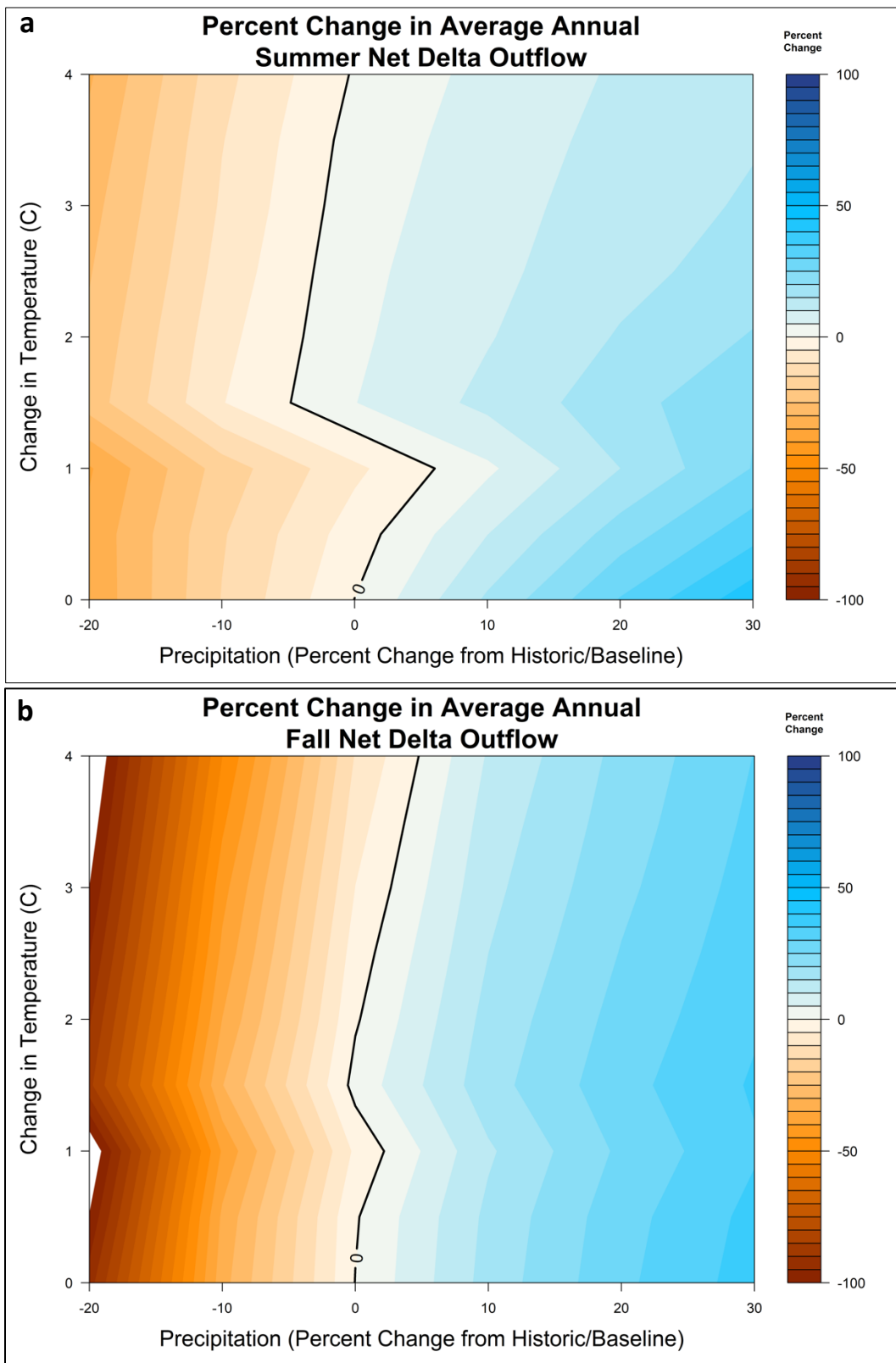


Figure 24 a-b Summer and Fall Net Delta Outflow System Response Surfaces

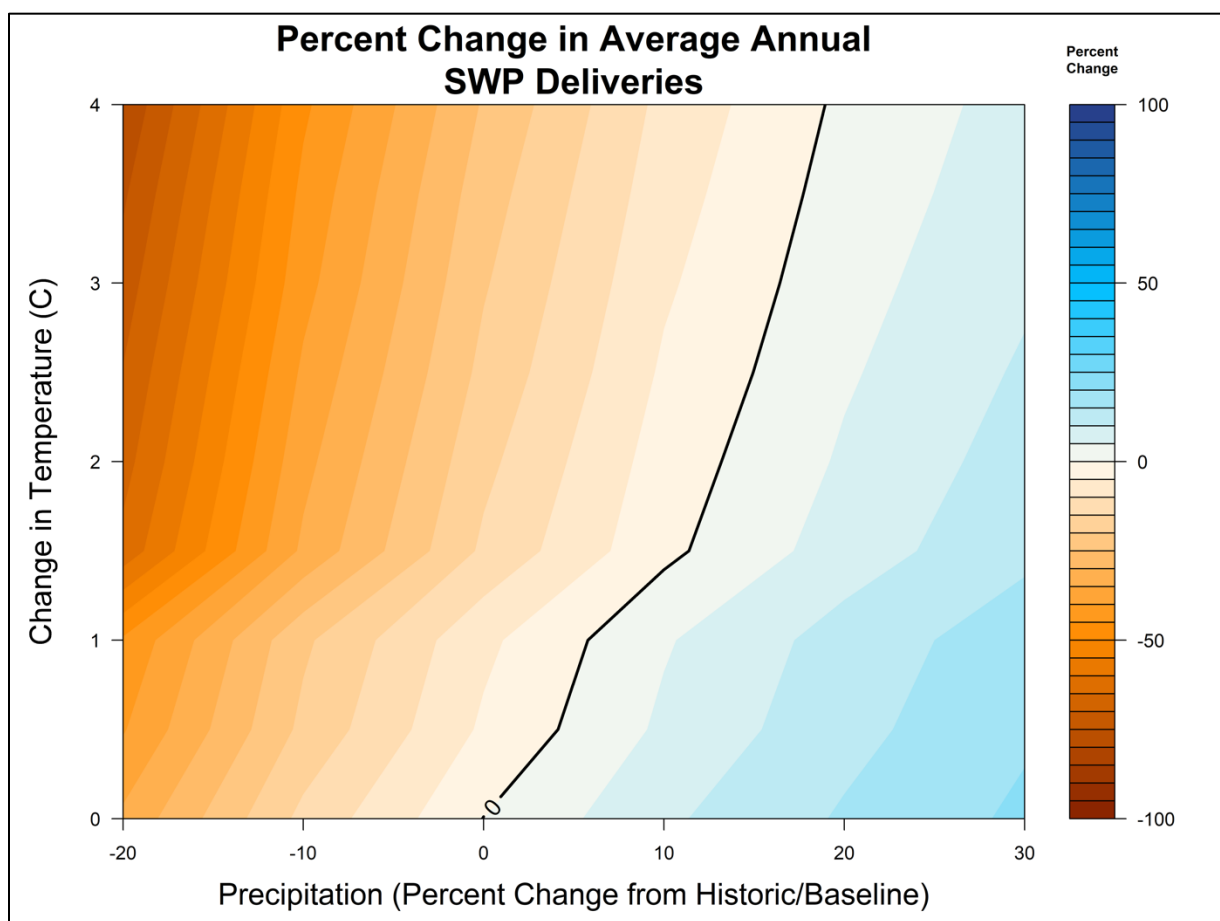


Performance Metric 4: Average Annual SWP Deliveries

The response surface for average annual SWP deliveries shows sensitivity to changes in temperature, precipitation, and sea-level rise (as would be expected). In the simulations, sea-level was implemented in three steps: (1) no sea-level rise at 0°C temperature change, (2) 15 cm of sea-level rise at 0.5 and 1.0°C temperature change, and (3) 45 cm of sea-level rise at 1.5°C and above temperature change (Table 5). These changes are evident in the response surface as inflection points where SWP deliveries decrease substantially (see Figure 25).

As noted above, each color band represents a change in system performance of 5 percent. For SWP deliveries, the performance bands become narrower to the left (less precipitation) and wider to the right (more precipitation), indicating that as precipitation decreases, SWP deliveries diminish faster than they improve as precipitation increases. Put another way, SWP deliveries are more sensitive to decreases in precipitation than increases in precipitation.

Figure 25 Average Annual SWP Deliveries System Response Surface

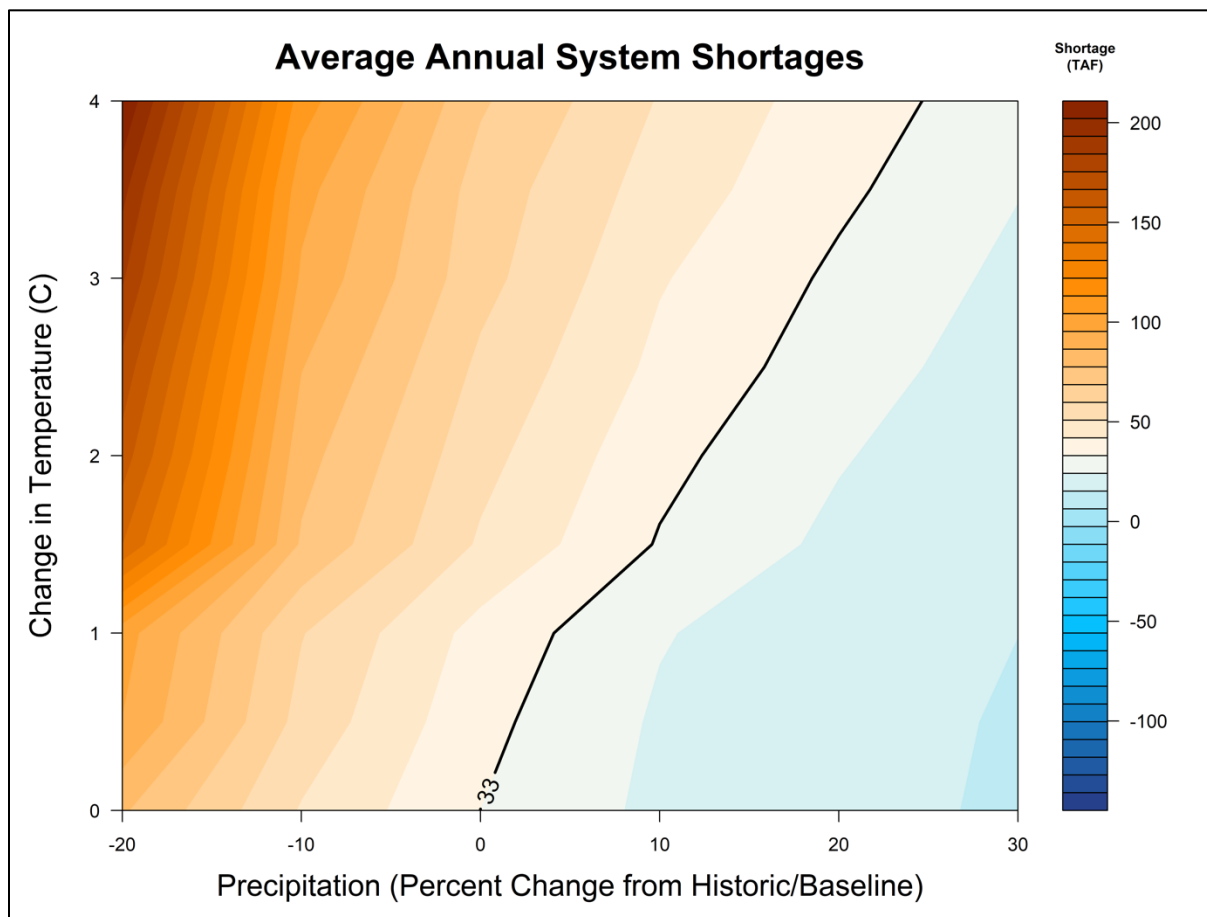


Performance Metric 5: Average Annual System Shortages

System shortages occur when there is not enough water in the system (precipitation, runoff, and storage) to meet all water demands, regulatory requirements, and health and safety required diversions. In the modeling simulations, these shortages typically result in the relaxation of Delta water quality or outflow requirements. The shortage amount is the amount of water that would be needed to meet all the requirements. Historically, these shortages have been rare but do occur periodically (i.e., 2014 and 2015).

The response surface for average annual system shortages (Figure 26) displays results in terms of absolute values of system shortages as opposed to percentage change since average annual system shortages cannot be smaller than zero and can become very large under extremely stressful conditions. Historically, average annual system shortages have been very low, averaging around 33,000 acre-feet per year, though some historical dry years have had much larger shortages and most years with normal or above normal precipitation have had no shortages at all. As the climate warms, system shortages increase by about 10,000 acre-feet per year per °C. Decreases in average annual precipitation will drive significant increases in system shortages.

Figure 26 Average Annual System Shortages System Response Surface



Risk

The sections above have described the SWP's exposure and sensitivity to climate change. By combining this information, probabilistic estimates of risk for each of the selected performance metrics can be developed. In this next step, the mid-century GCM-informed probability density function (pdf) of future Central Valley watershed climate conditions is superimposed on top of the response surface for each performance metric. This graphically illustrates the probabilistic range of future system performance.

The year 2050 conditional climate probability density is summarized in Table 8. Table 8 was developed by assigning a bivariate normal distribution to the shifts in mean annual temperature and precipitation of the ensemble of CMIP5 GCM output for the period of 2035–2065 relative to 1970–2000 (see Annex A: GCM Likelihood Function for the detailed steps for generating the GCM probability density function).

Table 9 Conditional Climate Probability Density of Each Climate Change Shift, 1970–2000 to 2035–2065

| Temp. (C) | 4 | 0.00000 | 0.00000 | 0.00001 | 0.00005 | 0.00007 | 0.00001 | 0.00000 |
|---|-----|---------|---------|---------|---------|---------|---------|---------|
| Increase Over Historical | 3.5 | 0.00000 | 0.00000 | 0.00017 | 0.00131 | 0.00145 | 0.00023 | 0.00001 |
| | 3 | 0.00000 | 0.00006 | 0.00244 | 0.01520 | 0.01370 | 0.00176 | 0.00003 |
| | 2.5 | 0.00000 | 0.00044 | 0.01540 | 0.07790 | 0.05670 | 0.00590 | 0.00009 |
| | 2 | 0.00001 | 0.00149 | 0.04260 | 0.17500 | 0.10300 | 0.00871 | 0.00011 |
| | 1.5 | 0.00001 | 0.00223 | 0.05180 | 0.17200 | 0.08230 | 0.00563 | 0.00006 |
| | 1 | 0.00001 | 0.00147 | 0.02760 | 0.07450 | 0.02880 | 0.00160 | 0.00001 |
| | 0.5 | 0.00000 | 0.00042 | 0.00646 | 0.01410 | 0.00443 | 0.00020 | 0.00000 |
| | 0 | 0.00000 | 0.00005 | 0.00066 | 0.00118 | 0.00030 | 0.00001 | 0.00000 |
| | | 0.7 | 0.8 | 0.9 | 1 | 1.1 | 1.2 | 1.3 |
| Precipitation (relative to historical) | | | | | | | | |

Figure 27 through Figure 32 show the mid-century GCM-informed pdf for each of the performance metrics at 2050 conditions. As the circles in the climate probability space get lighter in color, the conditional probability density of that outcome falls. The mid-century climate probability density is roughly centered at no change in precipitation and about 2°C change in temperature, with significant uncertainties in both precipitation and temperature extending from about -20 percent to +26 percent change in precipitation and from +0.5°C to +3.5°C change in temperature. Despite this wide range of uncertainty, it is clear from this series of graphics that for all metrics except seasonal NDO, the majority of the GCM-informed pdf at 2050 overlays decreased SWP performance. At 2050, only a small portion of the GCM-informed pdf for each performance metric goes past the black line and into the blue areas of system performance (where performance would actually be better than historical). This situation is especially acute for average Oroville September storage, where only a tiny sliver of GCM-informed pdf at 2050 reaches into the blue area. For the seasonal NDO, Figure 29 and Figure 30, the GCM-informed pdf at 2050 is generally evenly distributed across higher and lower levels of NDO.

Figure 27 Average Annual Oroville End-of-April Storage System Response Surface With CMIP5 GCM pdf at 2050

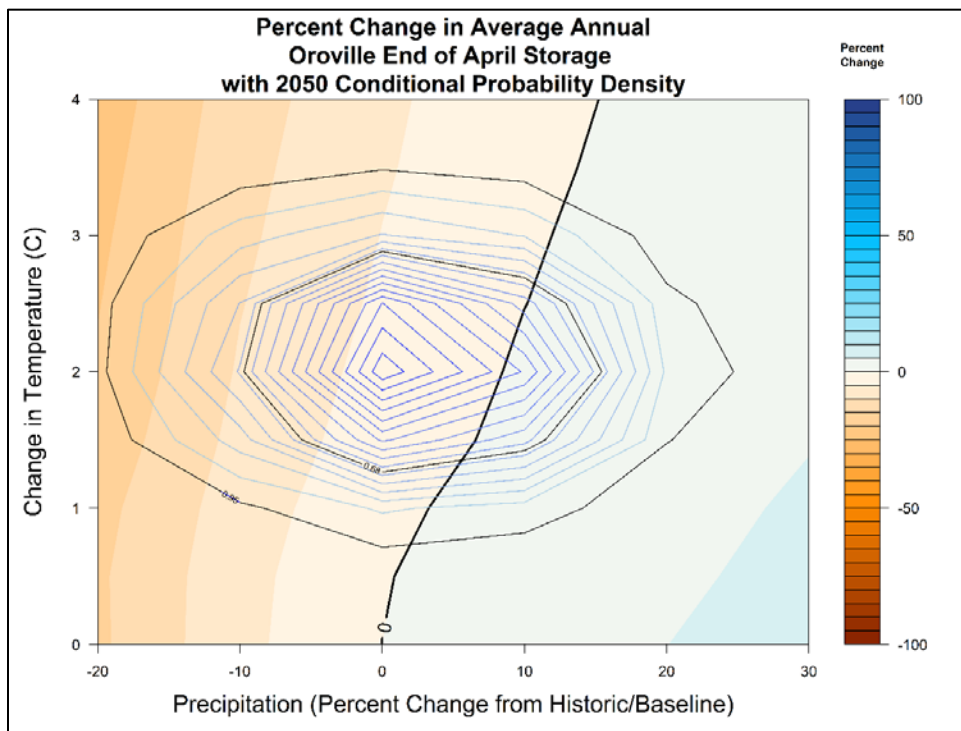


Figure 28 Average Annual Oroville Carryover Storage System Response Surface With CMIP5 GCM pdf at 2050

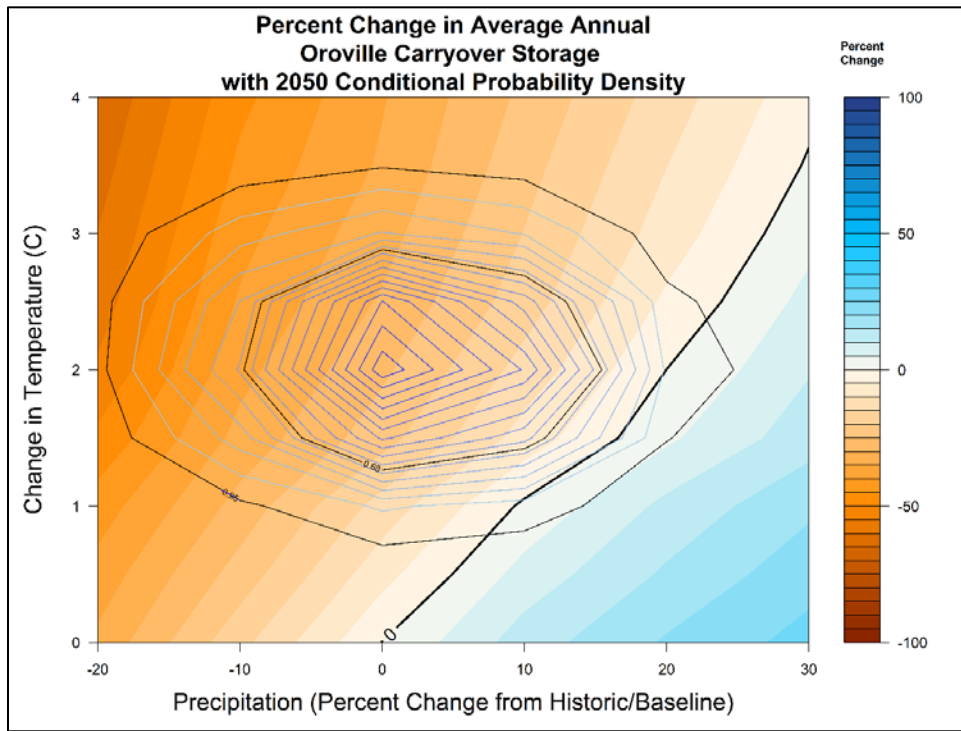


Figure 29 a-b Average Annual Winter and Spring Net Delta Outflow System Response Surface With CMIP5 GCM-Informed pdf at 2050

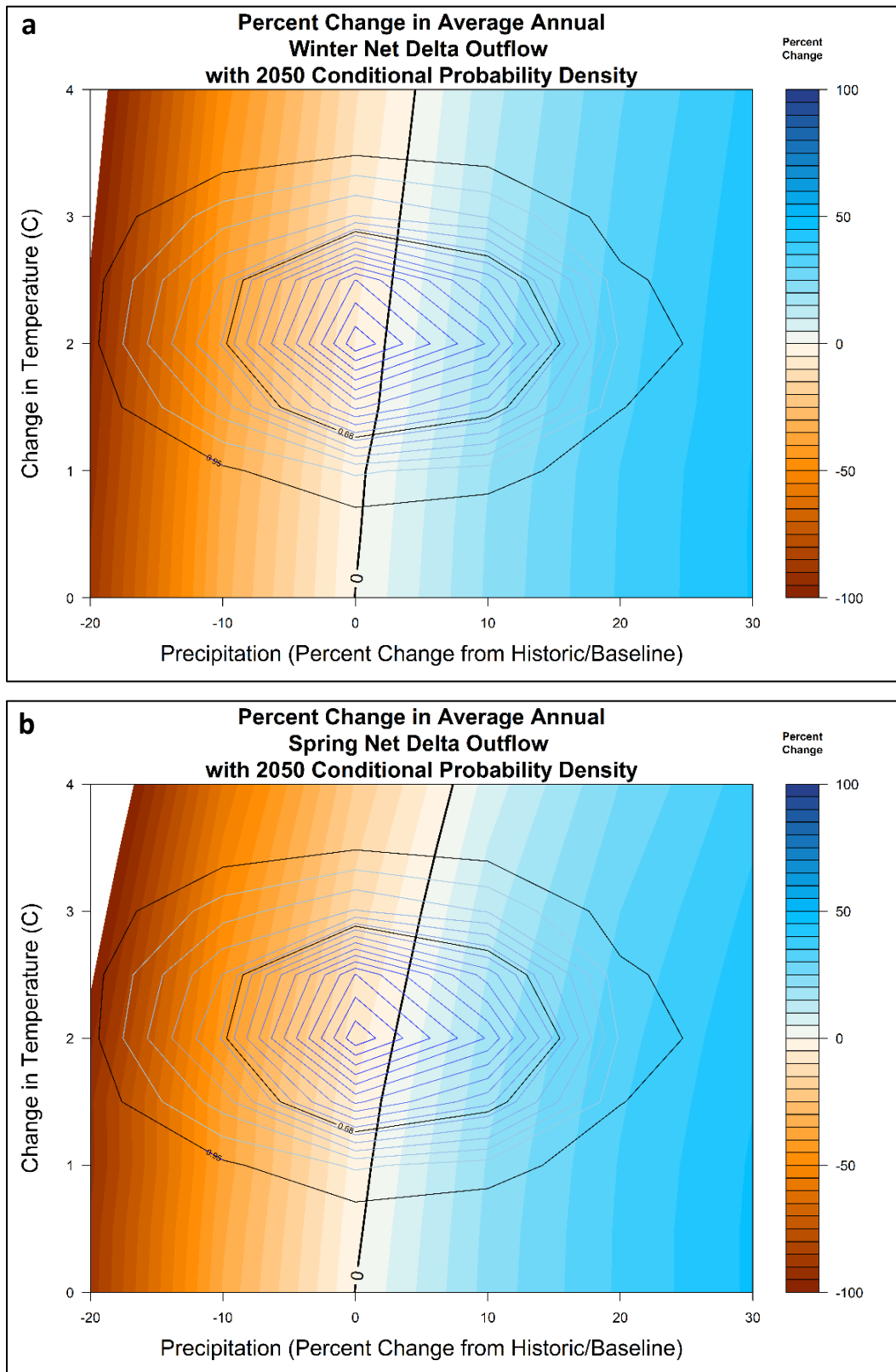


Figure 30 a-b Average Annual Summer and Fall Net Delta Outflow System Response Surfaces With CMIP5 GCM-Informed pdf at 2050

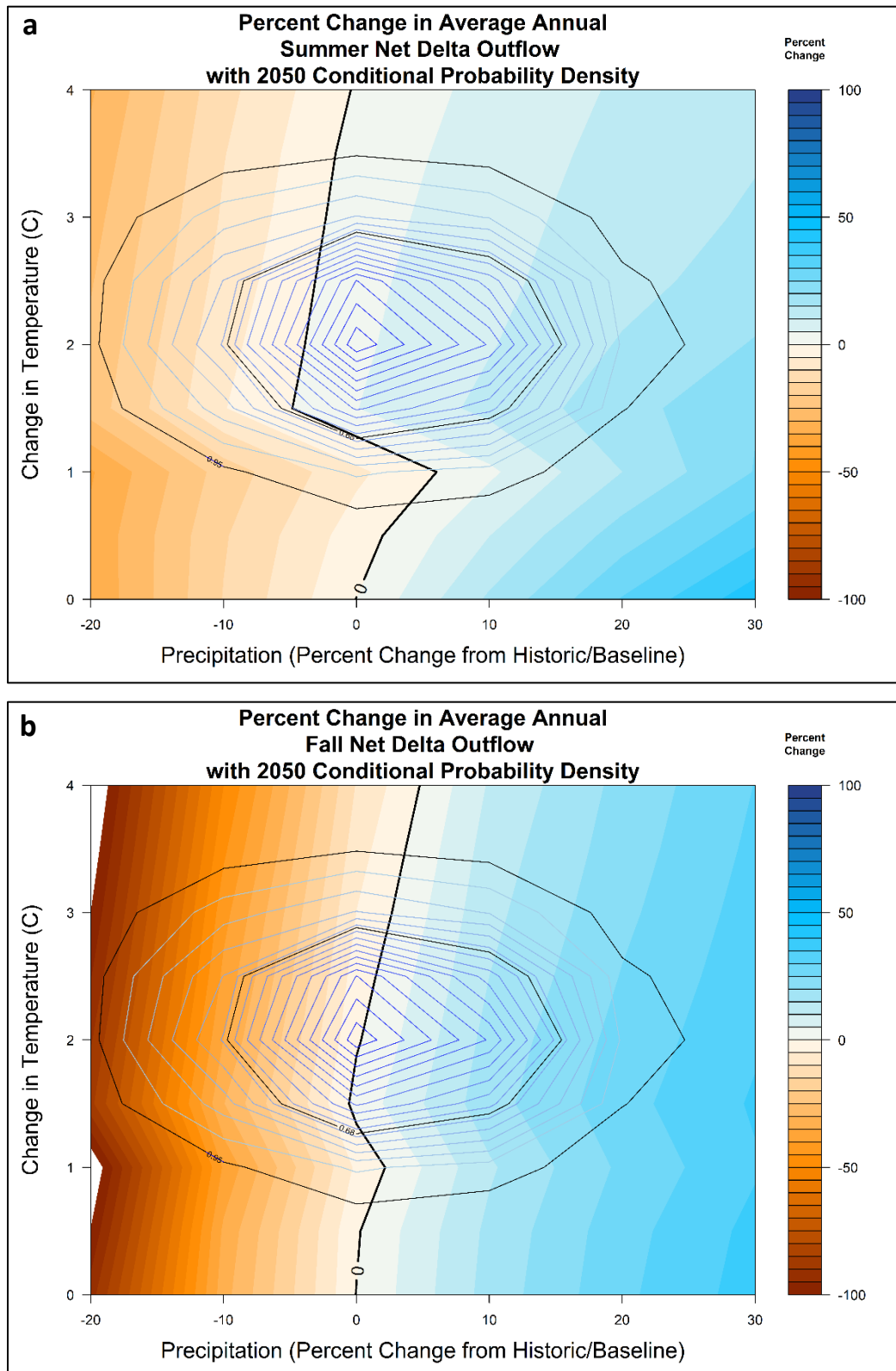


Figure 31 Average Annual SWP Deliveries Systems Response Surface With CMIP5 GCM-Informed pdf at 2050

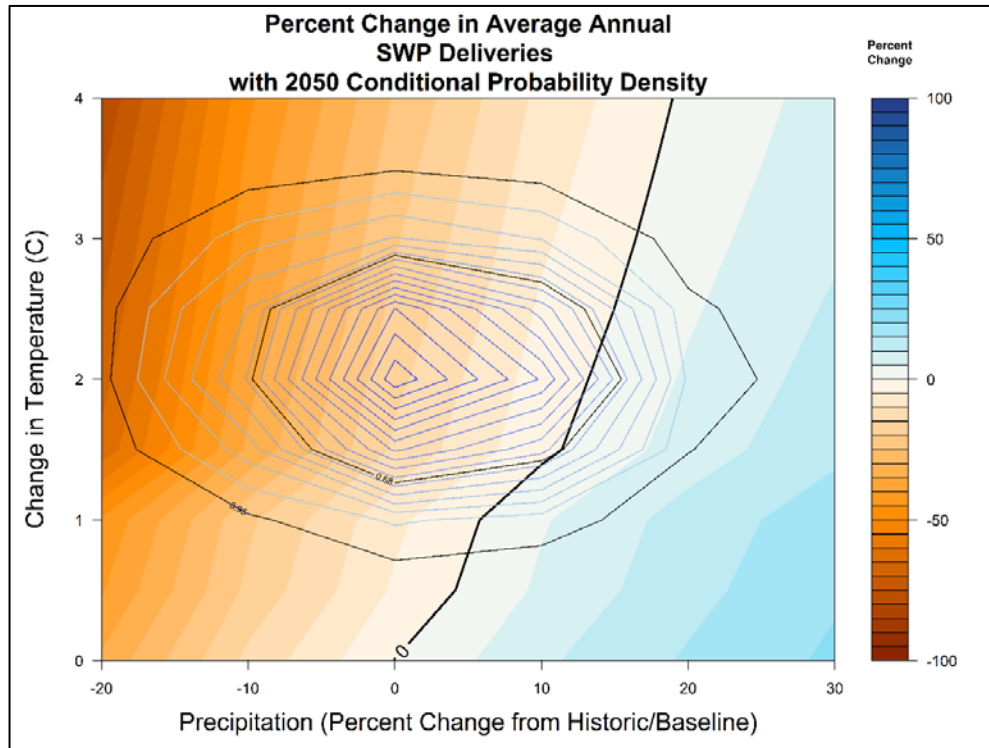


Figure 32 Average Annual System Shortage Response Surface With CMIP5 GCM-Informed pdf at 2050

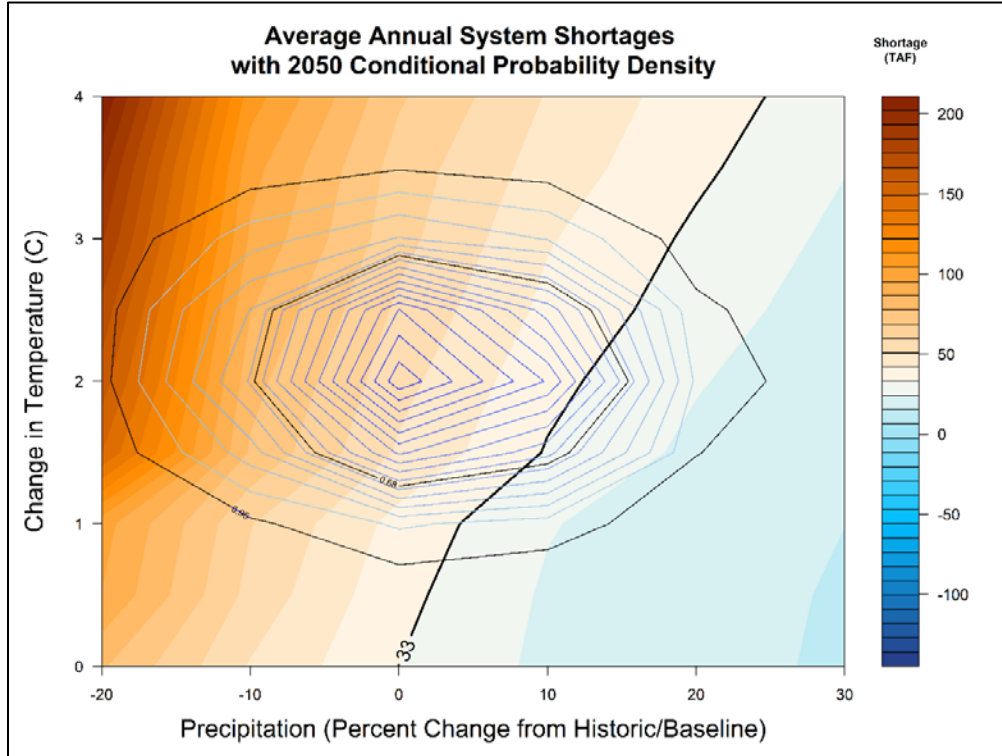


Table 10 Probability That Mid-Century Long-Term Average Performance Will Be Inferior to Current Average Performance

| Performance Metric | Probability that Mid-Century Performance Will be Inferior to Current Performance |
|----------------------------|--|
| Oroville April Storage | 76% |
| Oroville Carryover Storage | 95% |
| Winter Net Delta Outflow | 65% |
| Spring Net Delta Outflow | 65% |
| Summer Net Delta Outflow | 21% |
| Fall Net Delta Outflow | 56% |
| SWP Deliveries | 93% |
| System Shortages | 87% |

Long-term average system performance over a wide range of hydrologic conditions is summarized in Table 9 and depicted in Figures 33 through 38. While this is one important measure of changing risk, regulators, water managers, and SWP contractors are often focused on annual conditions and the risks associated with changing annual conditions, particularly conditions in the driest years. The analysis below provides information about the changing distribution of annual performance (i.e., how does system performance change across the entire distribution of hydrologic conditions from the wettest years to the driest years) for each of the performance metrics.

The cdf provides the probability that the system performance will be at or below any given value of system performance, while the pdf provides a measure of the relative likelihood of one level of performance over another or the probability that system performance will fall within a given range. The cdf and pdf take into account the yearly system performance data across all 54 different combinations of temperature and precipitation and weights them by the conditional GCM-informed probability density associated with the combination of temperature and precipitation change that produced the simulation. The cdf and pdf for each performance metric can be calculated at current conditions and at any future time period. Comparing the cdf and pdf for current conditions and mid-century conditions illustrates the shift in the distribution of annual performance.

For each performance metric, the 25th, 50th, and 75th percentile values of performance are calculated from the cdf and provided for both current conditions and 2050 conditions (notated as P25, P50, and P75 in the light blue table below cdf curves). The mode, or most likely level of system performance, is calculated from the pdf for both current conditions and 2050 conditions (light blue table below pdf curves). The 25th, 50th, and 75th percentile values help illustrate how system performance will change in dry years, median years, and wetter years, respectively, while the mode provides a measure of the expected value of system performance across the range of year types and climate uncertainty.

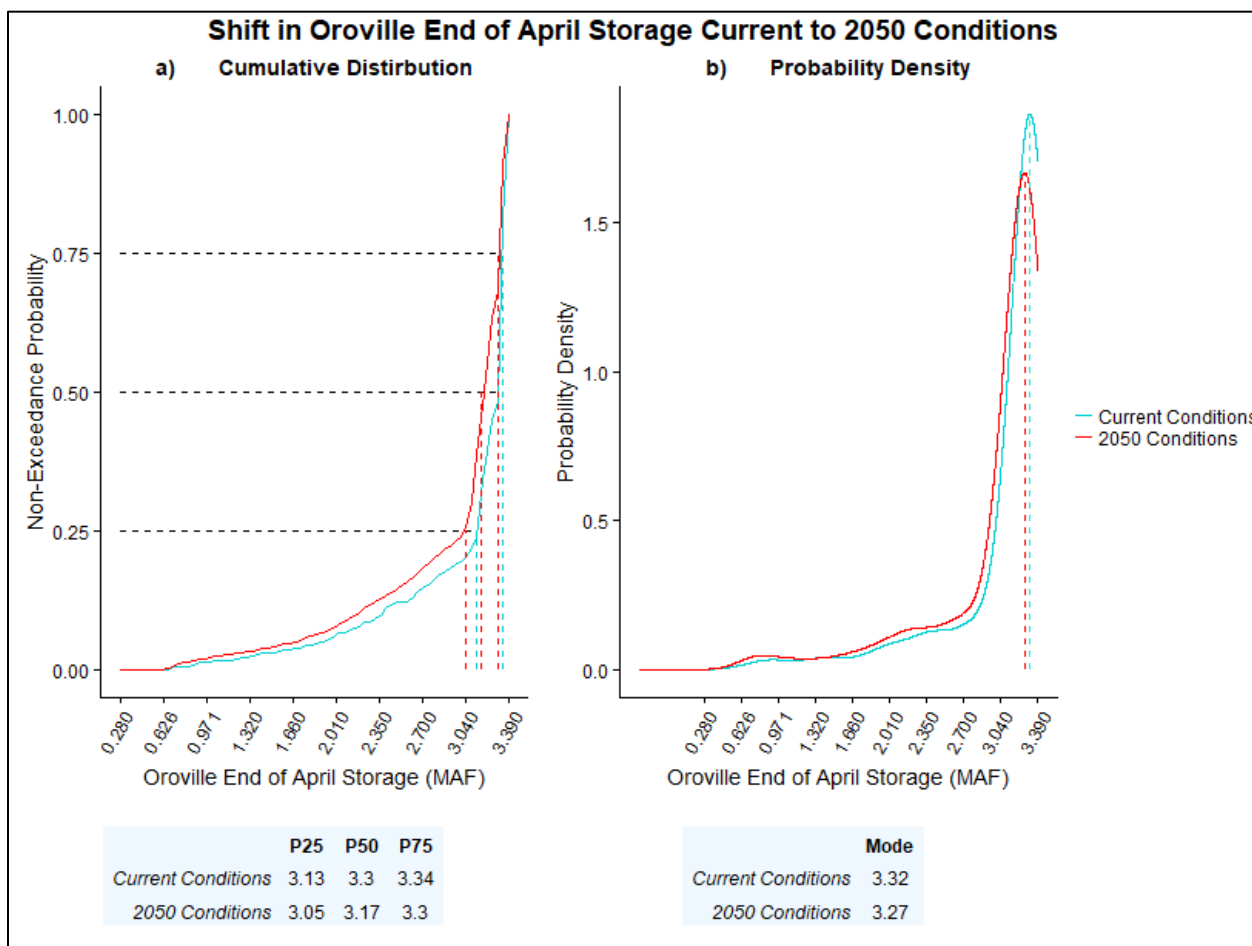
Vulnerability of Oroville April Storage

For Oroville end-of-April storage (Figure 33), the major shift in performance is during dry-to-median years. The 25th percentile performance falls by nearly 100,000 acre-feet and 50th percentile performance falls by 130,000 acre-feet. During wetter years (75th percentile and above), Oroville end-of-April storage is nearly identical at current and 2050 conditions. This is because Oroville is full in these years and any

additional inflow (resulting from earlier runoff of snowmelt) to the reservoir would not result in additional storage. Future conditions will almost certainly be warmer, resulting in an increasing amount of winter precipitation entering the reservoir by April and a decreasing amount remaining higher in the watershed until later in the spring and summer; however, it appears that climate change will still result in significant reductions to Oroville end-of-April storage. This is likely the result of lower carryover storage (September 30th storage) (i.e., starting out the winter with lower storage levels will result in lower end-of-winter storage conditions in all but the wettest years). Some of the reduction in April storage may also result from high temperatures leading to higher evapotranspiration rates, sublimation rates, and reduced soil moisture all contributing to reduced runoff and inflow to the reservoir.

The pdf shows that the most likely future outcome for end-of-April storage in Oroville is slightly reduced from current conditions to 2050 conditions with a loss of about 50,000 acre-feet (1.5 percent).

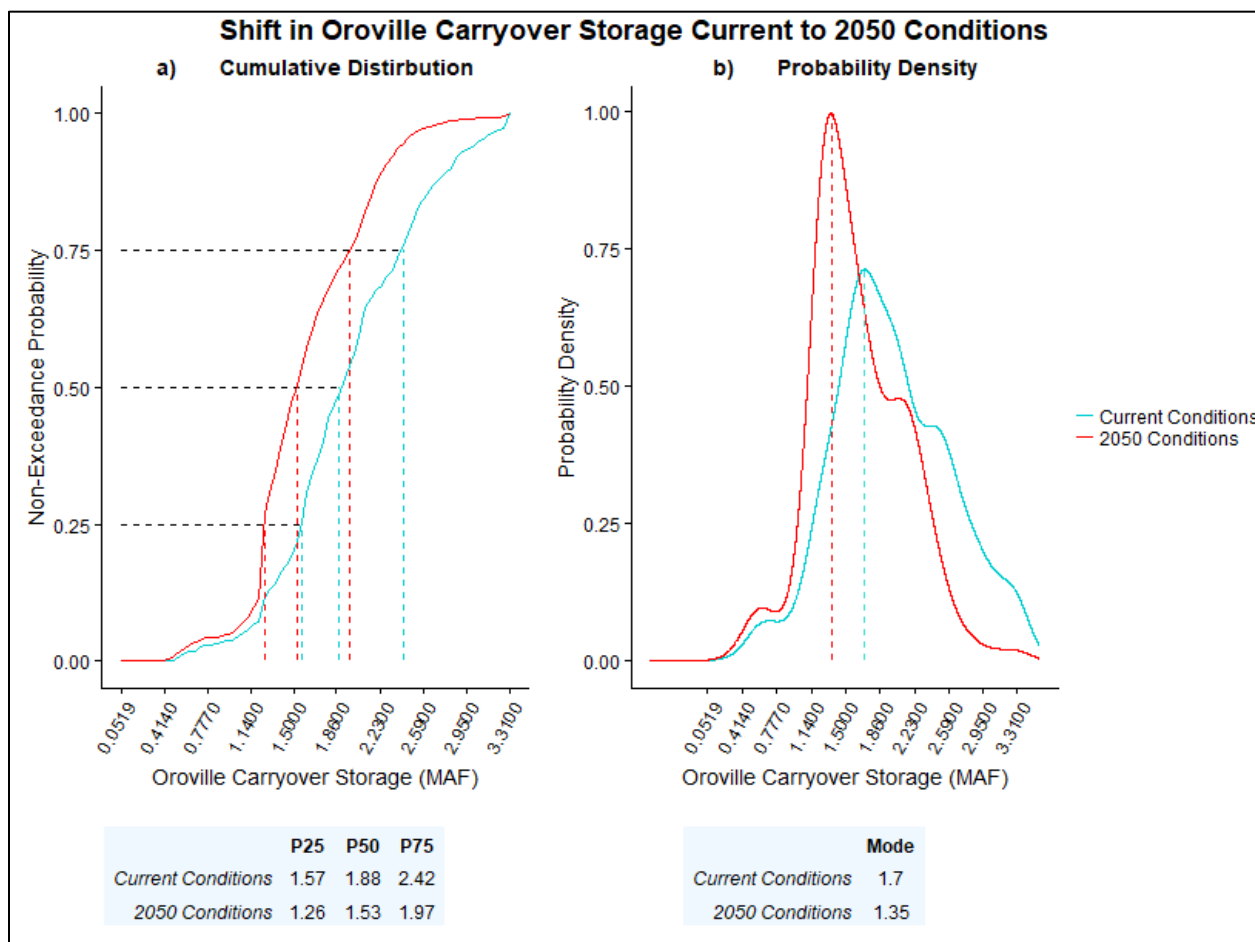
Figure 33 a) Cumulative Distribution and b) Probability Density for End of April Storage in Oroville



Vulnerability of Oroville Carryover Storage

For Oroville carryover storage (Figure 34), the effect of climate change is exactly opposite from the effect on Oroville end-of-April storage. The impacts are felt more strongly toward the wetter end of the spectrum with 50th and 75th percentile 2050 performance around 350,000 and 450,000 acre-feet less than current conditions, respectively. To put it another way, even during the very wettest years (above 75th percentile) under 2050 conditions, Oroville is only slightly fuller (1.97 maf) than current levels during median years (1.88 maf). At the drier (25th percentile) end of the spectrum, where carryover storage at 2050 performance is 310,000 acre-feet less than current conditions, performance is driven by a management target simulated in the model that Oroville storage remain above at least 1 maf. Thus, when storage in Oroville nears this level, water allocations for other purposes are reduced to the extent possible to maintain this minimum target. At 2050 conditions, nearly 25 percent of years approach this minimum storage target versus approximately 12 percent of years under current conditions.

Figure 34 a-b Cumulative Distribution and Probability Density for September 1st Storage in Oroville



The pdf shows very significant differences in the most likely levels of Oroville carryover storage, with the most likely future outcome falling from a current value of 1.7 maf to a 2050 storage level of 1.35 maf (a loss of 350,000 acre-feet). Despite the future climate uncertainty, the likelihood of ending September at much lower levels of storage in the future is actually higher than the likelihood under current conditions. Put another way, there is more certainty that carryover storage levels in Oroville will be around 1.39 maf by mid-century than there is certainty today that carryover storage levels in Oroville will be around 1.73 maf.

Vulnerability of Seasonal Net Delta Outflow

The annual cdf and pdf of seasonal net Delta outflow (Figure 35 and Figure 36) give a more nuanced picture than the response surfaces (Figure 29 and Figure 30) of how Delta outflows are likely to change because of climate change. The cdf and pdf show that changes in NDO are likely to be relatively small on an annual level. Slight shifts are seen in all seasons, with winter, spring, and fall NDO all increasing slightly above the 75th percentile, and summer NDO increasing slightly at all levels below the 80th percentile then decreasing above the 80th percentile. Increasing summer NDO, as noted above, is likely the result of increased outflow necessary to repel higher sea-levels and associated salinity intrusion into the Delta. The relatively small shifts in summer NDO indicated that DWR and Reclamation will continue to be able to meet Delta regulatory requirements, but there will be fewer years in which summer NDO exceeds required conditions.

Figure 35 Winter and Spring Net Delta Outflow a) Cumulative Distribution and b) Probability Density

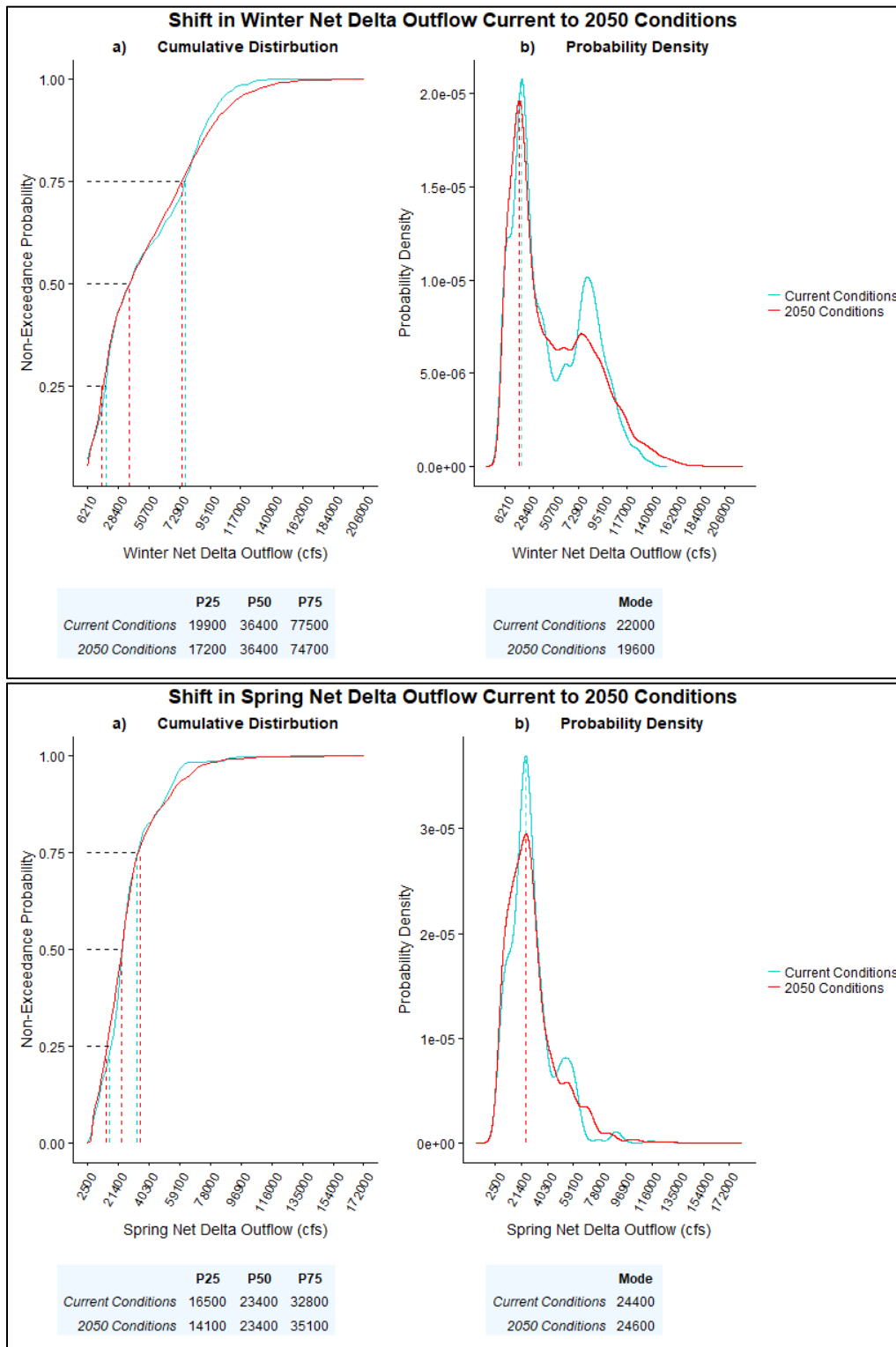
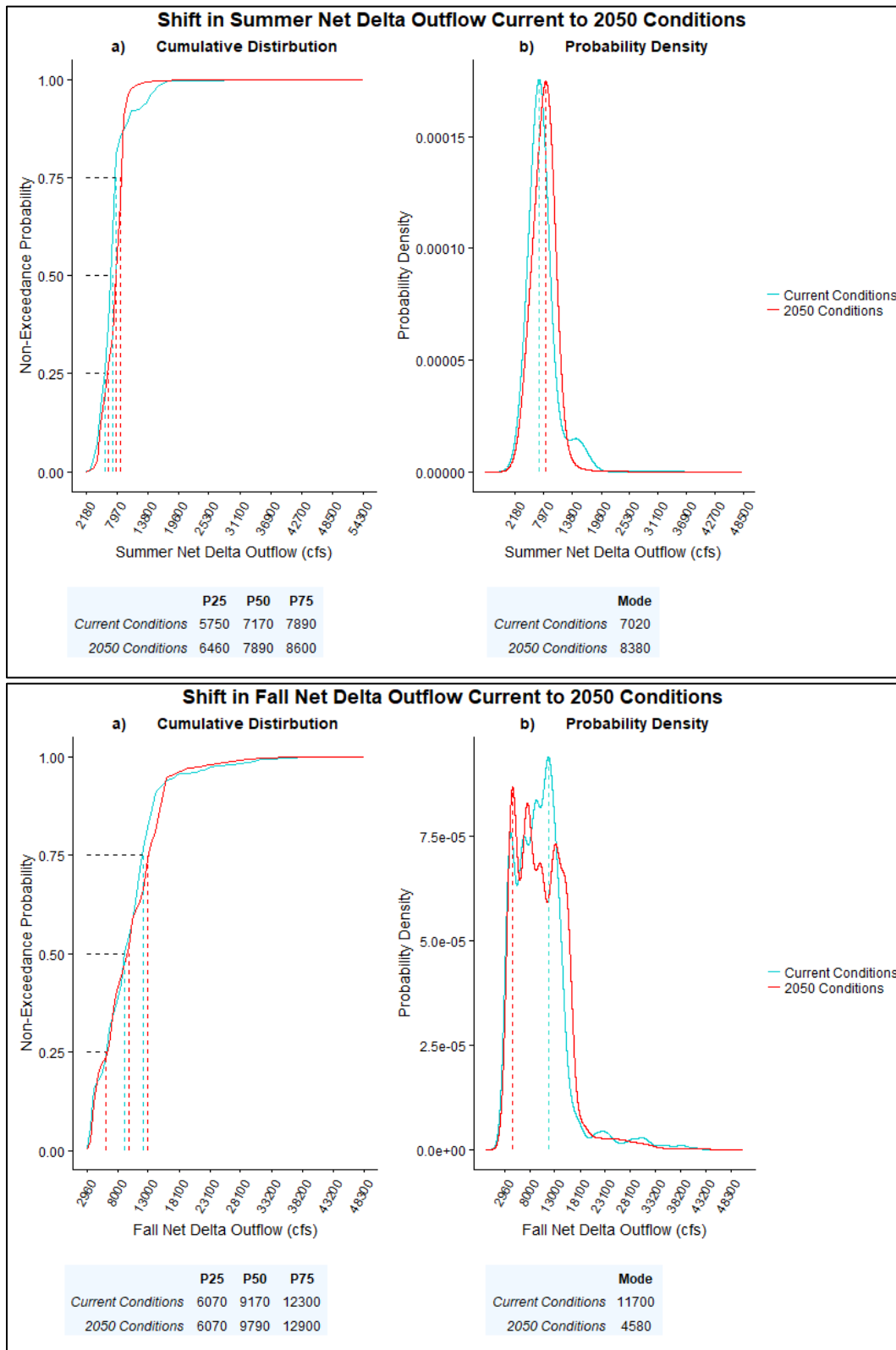


Figure 36 a-b Summer and Fall Net Delta Outflow a) Cumulative Distribution and b) Probability Density



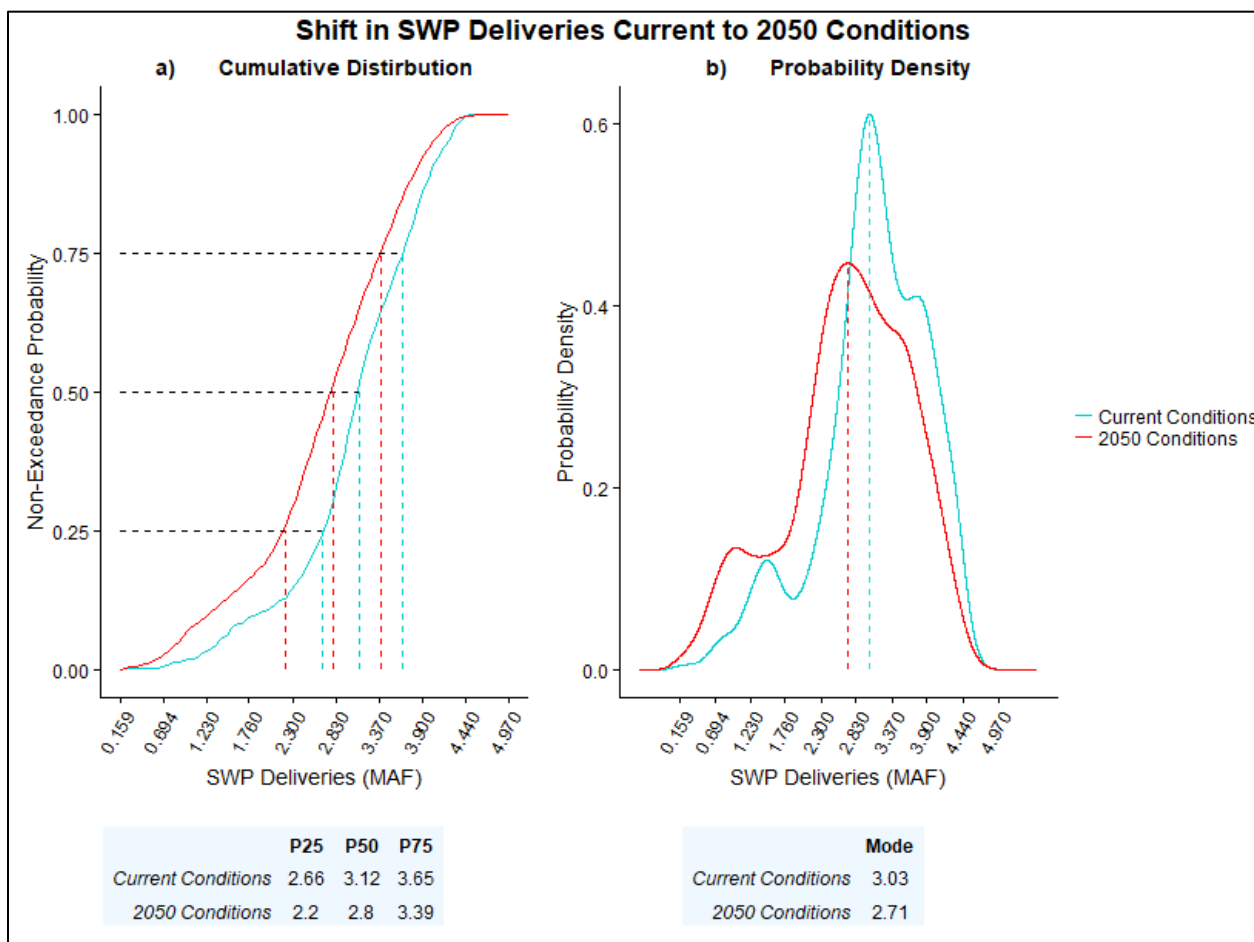
Vulnerability of SWP Deliveries

SWP deliveries (Figure 37) show a significant loss in performance across the entire range of non-exceedance probabilities, with the most acute loss of performance coming at the drier end of the range. Twenty-fifth percentile deliveries fall by over 450,000 acre-feet between current conditions and 2050 conditions — a 17 percent reduction. Median performance falls by over 300,000 acre-feet (10 percent) and 75th percentile performance falls by 260,000 acre-feet (7 percent).

This is an important result, indicating that not only will SWP deliveries be less reliable in the future, but the largest reductions will occur in the driest years, placing additional stress on SWP water contractors.

The pdf shows that the most likely level of SWP deliveries in 2050 is about 300,000 acre-feet less than current conditions and is quite a bit less certain, with deliveries that are less than current levels being more likely and deliveries that are higher than current levels being less likely.

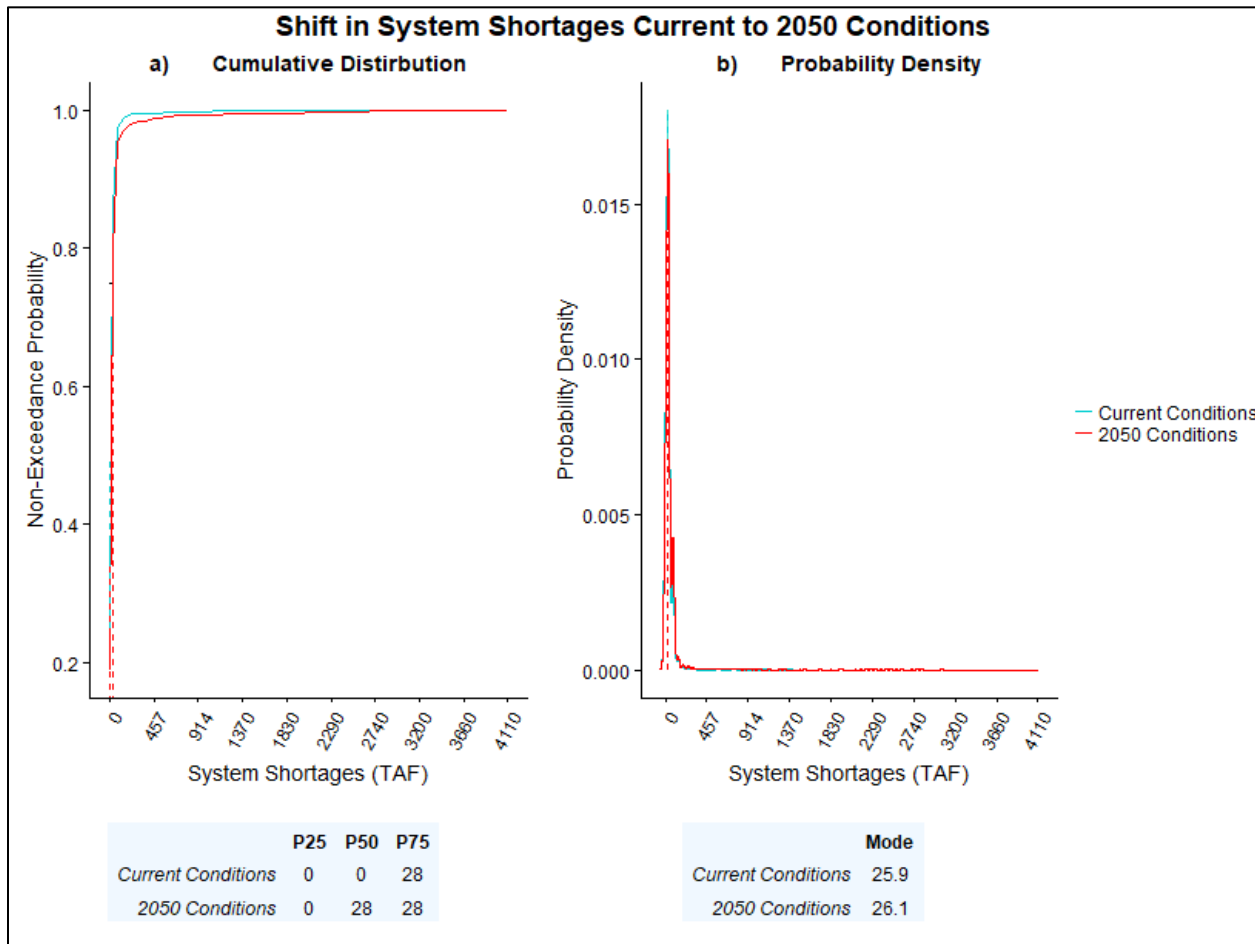
Figure 37 a-b Cumulative Distribution and Probability Density for Annual SWP Deliveries



Vulnerability of System Shortages

The cdf and pdf of system shortages (Figure 38) also provide a more nuanced picture of the likelihood of system shortages in the future than did the response surface of system shortages (Figure 32). The cdf and pdf illustrate that system shortages are rare under current conditions and will continue to be so under 2050 conditions. A small increase in magnitude and frequency of system shortages is likely to occur by 2050, but shortages of greater than a 1 maf would still be expected to occur in less than 1 percent of years.

Figure 38 a-b Cumulative Distribution and Probability Density for Annual System Shortages



Vulnerability

The analysis above suggests that there is a high likelihood that SWP storage and deliveries will diminish significantly in the future as the climate warms. Reductions in Oroville carryover storage mean that California will be vulnerable to future droughts, and these droughts will enter each winter with a smaller cushion if winter rains do not materialize. Lower storage levels in the future will also likely reduce the amount of hydroelectric generation from the Hyatt-Thermalito hydroelectric complex and will reduce recreational opportunities on Lake Oroville.

There is little evidence to suggest that climate change will impede DWR's ability to meet today's regulatory standards at mid-century as evidenced by the performance results for summer and fall NDO and system shortage. Overall, for the metrics analyzed in this vulnerability assessment, the SWP appears

to be relatively robust in its ability to continue to meet today's regulatory requirements at mid-century with only minimal loss of reliability. The same cannot be said about SWP deliveries. Since SWP deliveries are made only after regulatory standards are met, SWP deliveries show considerable vulnerability to changing climate. Without significant adaptation, SWP delivery reliability is likely to diminish as the climate warms.

Adaptive Capacity

It is still unclear to what extent SWP facilities and operations can be adapted to ameliorate these losses in performance. Several structural improvements, such as improved Delta conveyance; non-structural improvements, such as upper meadow restoration in the UFRW; and operational improvements, such as forecast-based operations of reservoirs, have been suggested. A full analysis of the efficacy of these types of adaptation strategies has yet to be completed; however, initial assessments of some strategies appear promising. Suggested adaptation strategies, such as those evaluated in California Water Plan 2013 and the Reclamation Sacramento-San Joaquin Basin Study, range in cost from a few million dollars to billions of dollars, with a range in social acceptability from "highly acceptable with nearly no social resistance" to "highly contentious." These issues will be evaluated further in DWR's Climate Action Plan Phase III: Adaptation Plan.

Other Considerations and Next Steps

The analysis shown here suggests that vulnerabilities to the SWP from persistent long-term changes in climate will be significant. It is very likely that the performance of the SWP will diminish over the coming decades if nothing is done to adapt to climate change; however, this new way of evaluating the system and assessing vulnerabilities provides opportunities to improve planning for climate change. Decision scaling allows planners to quantify the risks and costs associated with both the status quo and those of various adaptation strategies. Planners can then use this information to make informed decisions about which adaptation strategies will be most likely to improve conditions for various performance metrics. Unfortunately, the uncertainty associated with future climate conditions is here to stay and will likely not be substantially reduced in the near future. Therefore, our planning objectives need to acknowledge and accommodate this uncertainty. It is not feasible to plan for every possible climate outcome; however, with these quantitative assessments of future risk, quantitative adaptation objectives that address this uncertainty can be established.

An example quantitative climate adaptation objective might be: *For mid-century conditions, decision scaling analysis indicates that there is a 22 percent probability that long-term average annual SWP deliveries will fall below 2 maf. Implement adaptation strategies that reduce the probability of this condition to no more than 5 percent.*

Objectives like this acknowledge that we cannot plan for all "tail end" probabilities and there will always be a residual risk. This objective also acknowledges that climate adaptation is a moving target. Climate change will not stop at mid-century; indeed, the impacts are expected to become increasingly more severe toward the end of the century. Thus, adaptation objectives and the strategies we implement to achieve those objectives will need to be continually rolled out in the future to keep up with impacts.

Recommendations for Future Applications of Decision Scaling

The analysis suggests that SWP performance will very likely deteriorate over the coming decades if no action is taken to adapt to climate change; however, there are opportunities for improved climate change planning. Applications of decision scaling (1-9 identified below) within three major categories are recommended for future study to support adaptation planning.

Resource Management Strategies

Among 37 resource management strategies (RMS) identified in the California Water Plan Update 2013 (Water Plan), there are several which address vulnerabilities described in this report, are technically feasible, and for which DWR has the capacity as well as the authority to implement (see Annex C: Resource Management Strategy Screening). As a next step, DWR's Climate Change Program will use the decision scaling platform built for this study to conduct a systematic evaluation of a sample of proposed climate change adaptation strategies drawn from the 37 RMS including, but not limited to:

- (1) The effect of monthly reservoir inflow forecasting ability on system operation (Annex D: Adaptation Strategies — Seasonal Forecasting).
- (2) Weather modification or “cloud-seeding” (Annex E: Adaptation Strategies – Enhanced Precipitation).
- (3) Incorporation of improved multi-objective upper watershed management (Annex F: Adaptation Strategies — Upper Watershed Management)

Supplemental Analysis

The decision scaling platform built for this study establishes a probabilistic framework and set of tools that allow evaluation of a much larger range of historical and potential future changes in inter-annual variability and drought length and severity (4). The platform, through its use of the system operations model CalLite 3.0, also reduces concerns related to accuracy of modelling regulations and institutional constraints thus enabling an exploration of the sensitivity of water indexing methods to climate change and potential ways of adapting water year typing methods to support water management decisions (5) (see Annex G: Water Year Typing). Although considered to some extent in this report, further investigation into the presence and causes of trends in seasonal and elevation-dependent warming would help prioritize adaptive strategies that are evaluated in studies using this platform (6).

Groundwater

While climate change risks to the groundwater component of water supply have not been evaluated here, DWR's Flood Managed Aquifer Recharge program (California Department of Water Resources 2018) has adopted the decision scaling platform to evaluate using flood waters to recharge groundwater aquifers (7). In addition, DWR's Climate Change Program has drafted a simplified strategy for evaluating the potential benefits of increased groundwater storage north and/or south of Delta (see Annex H: Groundwater) using CalLite 3.0 (8). If simplified modeling of groundwater in CalLite 3.0 is found infeasible, shifting the operations model used in this study from CalLite 3.0 to CalSim-III, which features a dynamic link to the California Central Valley Groundwater-Surface Water Model (C2VSIM), would enable exploration of climate change risks and adaptation strategies based on modelling of the integrated surface-groundwater system (9) (see Annex I: Move From CalLite 3.0 to CalSim-III Operations Modeling).

References

- AghaKouchak A, L Cheng, O Mazdiyasni, and A Farahmand. 2014, "Global warming and changes in risk of concurrent climate extremes: Insights from the 2014 California drought." *Geophys. Res. Lett.*, 41, 8847-8852.
- Anderson EA. 1976. "A point energy and mass balance model of a snow cover" *NOAA Tech. Rep. NSW* 19, Natl. Oceanic and Atmos. Admin., Silver Spring, MD., 1-150.
- Bay-Delta Office. 2007. *California Central Valley Unimpaired Flow Data: 4th edition*. California Department of Water Resources, 1-53.
- Brown C. and RL Wilby. 2012. "An alternate approach to assessing climate risks" *EOS, Transactions, American Geophysical Union*, 92, 401-412.
- Brown CM, JR Lund, X Cai, PM Reed, EA Zagona, A Ostfeld, J Hall, GW Characklis, W. Yu, and L. Brekke. 2015. "The future of water resources systems analysis: Toward a scientific framework for sustainable water management" *Water Resources Research*. 51. 6110-6124.
- Brown C, Y Ghile, M Laverty, and K Li. 2012. "Decision Scaling: Linking bottom-up vulnerability analysis with climate projections in the water sector." *Water Resources Research*. 48. W09537.
- California Department of Fish and Wildlife. 2014 "CDFW moves to prevent fish loss, evacuates fish at American River and Nimbus Hatcheries" California Department of Fish and Wildlife, 16 June, hatcheries.
- California Department of Water Resources. 2013. "California Water Plan 2013: Investing in Innovation and Infrastructure" Bulletin 160-13, 3 - Resource Management Strategies. 1-858.
- California Department of Water Resources. 2014a. "Water year 2014 ends as 3rd driest in precipitation." California Department of Water Resources, Available at <http://www.water.ca.gov/waterconditions/>.
- California Department of Water Resources. 2014b. Year's final snow survey comes up dry. California Department of Water Resources. 1 May. Available at <http://www.water.ca.gov/news/newsreleases/2014/050114.pdf>.
- California Department of Water Resources. 2015a. California Climate Science and Data for Water Resources Management. California Climate Science and Data, June 2015, 1-28.
- California Department of Water Resources. 2015b. California's most significant droughts: comparing historical and recent conditions. California Department of Water Resources.
- California Department of Water Resources. 2016. Precipitation Enhancement: A Resource Management Strategy of the California Water Plan. California Department of Water Resources.

California Department of Water Resources. 2017. California Climate Risk: Evaluation of Climate Risks for California Department of Water Resources. California Department of Water Resources. Available online at <https://www.water.ca.gov/-/media/DWR-Website/Web-Pages/Programs/All-Programs/Climate-Change-Program/Files/California-Climate-Risk-Evaluation-of-Climate-Risks-for-California-Department-of-Water-Resources.pdf>.

California Department of Water Resources. 2018. FLOOD-MAR: Using Flood Water for Managed Aquifer Recharge to Support Sustainable Water Resources. California Department of Water Resources. Available online at https://water.ca.gov/-/media/DWR-Website/Web-Pages/Programs/All-Programs/Flood-MAR/DWR_FloodMAR-White-Paper_06_2018_updated.pdf.

California Department of Water Resources and United States Bureau of Reclamation. 2011. *CalLite: Central Valley Water Management Screening Model (Version 2.0) Reference Manual*, vol. October 2011. 161 pp., California Department of Water Resources, Sacramento, California.

Cayan DR, T Das, DW Pierce, TP Barnett, M Tyree, and A Gershunov. 2010. "Future Dryness in the Southwest US and the Hydrology of the Early 21st Century Drought." Proceedings of the National Academy of Sciences of the United States of America, 107, 21271-21276.

Cayan D. et al. 2013. "Future climate: Projected average." in Assessment of Climate Change in the Southwest United States: A Report Prepared for the National Climate Assessment. A report by the Southwest Climate Alliance. edn., edited by G Garfin, A Jardine, R Merideth, M Black, and S LeRoy. pp. 101–125, Island Press, Washington, D.C., USA.

Charnes A and WW Cooper. 1961. *Management Models and Industrial Applications of Linear Programming*. Wiley. New York.

Connell-Buck CR, J Medellin-Azuara, JR Lund, and K Madani. 2011. "Adapting California's water system to warm vs. dry climates." Climate Change. 109, 133–149.

Dettinger, M. D. and M. L. Anderson (2015), Storage in California's Reservoirs and Snowpack in this Time of Drought, *San Francisco Estuary and Watershed Science*, 13, 1-5.

Dettinger, M. D. and D. R. Cayan (2014), Drought and the California Delta - A Matter of Extremes, *San Francisco Estuary and Watershed Science*, 12, 1-6.

Diffenbaugh, N. S. and M. Ashfaq (2010), Intensification of hot extremes in the United States, *Geophys. Res. Lett.*, 37, L15701.

Diffenbaugh, N. S., D. L. Swain, and D. Touma (2015), Anthropogenic warming has increased drought risk in California, *Proc. Natl. Acad. Sci. U. S. A.*, 112, 3931-3936.

Draper, A. J., A. Munevar, S. K. Arora, E. Reyes, N. L. Parker, F. I. Chung, and L. E. Peterson (2004), CalSim: Generalized model for reservoir system analysis, *Journal of Water Resources Planning and Management-ASCE*, 130, 480-489.

Forsythe, W. C., E. J. Rykiel Jr., R. S. Stahl, H. Wu, and R. M. Schoolfield (1995), A model comparison for daylength as a function of latitude and day of year, *Ecol. Model.*, 80, 87-95.

Gleick, P. H. (1987), The Development and Testing of a Water-Balance Model for Climate Impact Assessment - Modeling the Sacramento Basin, *Water Resour. Res.*, 23, 1049-1061.

Griffin, D. and K. J. Anchukaitis (2014), How unusual is the 2012-2014 California drought?, *Geophys. Res. Lett.*, 41, 9017-9023.

Griffith D, Solak M, Almy R, Gibbs D. 2005. "The Santa Barbara Cloud Seeding Project in Coastal Southern California, Summary of Results and Their Implications." *Journal of Weather Modification* 37(April):21-27.

Griggs, G, Árvai, J, Cayan, D, DeConto, R, Fox, J, Fricker, HA, Kopp, RE, Tebaldi, C, Whiteman, EA (California Ocean Protection Council Science Advisory Team Working Group). Rising Seas in California: An Update on Sea-Level Rise Science. California Ocean Science Trust, April 2017.

Groves, D. G. and E. Bloom (2013), Robust Water-Management Strategies for the California: Water Plan Update 2013 Proof-of-Concept Analysis, *RAND Corporation, California Water Plan Update 2013*, 1-72.

Hallegatte, S., A. Shah, C. Lempert, C. Brown, and S. Gill (2012), Investment Decision Making under Deep Uncertainty: Application to Climate Change.

Hamon, W. R. (1961), Estimating potential evapotranspiration, *J. Hydr. Eng. Div. -ASCE*, 87, 107-120.

Harou, J. J., J. Medellin-Azuara, T. Zhu, S. K. Tanaka, J. R. Lund, S. Stine, M. A. Olivares, and M. W. Jenkins (2010), Economic consequences of optimized water management for a prolonged, severe drought in California, *Water Resour. Res.*, 46, W05522.

Heim, R. R. (2002), A review of twentieth-century drought indices used in the United States, *Bull. Am. Meteorol. Soc.*, 83, 1149-1165.

Higgins, R. W., V. B. S. Silva, W. Shi, and J. Larson (2007), Relationships between climate variability and fluctuations in daily precipitation over the United States, *J. Clim.*, 20, 3561-3579.

Hirsch, R. M. (2011), A Perspective on Nonstationarity and Water Management, *J. Am. Water Resour. Assoc.*, 47, 436-446.

Howitt, R. E., D. MacEwan, J. Medellin-Azuara, J. R. Lund, and D. A. Sumner (2015), Economic Analysis of the 2015 Drought for California Agriculture, *Center for Watershed Sciences, University of California – Davis, Davis, CA*, 1-16.

Howitt, R. E., J. Medellin-Azuara, D. MacEwan, J. R. Lund, and D. A. Sumner (2014), Economic Analysis of the 2014 Drought for California Agriculture, *Center for Watershed Sciences, University of California – Davis, Davis, CA*, 1-16.

- IPCC (2012), *Managing the Risks of Extreme Events and Disasters to Advance Climate Change Adaptation: A Special Report of Working Groups I and II of the Intergovernmental Panel on Climate Change - Summary for Policymakers*, 1-19 pp., Cambridge University Press, Cambridge, UK, and New York, NY, USA.
- IPCC (2013), *Climate Change 2013: The Physical Science Basis. Working Group I Contribution to the Fifth Assessment Report of the Intergovernmental Panel on Climate Change*, 1-1535 pp., Cambridge University Press, New York.
- Islam, N. et al. (2014), Central Valley Water Management Screening Model for Water Management Alternatives, International Environmental Modelling and Software Society (iEMSs) 7th Intl. Congress on Env. Modeling and Software, June 15-19.
- Joyce, B., D. Purkey, D. Yates, D. Groves, and A. Draper (2010), Integrated scenario analysis for the 2009 California water plan update, Vol. 4, *California Dept. of Water Resources, Vol. 4*, 1-112.
- Killam, D., A. Bui, S. LaDochy, P. Ramirez, J. Willis, and W. C. Patzert (2014), California Getting Wetter to the North, Drier to the South: Natural Variability or Climate Change?, *Climate*, 2, 168-180.
- Kopp, R. E., A. C. Kemp, K. Bittermann, B. P. Horton, J. P. Donnelly, W. R. Gehrels, C. C. Hay, J. X. Mitrovica, E. D. Morrow, and S. Rahmstorf (2016), Temperature-driven global sea-level variability in the Common Era, *Proc. Natl. Acad. Sci. U. S. A.*, 113, E1441.
- LaDochy, S., P. Ramirez, D. Killam, A. Bui, W. C. Patzert, and J. Willis (2011), California temperature and precipitation trends: climate variability or global warming, 91st Meeting of the American Meteorology Society 2011, Seattle, Washington, January 22-27.
- Lempert, R. J., D. G. Groves, S. W. Popper, and S. C. Bankes (2006), A general, analytic method for generating robust strategies and narrative scenarios, *Management Science*, 52, 514-528.
- Livneh, B., E. A. Rosenberg, C. Lin, B. Nijssen, V. Mishra, K. M. Andreadis, E. P. Maurer, and D. P. Lettenmaier (2013), A Long-Term Hydrologically Based Dataset of Land Surface Fluxes and States for the Conterminous United States: Update and Extensions, *J. Clim.*, 26, 9384-9392.
- Lohmann, D., R. Raschke, B. Nijssen, and D. P. Lettenmaier (1998), Regional scale hydrology: I. Formulation of the VIC-2L model coupled to a routing model, *Hydrolog. Sci. J.*, 43, 131-141.
- Lund, J. R., E. Hanak, W. E. Fleenor, W. A. Bennett, R. E. Howitt, J. F. Mount, and P. B. Moyle (2010), *Comparing Futures for the Sacramento-San Joaquin Delta*, Freshwater Ecology Series, vol. 3, 232 pp., Univ California Press, Berkeley; 2120 Berkeley Way, Berkeley, CA 94720 USA.
- Mao, Y., B. Nijssen, and D. P. Lettenmaier (2015), Is climate change implicated in the 2013-2014 California drought? A hydrologic perspective, *Geophys. Res. Lett.*, 42, 2805-2813.

- Margulis, S. A., G. Cortes, M. Girotto, L. S. Huning, D. Li, and M. Durand (2016), Characterizing the extreme 2015 snowpack deficit in the Sierra Nevada (USA) and the implications for drought recovery, *Geophys. Res. Lett.*, 43, 6341-6349.
- McEnery, J., J. Ingram, Q. Duan, T. Adams, and L. Anderson (2005), NOAA'S Advanced Hydrologic Prediction Service – Building pathways for Better Science in Water Forecasting, *Bulletin of the American Meteorological Society*, March, 375-385.
- Meko, D. M., C. A. Woodhouse, and R. Touchan (2014), Klamath/San Joaquin/Sacramento Hydroclimatic Reconstructions from Tree Rings, *Draft Final Report to California Department of Water Resources, Agreement 4600008850*.
- Moriasi, D. N., J. G. Arnold, M. W. Van Liew, R. L. Bingner, R. D. Harmel, and T. L. Veith (2007), Model evaluation guidelines for systematic quantification of accuracy in watershed simulations, *Trans. ASABE*, 50, 885-900.
- Mote, P. W., A. F. Hamlet, M. P. Clark, and D. P. Lettenmaier (2005), Declining mountain snowpack in western north America, *Bull. Am. Meteorol. Soc.*, 86, 39-49.
- Mount, J. and R. Twiss (2005), Subsidence, sea level rise, and seismicity in the Sacramento-San Joaquin Delta, *San Francisco Estuary and Watershed Science*, 3.
- Nash, J. E. (1957), The form of the instantaneous unit hydrograph, *International Association of Science and Hydrology*, 3, 114-121.
- National Research Council (2012), Sea-Level Rise for the Coasts of California, Oregon, and Washington: Past, Present, and Future, 1-217.
- NOAA (2014), California Drought: 2014 Service Assessment, *U. S. Department of Commerce and National Oceanic and Atmospheric Administration*, 1-72.
- NOAA (2016), Mean Sea Level Trend 9414290 San Francisco, California, *NOAA Tides and Currents*, https://tidesandcurrents.noaa.gov/slrends/slrends_station.shtml?stnid=9414290.
- Null, S. E. and J. R. Lund (2006), Re-Assembling Hetch Hetchy: Water Supply Implications of Removing O'Shaughnessy Dam, *Journal of the American Water Resources Association*, 42, 395-408.
- Null, S. E., J. Medellin-Azuara, A. Escriva-Bou, M. Lent, and J. R. Lund (2014), Optimizing the dammed: Water supply losses and fish habitat gains from dam removal in California, *J. Environ. Manage.*, 136, 121-131.
- Null, S. E. and J. H. Viers (2013), In bad waters: Water year classification in nonstationary climates, *Water Resour. Res.*, 49, 1137-1148.

Olivares, M. A., J. Haas, R. Palma-Behnke, and C. Benavides (2015), A framework to identify Pareto-efficient subdaily environmental flow constraints on hydropower reservoirs using a grid-wide power dispatch model, *Water Resour. Res.*, 51, 3664-3680.

Pavia, E. G., F. Graef, and R. Fuentes-Franco (2016), Recent ENSO-PDO precipitation relationships in the Mediterranean California border region, *Atmos. Sci. Lett.*, 17, 280-285.

Pierce, D. W., J. F. Kalansky, and D. R. Cayan, (Scripps Institution of Oceanography). 2018. Climate, Drought, and Sea Level Rise Scenarios for the Fourth California Climate Assessment. California's Fourth Climate Change Assessment, California Energy Commission. Publication Number: CNRA-CEC-2018-006.

Quiring, S. M. (2009), Developing Objective Operational Definitions for Monitoring Drought, *J. Appl. Meteorol. Climatol.*, 48, 1217-1229.

Rheinheimer, D. E., S. E. Null, and J. R. Lund (2015), Optimizing Selective Withdrawal from Reservoirs to Manage Downstream Temperatures with Climate Warming, *J. Water Resour. Plann. Manage.*, 141, 04014063.

Richter, B. D., J. V. Baumgartner, R. Wigington, and D. P. Braun (1997), How much water does a river need?, *Freshwat. Biol.*, 37, 231-249.

Schneider, U., A. Becker, P. Finger, A. Meyer-Christoffer, M. Ziese, and B. Rudolf (2014), GPCC's new land surface precipitation climatology based on quality-controlled in situ data and its role in quantifying the global water cycle, *Theor. Appl. Climatol.*, 115, 15-40.

Schwarz, Andrew, Patrick Ray, Sungwook Wi, Casey Brown, Minxue He, Matthew Correa. (California Department of Water Resources). 2018. Climate Change Risks Faced by the California Central Valley Water Resource System. California's Fourth Climate Change Assessment. Publication number: CCCA4-EXT-2018-001.

Seager, R., M. Hoerling, S. Schubert, H. Wang, B. Lyon, A. Kumar, J. Nakamura, and N. Henderson (2015), Causes of the 2011-14 California Drought*, *J. Clim.*, 28, 6997-7024.

Steinschneider, S. and C. Brown (2013), A semiparametric multivariate, multisite weather generator with low-frequency variability for use in climate risk assessments, *Water Resour. Res.*, 49, 7205-7220.

Swain, D. L. (2015), A tale of two California droughts: Lessons amidst record warmth and dryness in a region of complex physical and human geography, *Geophysical Research Letters*.

Swain, D. L., M. Tsiang, M. Haugen, D. Singh, A. Charland, B. Rajaratnam, and N. S. Diffenbaugh (2014), The Extraordinary California Drought of 2013/2014: Character, Context, and the Role of Climate Change, *Bull. Am. Meteorol. Soc.*, 95, S7.

Swetnam, T. W. and J. L. Betancourt (1998), Mesoscale disturbance and ecological response to decadal climatic variability in the American Southwest, *J. Clim.*, 11, 3128-3147.

SWRCB (State Water Resources Control Board). 2000. Revised Water Right Decision 1641: Implementation of Water Quality Objectives for the San Francisco Bay/Sacramento-San Joaquin Delta Estuary. California EPA. Available at:
http://www.waterboards.ca.gov/waterrights/board_decisions/adopted_orders/decisions/d1600_d1649/wrd1641_1999dec29.pdf

Tanaka, S. K., C. Buck, K. Madani, J. Medellin-Azuara, J. Lund, and E. Hanak (2011), Economic Costs and Adaptations for Alternative Regulations of California's Sacramento-San Joaquin Delta, *San Francisco Estuary and Watershed Science*, 9, 28.

U.S. Department of Agriculture (2014), California drought 2014: Farm and food impacts, *United States Department of Agriculture*, impacts.aspx.

U.S. Geological Survey (2014), California Water Science Center, Available online at
<http://ca.water.usgs.gov/data/drought/surfacewater.html>.

United States Drought Monitor (2014), California drought intensifies and U.S. drought spreads, *United States Drought Monitor*, 6 Feb, Available online at
<http://droughtmonitor.unl.edu/USDMNews/NewsArchive.aspx>.

van Vuuren, D.P., Edmonds, J., Kainuma, M. et al. (2011), The representative concentration pathways: an overview, *Climatic Change* 109: 5. <https://doi.org/10.1007/s10584-011-0148-z>

Wang, H. and S. Schubert (2014), Causes of the Extreme Dry Conditions Over California during Early 2013, *Bull. Am. Meteorol. Soc.*, 95, S11.

Whateley, S., S. Steinschneider, and C. Brown (2016), Selecting stochastic climate realizations to efficiently explore a wide range of climate risk to water resources systems, *Journal of Water Resources Planning and Management*, submitted.

Wilby, R. L. and S. Dessai (2010), Robust adaptation to climate change, *Weather*, 65, 180-185.

Williams, A. P., R. Seager, J. T. Abatzoglou, B. I. Cook, J. E. Smerdon, and E. R. Cook (2015), Contribution of anthropogenic warming to California drought during 2012-2014, *Geophys. Res. Lett.*, 42, 6819-6828.

Willis, A. D., J. R. Lund, E. S. Townsley, and B. Faber (2011), Climate Change and Flood Operations in the Sacramento Basin, California, *San Francisco Estuary and Watershed Science*, 9, 18.

Yoon, J., S. S. Wang, R. R. Gillies, B. Kravitz, L. Hipps, and P. J. Rasch (2015), Increasing water cycle extremes in California and in relation to ENSO cycle under global warming, *Nat. Commun.*

Zhang, Q. and S. J. Stanley (1999), Real-time water treatment process control with artificial neural networks, *Journal of Environmental Engineering-ASCE*, 125(2), 153-160, doi: 2(153).

Annex A: GCM Likelihood Function

Using Intergovernmental Panel on Climate Change (IPCC) Representative Concentration Pathways (RCP) scenarios of 4.5 and 8.5 of the CMIP5 ensemble in the region contributing flow to the CVS, the relative weights assigned to the climate states were obtained in five steps.

- 1) The vector of future mean annual precipitation and temperature changes was calculated from all climate projections.
- 2) The computed mean changes from the full ensemble of GCMs were reduced to 14 data points to account for the potential sampling biases because of the structural similarities in GCMs (Knutti et al. 2013). In so doing, all model runs were weighted equally and combined by arithmetic averaging within each model group.
- 3) The computed 14 data points were used to define a probability distribution function (pdf) for the domain of climate change. In this case, a bivariate Gaussian distribution was fit to the data (Whateley et al. 2014).
- 4) The Gaussian pdf was used to obtain the contingent normalized probability weights of the 54-plausible mean temperature and precipitation changes hereafter referred to as the GCM-informed pdf. Similar approaches have been taken by others (Borgomeo et al. 2015; Steinschneider et al. 2015; Tebaldi et al. 2005).
- 5) GCM-informed probabilities were applied to individual years in the development of cumulative density functions (cdf) of future system performance. Although each climate trace (i.e. “scenario”) has a likelihood based upon its shift in precipitation and temperature from the historical, each year within a given climate trace was treated as equally likely. Probability notions were thus extended from “scenario” (shift in precipitation and temperature) to the realization of any given year within a scenario.

Annex B: Spatial and Temporal Climate Trends

Because precipitation and temperature changes vary both spatially and temporally, the relationships of temperature and precipitation (for both observed and projected) with several geographical and time-scale factors, including elevation, latitude, and season, should be investigated. In doing so, the levels of precipitation and temperature changes can be incorporated in more detail, which would provide a more realistic distribution of climate changes across the large study area as a function of space as well as time. This study uses daily climate data from the National Climate Data Center (NCDC) to identify these relations.

Relationship of Observed Temperature, Precipitation With Elevation, Latitude, and Season

Relationship of Temperature with Elevation and Latitude

This study uses the correlation coefficient (R) to define the relationship between seasonal temperature (fall [September–November], winter [December–February], spring [March–May], summer [June–August]) and elevations in various latitude ranges. According to Ratner (2009): $R = 0$ defines no linear relationship, $R = -1$ or $+1$ represents perfect negative or positive linear relationship, $R = (-0.3, 0)$ or $(0, 0.3)$ reveals weak negative or positive linear relationship, $R = (-0.7, -0.3)$ or $(0.3, 0.7)$ indicates negative or positive moderate linear correlation, and $R = (-1, -0.7)$ or $(0.7, 1)$ identifies negative or positive strong linear correlation. Negative R is expected since temperature tends to decrease with increases in elevation. These coefficients are summarized in Table 10.

Table 11 Relationship Between Seasonal Temperatures and Elevations

| Data package | Trend | Correlation coefficient (R) |
|-----------------------------------|----------------------------------|---------------------------------|
| Missing data less than 10 percent | Fall temperature and elevation | -0.35 |
| | Winter temperature and elevation | -0.32 |
| | Spring temperature and elevation | -0.15 |
| | Summer temperature and elevation | -0.05 |
| Missing data less than 20 percent | Fall temperature and elevation | -0.28 |
| | Winter temperature and elevation | -0.27 |
| | Spring temperature and elevation | -0.07 |
| | Summer temperature and elevation | 0 |

According to Table 11, it was found that correlation coefficients (R) for relationships between temperatures and elevations in each latitude range are very weak, demonstrating that temperature does not have a clear linear relationship with elevations and latitudes. Most of the correlation coefficients are negative, showing negative correlations of temperatures with elevations and latitudes. The scatter plots used to derive these R coefficients are provided in the “Supplemental Figures” section below.

Table 12 Relationship Between Seasonal Temperatures and Elevations, Latitudes

| Data package | Trend | Latitude Range | Correlation Coefficient (R) | Number of Samples |
|-----------------------------------|----------------------------------|----------------|-----------------------------|-------------------|
| Missing data less than 10 percent | Fall temperature and elevation | (32 34] | -0.48 | 17 |
| | | (34 36] | -0.3 | 27 |
| | | (36 38] | -0.36 | 39 |
| | | (38 40] | -0.16 | 29 |
| | | (40 42] | -0.39 | 16 |
| | Winter temperature and elevation | (32 34] | -0.53 | 17 |
| | | (34 36] | -0.46 | 27 |
| | | (36 38] | -0.3 | 39 |
| | | (38 40] | -0.15 | 29 |
| | Spring temperature and elevation | (36 38] | -0.25 | 16 |
| | | (32 34] | 0 | 17 |
| | | (34 36] | -0.07 | 27 |
| | | (38 40] | -0.14 | 39 |
| | | (40 42] | -0.01 | 29 |
| | Summer temperature and elevation | (38 40] | -0.29 | 16 |
| | | (32 34] | 0.16 | 17 |
| | | (34 36] | 0.19 | 27 |
| | | (36 38] | -0.19 | 39 |
| | | (40 42] | 0.04 | 29 |
| Missing data less than 20 percent | Fall temperature and elevation | (38 40] | -0.08 | 16 |
| | | (32 34] | -0.29 | 30 |
| | | (34 36] | -0.23 | 39 |
| | | (36 38] | -0.25 | 52 |
| | | (38 40] | -0.2 | 45 |
| | Winter temperature and elevation | (40 42] | -0.24 | 25 |
| | | (32 34] | -0.31 | 30 |
| | | (34 36] | -0.3 | 39 |
| | | (36 38] | -0.3 | 52 |
| | Spring temperature and elevation | (38 40] | -0.14 | 45 |
| | | (40 42] | -0.25 | 25 |
| | | (32 34] | 0.05 | 30 |
| | | (34 36] | 0.02 | 39 |
| | Summer temperature and elevation | (36 38] | -0.01 | 52 |
| | | (38 40] | 0.04 | 45 |
| | | (40 42] | -0.02 | 25 |
| | | (32 34] | 0.05 | 30 |
| | | (34 36] | 0.11 | 39 |

Relationship Between Temperature and Season

This study divides temperature data into four seasons: winter (December, January, and February), spring (March, April, and May), summer (June, July, and August), and fall (September, October, and November) as well as an annual dataset that includes all data. Thiel Sen slopes are computed for each station in these five datasets, boxplots of which are shown in Figure 39. The daily temperature data used to conduct this analysis went through quality checks for two missing rates; Figure 39 results from 94 stations for which missing data rate is less than 10 percent, while Figure 40 shows the results of trend analysis from 145 stations for which missing rate is less than 20 percent. In Figure 39 and Figure 40, red numbers represent medians of seasonal/temperature trend; black numbers are means of seasonal temperature trend.

According to these box plots, it was found that the warming trend is stronger in spring and summer than in winter and fall. The calculation processes are shown as follows:

Step 1: From temperature data of each station during 1950–2015, Sen's slope is computed for 4 datasets of spring, summer, fall, and winter. Then, boxplots are calculated as above (Figure 39 and Figure 40).

Step 2: From these boxplots, means of temperature trend slope (black numbers in boxplots) are attained (shown in the last column of Table 12 below).

Step 3: Finally, temperature increases reflecting the spring, summer, fall and winter trends are calculated for 8 increasing temperature shifts (temperature increase of 0.5; 1; 1.5; 2; 2.5; 3; 3.5; 4°C).

Table 13 Means of Seasonal Warming Pattern (Average Increase Per Decade)

| SEASON | Mean T1 (10%) Black (Deg.C/decade) | Mean T2 (20%) Black (Deg.C/decade) | AVG increase per decade |
|--------|------------------------------------|------------------------------------|-------------------------|
| Winter | 0.112 | 0.12 | 0.116 |
| Spring | 0.261 | 0.269 | 0.265 |
| Summer | 0.189 | 0.194 | 0.1915 |
| Fall | 0.038 | 0.049 | 0.0435 |

The average annual temperature increase per decade across all stations was found to be 0.154°C per decade. Thus, as an example, winter months will have an increase of 0.38°C when the total annual temperature increase is 0.5°C, $(0.5^\circ\text{C} * 0.116^\circ\text{C per decade [winter trend]} / 0.154^\circ\text{C per decade [annual trend]}) = 0.38^\circ\text{C}$. Likewise, seasonal warming is applied to other seasons (shown in Table 13 below) and incorporated into new sequences of temperature. All seasonal warming patterns are shown in Figure 41.

Table 14 Seasonal Warming Pattern Application for Eight Increase Levels

| JAN | FEB | MAR | APR | MAY | JUN | JUL | AUG | SEP | OCT | NOV | DEC | T increase |
|---------|---------|---------|---------|-------|--------|--------|--------|--------|--------|--------|-------|---|
| 0.116 | 0.116 | 0.265 | 0.265 | 0.265 | 0.1915 | 0.1915 | 0.1915 | 0.0435 | 0.0435 | 0.0435 | 0.116 | 0.154 |
| 0.38 | 0.38 | 0.86 | 0.86 | 0.86 | 0.62 | 0.62 | 0.62 | 0.14 | 0.14 | 0.14 | 0.38 | 0.5 Temperature increase of 0.5 degrees Celcius |
| 0.75 | 0.75 | 1.72 | 1.72 | 1.72 | 1.24 | 1.24 | 1.24 | 0.28 | 0.28 | 0.28 | 0.75 | 1 Temperature increase of 1 degrees Celcius |
| 1.13 | 1.13 | 2.58 | 2.58 | 2.58 | 1.87 | 1.87 | 1.87 | 0.42 | 0.42 | 0.42 | 1.13 | 1.5 Temperature increase of 1.5 degrees Celcius |
| 1.51 | 1.51 | 3.44 | 3.44 | 3.44 | 2.49 | 2.49 | 2.49 | 0.56 | 0.56 | 0.56 | 1.51 | 2 Temperature increase of 2 degrees Celcius |
| 1.88 | 1.88 | 4.30 | 4.30 | 4.30 | 3.11 | 3.11 | 3.11 | 0.71 | 0.71 | 0.71 | 1.88 | 2.5 Temperature increase of 2.5 degrees Celcius |
| 2.26 | 2.26 | 5.16 | 5.16 | 5.16 | 3.73 | 3.73 | 3.73 | 0.85 | 0.85 | 0.85 | 2.26 | 3 Temperature increase of 3 degrees Celcius |
| 2.64 | 2.64 | 6.02 | 6.02 | 6.02 | 4.35 | 4.35 | 4.35 | 0.99 | 0.99 | 0.99 | 2.64 | 3.5 Temperature increase of 3.5 degrees Celcius |
| 3.01 | 3.01 | 6.88 | 6.88 | 6.88 | 4.97 | 4.97 | 4.97 | 1.13 | 1.13 | 1.13 | 3.01 | 4 Temperature increase of 4 degrees Celcius |
| | | | | | | | | | | | | |
| Winter | Spring | Summer | Fall | | | | | | | | | |
| 0.116 | 0.265 | 0.1915 | 0.0435 | | | | | | | | | |
| Dec-Feb | Mar-May | Jun-Aug | Sep-Nov | | | | | | | | | |

Figure 39 Trend Slope of Temperature With Less Than 10 Percent Missing Data in 94 Stations

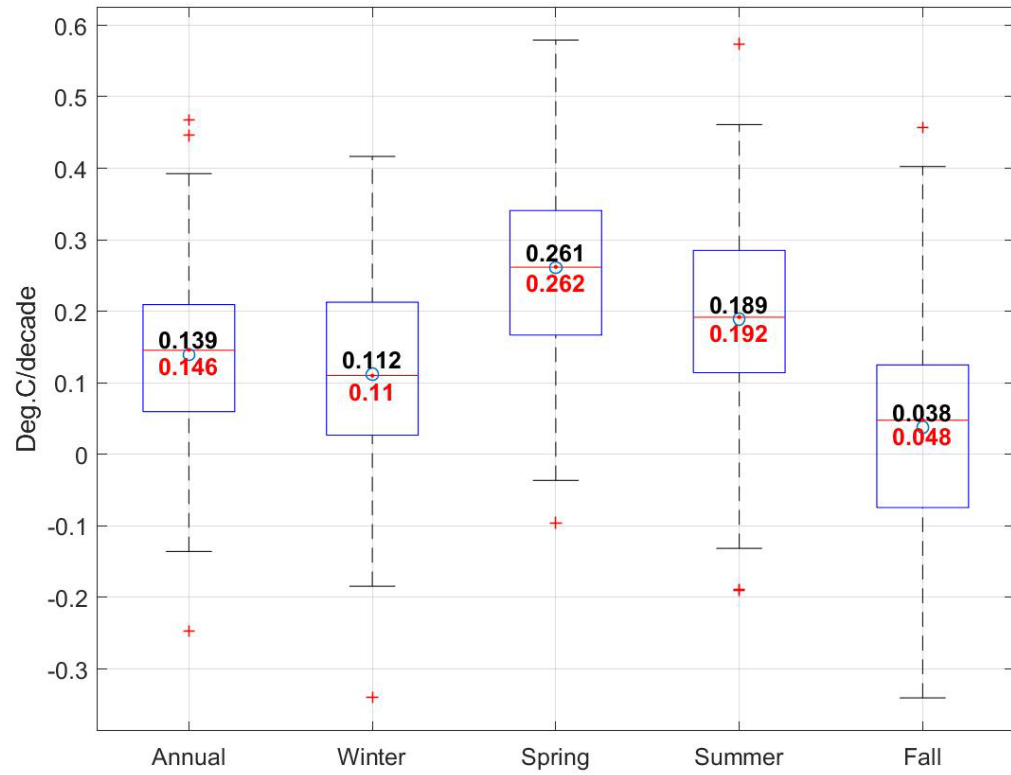


Figure 40 Trend Slope of Temperature With Less Than 20 Percent Missing Data in 145 Stations

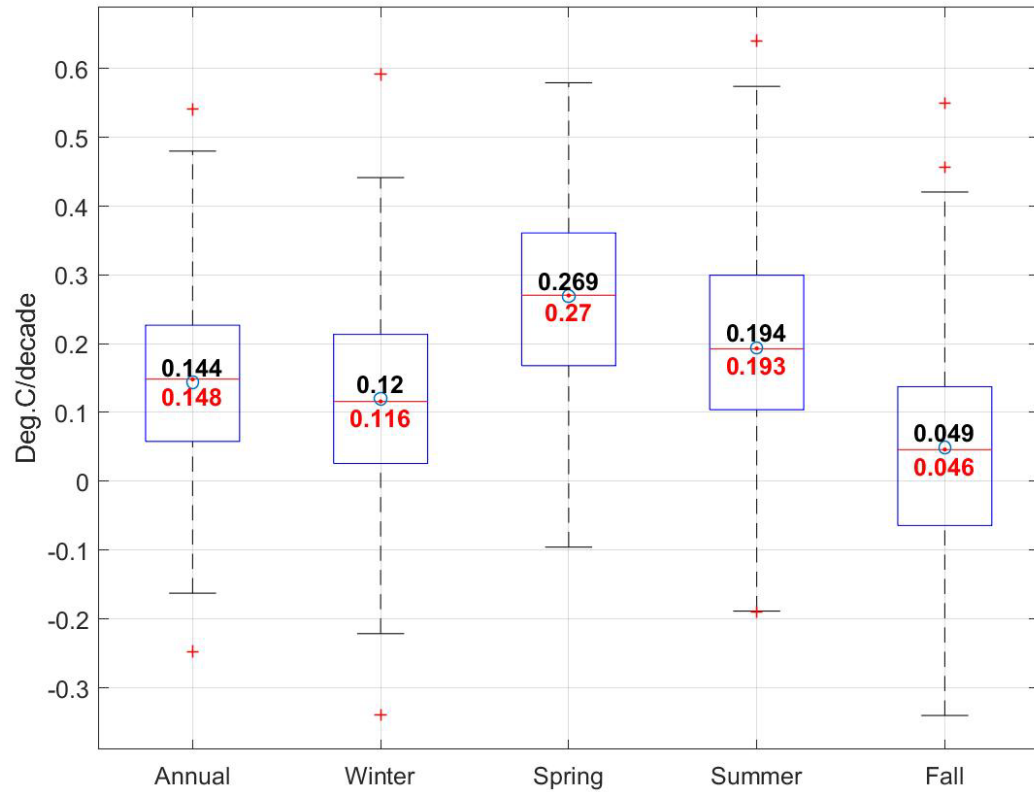
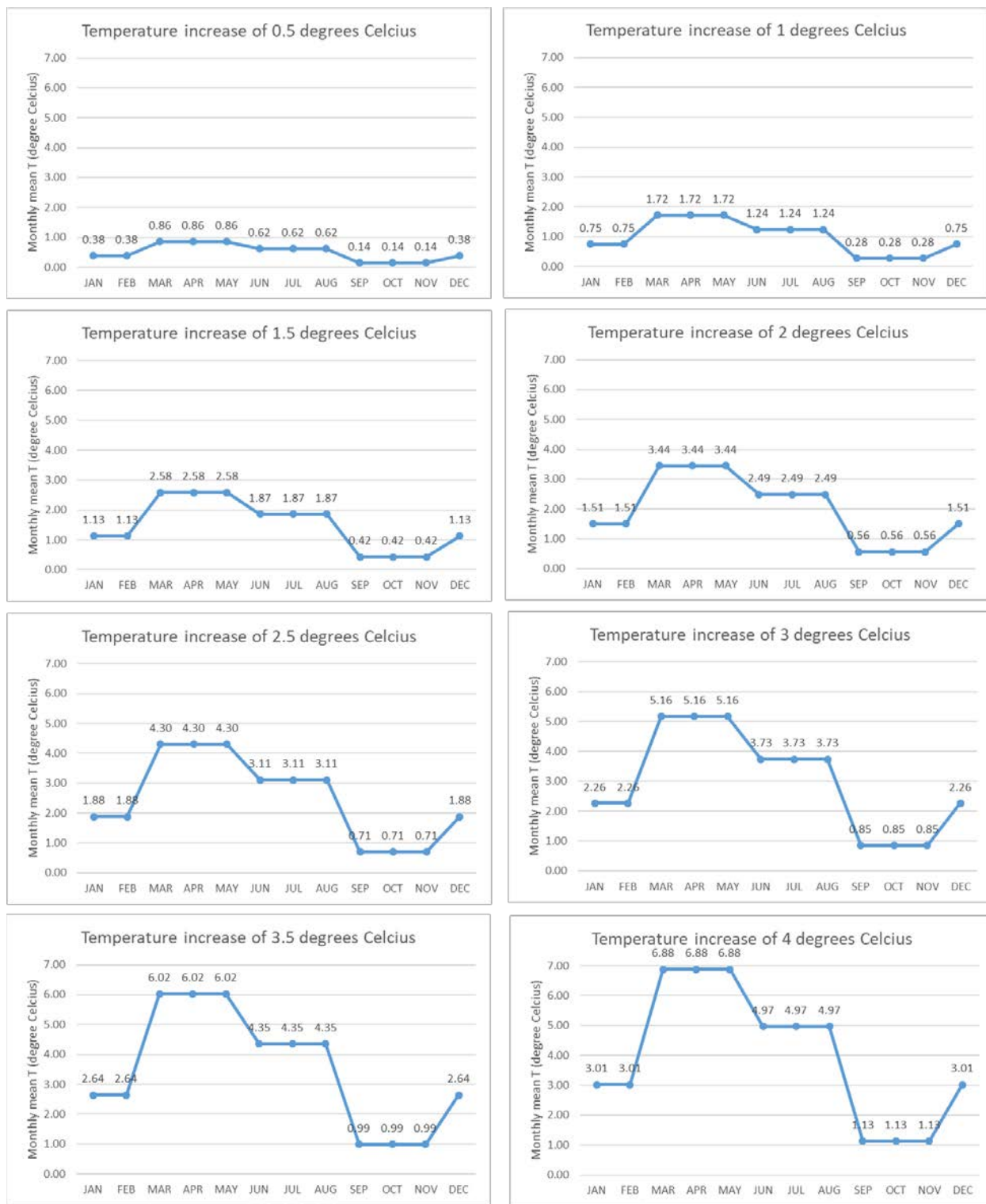


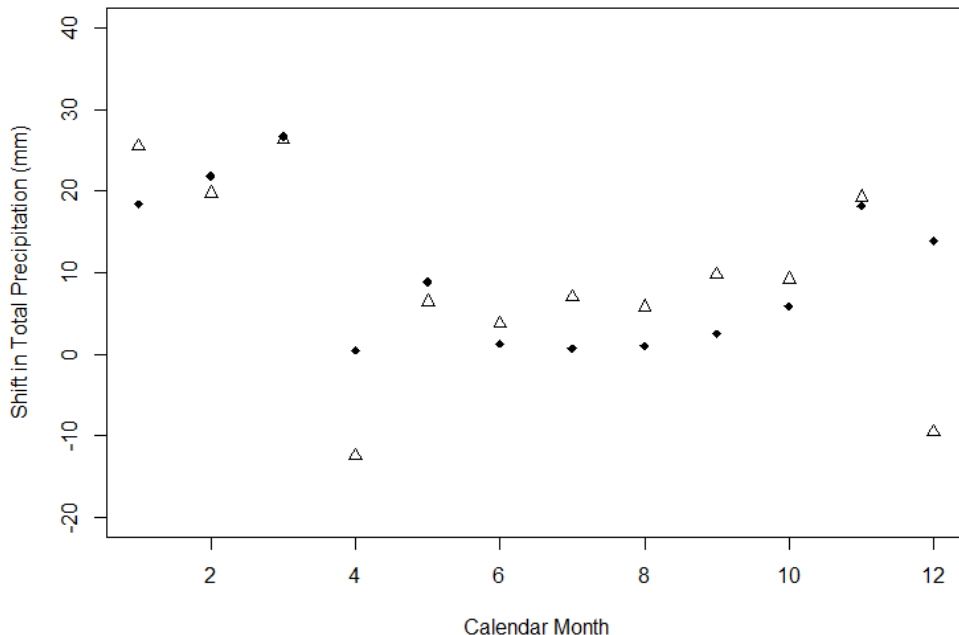
Figure 41 Seasonal Warming Patterns for Climate Projections



Relationship Between Precipitation and Elevation

In Figure 42, hollow triangles represent precipitation changes in high-elevation areas, while solid dots refer to low-elevation regions. High-elevation locations are considered as higher than 2000 m, and low-elevation locations lower than 2000 m. Ratios of differences between hollow triangles and solid dots vary from month to month which suggests that there is no trend of precipitation changes with elevation.

Figure 42 Differential Rate of Change in Precipitation Between Early Mid-20th Century (1920–1960) and Recent Past (1980–2011)

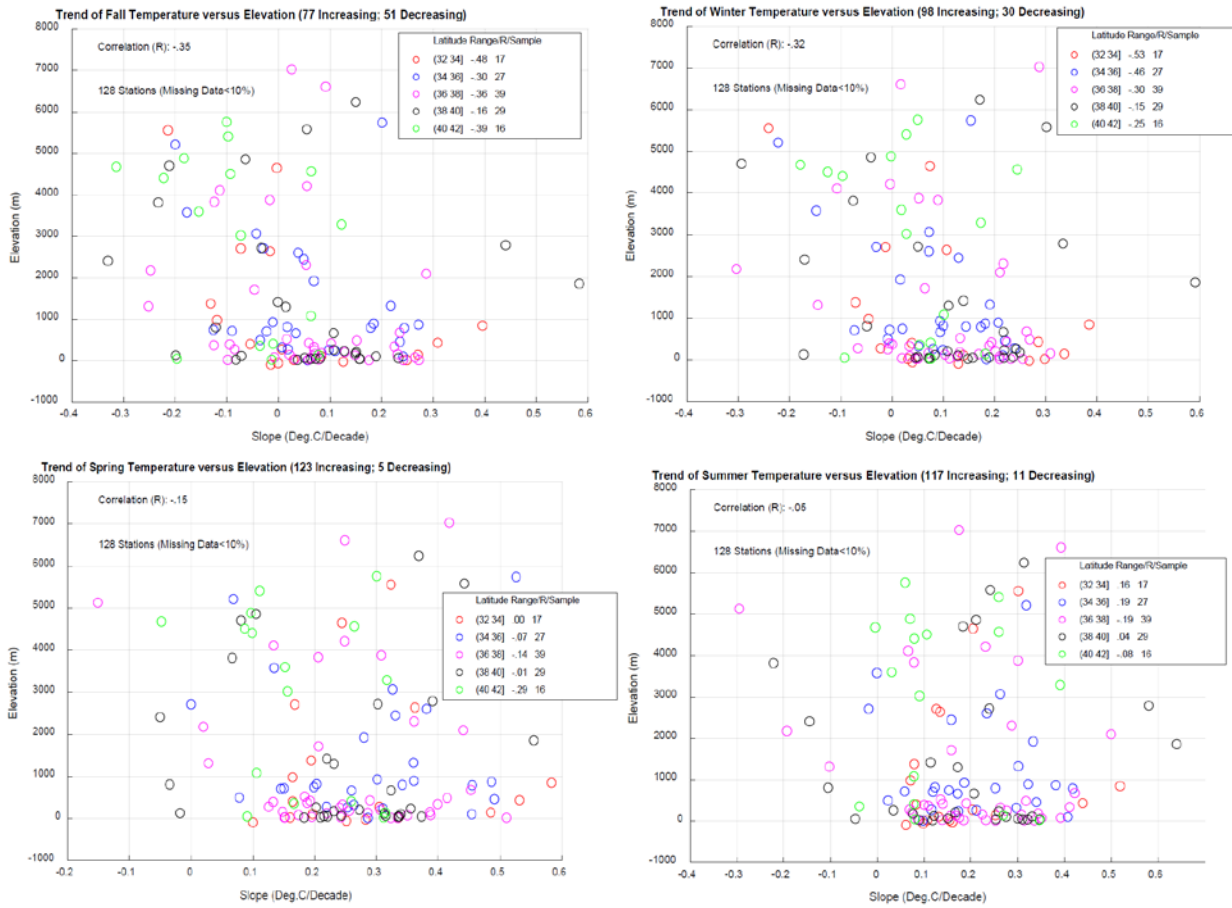


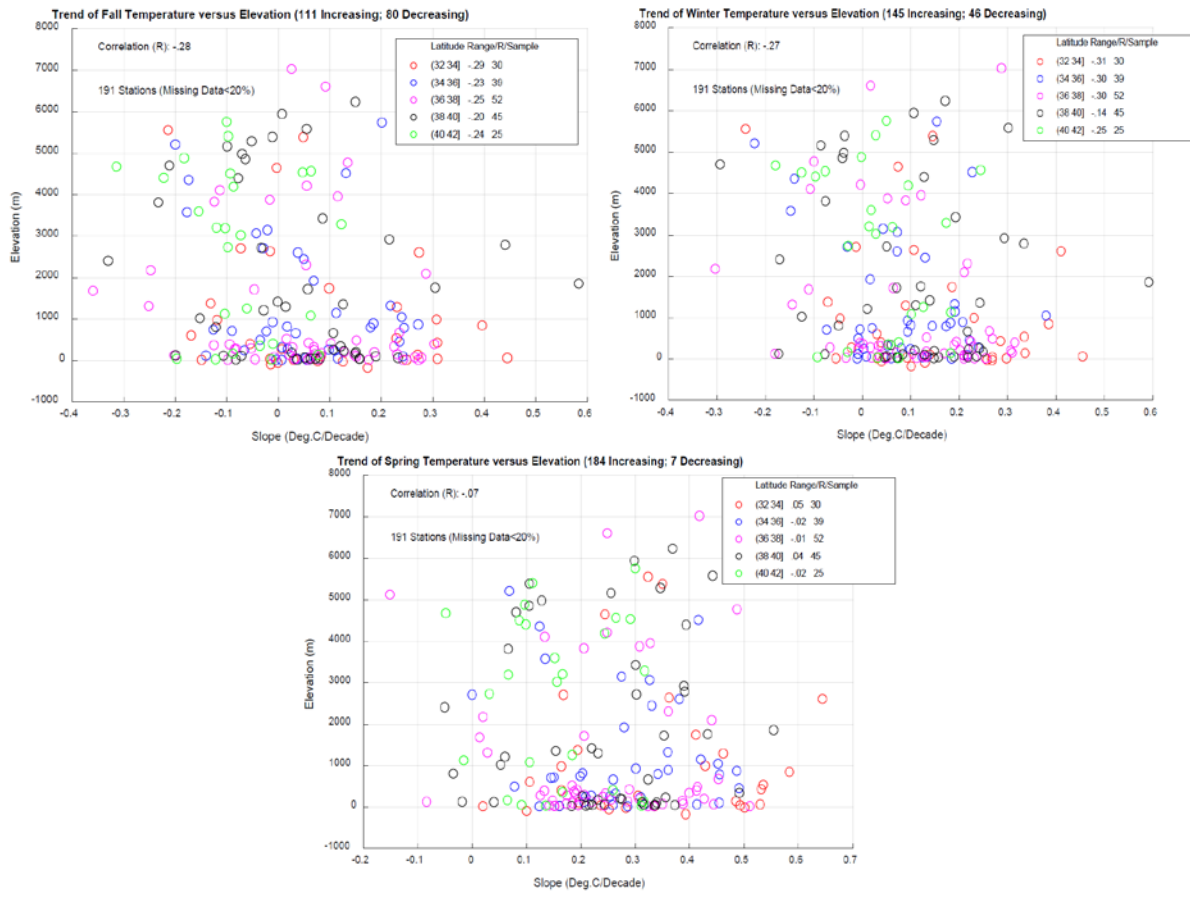
Note: Hollow triangles show changes in high-elevation (> 2000 m) grid cells of the Maurer et al. [2002] dataset, and solid dots show changes in low-elevation (< 2000 m) grid cells.

References

- Gilbert RO. 1987. *Statistical Methods for Environmental Pollution Monitoring*. Wiley, NY.
- Kendall MG. 1975. *Rank Correlation Methods*, 4th edition. Charles Griffin, London.
- Mann HB. 1945. "Non-parametric tests against trend." *Econometrica* 13:163-171.
- Maurer, E. P., A. W. Wood, J. C. Adam, D. P. Lettenmaier, and B. Nijssen (2002), A long-term hydrologically based dataset of land surface fluxes and states for the conterminous United States, *J. Clim.*, 15, 3237-3251.
- Ratner B. 2009. "A Closer Look: The correlation coefficient: Its values range between +1/-1, or do they?" *Journal of Targeting, Measurement and Analysis for Marketing* 17, 139 – 142. doi: 10.1057/jt.2009.5; <https://link.springer.com/content/pdf/10.1057%2Fjt.2009.5.pdf>.

Supplemental Figures





Annex C: Resource Management Strategies Screening

As an initial step toward adapting to long term hydrologic shifts due to a changing climate, DWR is developing an Adaptation Plan (AP) as part of Phase III of its Climate Action Plan (CAP). Potential adaption strategies explored in the forthcoming AP are drawn from the 37 resource management strategies (RMS)⁷ detailed in the California Water Plan Update 2013 (California Department of Water Resources 2013). The Climate Change Program has used four factors to drill down to a subset of screened RMS strategies that could address vulnerabilities of DWR's activities to climate change.

Factors Used to Screen RMS

Applicability

RMSs are considered in the context of their relationship to vulnerabilities identified in DWR's Vulnerability Assessment (VA). If the proposed actions do not address a specific vulnerability to DWR's activities identified within the VA, then they would be screened out from further consideration in the AP.

Authority

For the RMS to be a viable option for the immediate future, DWR would need decision-making authority to affect its implementation. A distinction is made between direct actions DWR can take and indirect actions taken to influence others to act. Direct actions would include such things as improved Delta conveyance, where DWR would be the project lead in terms of planning and implementation. Indirect actions could include topics such as outreach, education, and guidance, but also programs in which DWR is administering a public investment (e.g. implementation grants) in local or regional projects. Both direct and indirect actions are considered potential strategies for adaptation, but the distinction between them may influence applicability or feasibility in subsequent analyses.

Technical Feasibility

Some actions may meet the first two factors but are considered unlikely to be implemented for other reasons. If an action is deemed technically infeasible given current resources and technologies, it would be screened out from further consideration.

Capacity

Some actions may meet all three other factors, yet DWR does not possess the capacity to implement the action. For example, DWR may lack the expertise, tools, technology, or stakeholder relationships that would ensure full implementation. Otherwise, an action may prove cost-prohibitive even though the technical capacity is met, thus eliminating it from further evaluation in the AP.

⁷ A full listing of California Water Plan resource management strategies is provided on DWR's website at <https://water.ca.gov/Programs/California-Water-Plan/Water-Resource-Management-Strategies>

Annex D: Adaptation Strategies – Seasonal Forecasting Skill

Plan of Study

As a possible adaptation strategy, improving seasonal forecast skill (or reducing the residual error in runoff forecasts) would provide operators with better information about how much additional runoff they could depend on for the rest of the water year. This information would allow operators to more optimally release water to meet downstream demands while always leaving sufficient water in the reservoir to meet end-of-year minimum storage targets.

The decision scaling platform can be used to test whether investments in improved seasonal forecasting results in improved system performance. CalLite 3.0 calls three table files that simulate the information provided to operators for the monthly forecasts of inflow to Folsom, Oroville, and Shasta reservoirs. These table files (“sacramento_runoff_forecast.table,” “american_runoff_forecast.table,” and “feather_runoff_forecast.table”) provide the amount of runoff that remains in the watershed and is expected to arrive at the reservoir during the rest of the water year. Table 14 below shows the forecasts that are made for each of the reservoirs and the non-exceedance probabilities for runoff that are given in each month of the year.

Table 15 Non-Exceedance Runoff Values Given in Runoff Forecast Tables

| | Folsom | Shasta | Oroville |
|------------------|------------|------------|------------|
| January | NA | NA | 99 percent |
| February | 99 percent | 99 percent | 99 percent |
| March | 90 percent | 90 percent | 90 percent |
| April | 75 percent | 75 percent | 75 percent |
| May | 50 percent | 50 percent | 50 percent |
| June | 50 percent | NA | NA |
| July | 50 percent | NA | NA |
| August | 50 percent | NA | NA |
| September | 50 percent | NA | NA |

In the pre-processing routine that is used to create the input files to CalLite 3.0, these three tables are synthetically generated by taking a perfect runoff forecast for the year and then adding an stochastic error factor to that forecast so that the distribution of error in the forecasts mimics the distribution of errors that has been observed in the historical forecasts published in DWR’s Bulletin 120. A random normal distribution number generator was used to generate a factor within the mean and standard deviation of the error distribution to apply to each perfect forecast in the simulations. A comprehensive study was conducted to develop the error values for these historical forecasts. All monthly runoff forecasts produced by DWR from 1996–2015 were compiled and compared to actual runoff values. Table 15 below provides the mean and standard deviation used in each forecast.

Table 16 Mean and Standard Deviation of Historical Runoff Forecasts

| | Folsom | | Shasta | | Oroville | |
|-----------------|--------|--------|--------|--------|----------|--------|
| | Mean | Std | Mean | Std | Mean | Std |
| January | NA | NA | NA | NA | 0.51 | 0.2674 |
| February | 0.64 | 0.1619 | 0.50 | 0.1746 | 0.58 | 0.1912 |
| March | 0.43 | 0.3159 | 0.28 | 0.2173 | 0.39 | 0.2804 |
| April | 0.165 | 0.2915 | 0.118 | 0.2080 | 0.147 | 0.2436 |
| May | 0.014 | 0.1929 | 0.02 | 0.1844 | 0.012 | 0.1611 |

To evaluate the efficacy of improving seasonal runoff forecasts, an analysis could be done to reduce the mean and standard deviation of the error distribution that has historically been observed so that the new error distribution would reflect the level of improvement that might be possible if more monitoring, research, and tools were devoted to improving the forecasts. California State Climatologist, Dr. Michael Anderson, suggests mean error could be reduced to 0.05 for the April forecasts and to 0.15–0.25 for months earlier in the year; likewise, standard deviation could potentially be reduced to 0.10–0.15. Such seasonal forecast skill improvements could be realized through hydrologic modeling that leverages high-resolution (50 meter) maps of snow water equivalent derived from modern observation techniques such as the NASA's Airborne Snow Observatory project (ASO)^{8,9}.

Note: When developing this analysis, special attention should be given to how CalLite 3.0 uses the forecast information. CalLite 3.0 has two different methods for generating water supply forecasts (Water Supply Index/Delivery Index [WSI/DI] and Forecast Allocation Model [FAM]), which may be affected by the runoff forecasts. All current and past CalLite 3.0 runs have used a WSI/DI approach.

⁸ Behrangi, A., Bormann, K. J., & Painter, T. H. (2018). Using the Airborne Snow Observatory to assess remotely sensed snowfall products in the California Sierra Nevada. *Water Resources Research*, 54.

⁹ NASA Airborne Snow Observatory Factsheet for the San Joaquin River Restoration Program. Available online at http://www.restoresjr.net/?wpfb_dl=2127

Annex E: Adaptation Strategies – Enhanced Precipitation

Plan of Study

Precipitation enhancement, or “cloud seeding,” is identified in the California Water Plan 2013 Update as a resource management strategy to help manage water shortages. Cloud seeding has been identified as a candidate for evaluation with the decision scaling platform due to its technical feasibility, DWR’s capacity and authority to implement the strategy, and its applicability to the vulnerabilities to climate change discussed in this report (see Annex C: Resource Management Strategy Screening).

Winter orographic cloud seeding (seeding of colder clouds formed by wind uplift over mountain ranges) has been practiced by many entities throughout California since the early 1950s. Weather modification projects currently operate in mostly southern Sierra watersheds (see Figure 43). Winter orographic cloud seeding projects disperse silver iodide or liquid propane into clouds to artificially initiate ice nucleation and freezing of supercooled liquid water (SLW), thereby augmenting precipitation falling as rain or snow.

Studies of cloud seeding projects in California have found statistically significant water-year total streamflow increases ranging from 2-24% in several major watersheds in the Sierra Nevada mountains (Silverman, 2010). DWR estimates that an additional 400,000 acre-feet could be realized from the expansion of cloud seeding projects in California, particularly in the Pit River-McCloud River Basin (California Department of Water Resources 2016).

The best estimates of expected increases in runoff from cloud seeding projects can be made through dynamical weather modeling, which provides information on the average temperature and frequency of occurrence of clouds and weather systems with SLW, a key driver of winter orographic cloud seeding effectiveness for a given area. As dynamical modeling would require extensive computing resources and data collection, the could seeding adaptation strategy would be evaluated based on more simplified estimates of expected streamflow increases derived from a literature review of studies conducted to date for watersheds in California and other western states.

Using the decision scaling platform, simulated monthly streamflows in expanded cloud seeding operation candidate watersheds would be augmented based on expected annual runoff increases and applied equally for all incremental climate perturbations. With the modified streamflows as input, the water system operations model, Callite 3.0, would simulate effects of these augmented flows on storage and other performance metrics. A method to adjust the amount of monthly flow augmentation according to the average temperature and rainfall of the simulated climate could be developed with further research to more accurately represent the effectiveness of cloud seeding operations in warmer and drier climates.

Figure 43 Weather Modification Projects in California during 2016



Annex F: Adaptation Strategies – Upper Watershed Management

Plan of Study

Land cover plays a key role in watershed management since it can absorb and navigate water in watersheds. Moreover, it affects the micro and macro climate in watersheds, which should be considered in management plans. To improve watershed management, it is necessary to assess the impacts of land cover change on the watershed. Thus, a hydrological model which can cope with land cover change assessment is proposed.

In its current configuration, the Sacramento Soil Moisture Accounting (SAC-SMA) is not capable of accounting for changes in land cover. SAC-SMA has no controls of water movement to satisfy evaporation. In this model, if the potential evaporation rate is not satisfied from the upper layer, it will withdraw water directly from the lower layer without considering the interaction between these two layers. Indeed, the model has a single evapotranspiration component and reduces the water content of each zone based on a residual of the potential evaporation from the upper to the lower zones. In dry basins, there is no water moving from the lower layer to the upper layer. Consequently, soil moisture in SAC-SMA's lower zone is underestimated. In addition, SAC-SMA does not consider the effects of vegetation, which absorbs water from the soil as a function of root depth, root distribution, and water demand. Under severely dry conditions, the upper and lower soil moisture can be further underestimated since vegetation resistance and transpiration withdrawals are not considered.

This proposal aims to build an evapotranspiration component into SAC-SMA that is explicitly connected to land cover, thus providing information which may help manage the Upper Feather River watershed. This plan of study would use the “Noah” parameterization of evapotranspiration (Koren et al. 2010), which computes overall evapotranspiration from the root zone and splits it into soil layer evapotranspiration based on layer saturation and root distribution. The parameterization combines the Penman potential evaporation approach and the canopy resistance-based model of Ek and Mahrt (1991). Additionally, the dynamic vegetation processes described in Terink et al. (2015) will be incorporated to consider canopy storage effects. See *Supplementary Material: Parameterization of Evaporation in the “Noah” Land Surface Scheme* at the end of this annex for a detailed presentation of the parameterization.

Conclusion

More consistent water subtraction for evapotranspiration from upper and lower layers could be achieved by implementing vegetation effects based on canopy resistance parameterization. A new evapotranspiration computation module could be coupled with the SAC-SMA rainfall-runoff model to increase the accuracy and help evaluate effects on streamflows from land cover change. Moreover, the performance of this advanced SAC-SMA could be evaluated by intercomparison with the Variable Infiltration Capacity (VIC)-model, which also integrates the effects of vegetation.

References

Koren V et al. 2010. “Modification of Sacramento Soil Moisture Accounting Heat Transfer Component (SAC-HT) for Enhanced Evapotranspiration.” NOAA Technical Report NWS 53

Terink W et al. 2015. “SPHY v2.0: Spatial Processes in Hydrology.” Geosci. Model Dev., 8, 2009-2034

Supplementary Material: Parameterization of Evaporation in the "Noah" Land Surface Scheme

Actual evaporation is estimated from the Penman equation adjusted by soil moisture and canopy resistance effects. It contains three components: direct evaporation from the top soil layer, evaporation of precipitation intercepted by the canopy, and transpiration via canopy and roots.

3.1. Noah Direct Evaporation From the Top Soil Layer

$$E_{dir} = (1 - \sigma) \times E_p \times \left(\frac{\theta_1 - \theta_{min}}{\theta_s - \theta_{min}} \right)^{fx}$$

σ : green vegetation fraction = Par(32)

E_p = pet: potential evaporation

θ_1 : soil moisture in the upper soil layer = Par(33)

θ_s : air dry (minimum) soil moisture = Par(34)

θ_{min} : saturation (porosity) soil moisture = Par(35)

fx : empirical coefficient; $fx = 2$ as recommended from Ek et al. (2003)

3.2. Wet Canopy Evaporation

$$E_c = \sigma \times E_p \times \left(\frac{W_c}{W_{max}} \right)$$

There are two ways to compute maximum allowed canopy interception (maximum canopy storage) and intercepted canopy water content (canopy storage).

Method 1: Noah model

W_{max} : maximum allowed canopy interception

W_c : intercepted canopy water content = Par(36)

Chen et al. (1996): $W_{max} = 0.5 \text{ mm}$; $n = 0.5$

$$\frac{\partial W_c}{\partial t} = \sigma \times P - P_d - E$$

$$\rightarrow W_c = (\sigma \times P - P_d - E)t \text{ with } W_c = 0 \text{ at } t = 0$$

If W_c exceeds W_{max} , the excess precipitation P_d reaches the ground. Therefore, actual surface precipitation $P_s = (1 - \sigma) \times P + P_d$ with P is measured precipitation.

Method 2: Terink et al. (2015)

Maximum canopy storage

$$scan_{max} = 0.935 + 0.498 \times LAI - 0.00575 \times LAI^2 = W_{max}$$

Canopy storage

$$scan_t = scan_{t-1} + P_t$$

scan: canopy story at (t-1) [mm]

P_t : measured precipitation [mm]

Precipitation throughfall/effective precipitation is the precipitation that cannot be stored in canopy storage. It occurs if water stored in the canopy is bigger than maximum canopy storage.

$$Pe_t = \max(0, scan_t - scan_{max,t})$$

Update canopy storage after computing effective precipitation

$$scan_t = scan_t - Pe_t$$

Intercepted water

$$Int_t = \min(1.5 \times ET_{r,t}, scan_t) [mm]$$

Update

$$scan_t = scan_t - Int$$

$$scan_t = W_c$$

3.3. Canopy Evapotranspiration

$$E_t = \sigma \times E_p \times B_c \left[1 - \left(\frac{W_c}{W_{max}} \right)^n \right]$$

$$B_c = \frac{1}{R_a + R_c} = \frac{C_h}{1 + C_h R_c}$$

R_a : atmosphere resistance = 230 Ω

R_c : total canopy resistance

$$R_c = \frac{R_{c,min}}{F_{sr} \times F_q \times F_T \times F_{sm} \times LAI}$$

$R_{c,min}$: minimal stomatal resistance [s/m]

Solar radiation effect

$$F_{sr} = \frac{\frac{R_{c,min}}{R_{c,max}} + f}{1 + f}$$

$R_{c,max}$: maximum stomatal resistance; $R_{c,max} = 5000s/m$

$$f = 0.55 \times \frac{R_g}{R_{gl}} \times \frac{2}{LAI}$$

LAI: leaf area index; set to the universal value of 5 or extracted from land cover data (source:
https://neo.sci.gsfc.nasa.gov/view.php?datasetId=MOD15A2_M_LAI)

R_{gt} : solar radiation limit value

R_g : solar radiation

$$K_t = \frac{R_g}{R_0} = A(1 - \exp(-B \times T_d^C))$$

A: maximum clear sky characteristics of the study area, vary with elevation and pollution; A = 0.7

B: how soon maximum K_t is achieved as T_d increases; winter: 0.01; summer: 0.004

C: how soon maximum K_t is achieved as T_d increases; 2.4

T_d : the difference between daily maximum and minimum temperature

R_0 : extraterrestrial insulation is estimated from astronomical relationships

$$R_0 = 2 \times S_0 \times E_0 [\cos(lat) \times \cos(\delta) \times \sin(0.5 \times rot \times t_{rs}) \times rot + \sin(lat) \times \sin(\delta) \times 0.5 \times t_{rs}]$$

S_0 : solar constant; $S_0 = 117.54 \text{ cal/cm}^2\text{hr}$

E_0 : eccentricity correction

$$E_0 = 1.00011 + 0.034221 \times \cos\Gamma + 0.001280 \times \sin\Gamma + 0.000719 \times \cos 2\Gamma + 0.000077 \sin 2\Gamma$$

Γ : day angle

$$\Gamma = \frac{2\pi(N_d - 1)}{365}$$

N_d = day number, January 1 = day 1

Duffie and Beckman (1991):

$$E_0 = 1 + 0.033 \times \cos\left(\frac{2\pi \times N_d}{365}\right)$$

lat: latitude

δ : sun declination

$$\delta = 23.45 * \sin [360 / 365 * (284 + N_d)]$$

N_d = day number, January 1 = day 1

rot: angular velocity of the earth's rotation; rot = 0.2618 rad/hr

t_{rs} : daylight time in hours

$$t_{rs} = \frac{\arccos[-\tan(\delta)\tan(lat)] - \arccos[-\tan(\delta)\tan(lat)]}{rot}$$

Vapor pressure effect

$$F_q = \frac{1}{1 + h_s[q_s(T_a) - q_a]}$$

h_s : empirical parameter

q_a : water vapor mixing ratio [kg/kg]

$$q_a = q(T_a) = \frac{0.622 \times e}{P_a - (1 - 0.622 \times e)}$$

$$e = 446.02 \times \exp(0.0579 \times t_a)$$

e: water vapor pressure [Pa]

t_a : air temperature [degrees Celsius]

q_s : saturation mixing ratio [kg/kg]

Tables of Saturation Mixing Ratios

| Table for Fahrenheit Temperature | |
|---|--|
| Temperature (°F) Or Dew Point Temperature (°F) | Saturation Mixing Ratio (g / kg) Or Mixing Ratio (g / kg) |
| -40 | 0.12 |
| -30 | 0.21 |
| -20 | 0.35 |
| -10 | 0.58 |
| 0 | 0.94 |
| 10 | 1.52 |
| 15 | 1.89 |
| 20 | 2.34 |
| 25 | 2.88 |
| 30 | 3.54 |
| 35 | 4.33 |
| 40 | 5.28 |
| 45 | 6.40 |
| 50 | 7.74 |
| 55 | 9.32 |
| 60 | 11.19 |
| 65 | 13.38 |
| 70 | 15.95 |
| 75 | 18.94 |
| 80 | 22.43 |
| 85 | 26.48 |
| 90 | 31.16 |
| 95 | 36.56 |
| 100 | 43.22 |

| Table for Celsius Temperature | |
|---|--|
| Temperature (°C) Or Dew Point Temperature (°C) | Saturation Mixing Ratio (g / kg) Or Mixing Ratio (g / kg) |
| -40 | 0.1 |
| -30 | 0.3 |
| -20 | 0.8 |
| -10 | 1.8 |
| 0 | 3.8 |
| 5 | 5.4 |
| 10 | 7.6 |
| 15 | 10.6 |
| 20 | 14.7 |
| 25 | 20.1 |
| 30 | 27.2 |
| 35 | 36.6 |
| 40 | 49.0 |

Air temperature effect

$$F_T = 1 - 0.0016 \times (T_{ref} - T_a)^2$$

T_{ref} : empirical parameter; $T_{ref} = 298 K$

Soil moisture effect

$$F_{sm} = \sum_{i=1}^{nr} \frac{(\theta_i - \theta_w) \times d_i}{(\theta_f - \theta_w) \times d_{nr}}$$

θ_i : soil moisture content of soil layer I; maximum number of layers = 4;

$$\theta_1 = Par(33); \theta_2 = Par(37); \theta_3 = Par(38); \theta_4 = Par(39)$$

θ_f : field capacity = Par(40)

θ_w : wilting point = Par(41)

d_i : layer thickness; maximum number of layers = 4;

$$d_1 = Par(42); d_2 = Par(43); d_3 = Par(44); d_4 = Par(45)$$

d_{nr} : total root zone thickness = Par(42)+ Par(43)+ Par(44)+ Par(45)+

nr: number of root zone layers

T_a : air temperature

Parameters dependent on the vegetation class index

- 1: Evergreen Needleleaf Forest
- 2: Evergreen Broadleaf Forest
- 3: Deciduous Needleleaf Forest
- 4: Deciduous Broadleaf Forest
- 5: Mixed Forest
- 6: Woodland
- 7: Wooded Grassland
- 8: Closed Shrubland
- 9: Open Shrubland
- 10: Grassland
- 11: Cropland
- 12: Bare Ground
- 13: Urban and Built-up
- 14: Water

| Vegetation class | Noah parameters | | | | | SAC-HTCR parameters (see Sections 3.5, & 4) | | |
|------------------|-----------------|----------|-------|-------|-------|---|-------|-------------|
| | $R_{c,min}$ | R_{gl} | h_s | Z_o | N_r | D_{sg} | r_n | $R_{c,max}$ |
| 1 | 2 | 3 | 4 | 5 | 6 | 7 | 8 | 9 |
| 1 | 150 | 30 | 41.69 | 2.653 | 4 | 12 | -1.88 | 70 |
| 2 | 100 | 30 | 54.53 | 0.826 | 4 | 21 | -1.84 | 50 |
| 3 | 125 | 30 | 51.93 | 0.563 | 4 | 12 | -1.88 | 60 |
| 4 | 150 | 30 | 47.35 | 1.098 | 4 | 23 | -1.76 | 70 |
| 5 | 100 | 30 | 47.35 | 0.854 | 4 | 23 | -1.76 | 50 |
| 6 | 70 | 65 | 54.53 | 0.856 | 4 | 23 | -1.76 | 40 |
| 7 | 40 | 100 | 36.35 | 0.035 | 3 | 28 | -1.91 | 40 |
| 8 | 300 | 100 | 42.00 | 0.238 | 3 | 28 | -1.91 | 90 |
| 9 | 400 | 100 | 42.00 | 0.065 | 3 | 27 | -2.05 | 250 |
| 10 | 150 | 100 | 42.00 | 0.076 | 2 | 7 | -1.18 | 150 |
| 11 | 400 | 100 | 42.00 | 0.011 | 3 | 16 | -1.45 | 200 |
| 12 | 40 | 100 | 36.35 | 0.035 | 3 | 16 | -1.45 | 40 |
| 13 | 150 | 100 | 42.00 | 0.011 | 2 | 5 | -1.45 | 100 |
| 14 | 100 | 30 | 51.75 | 0.001 | 0 | 0 | -1.00 | 100 |

3.4. Total evapotranspiration

$$E_{total} = E_{dir} + E_c + E_t$$

Annex G: Adaptive Water Year Typing

DWR's water-year type calculation methodology is described on the California Data Exchange Center (CDEC) California Cooperative Snow Surveys website (http://cdec.water.ca.gov/cgi-progs/iodir_ss/wsihist). The Sacramento and San Joaquin water-year type indices classify the water available from Sacramento and San Joaquin river watersheds into one of five discrete states relative to long-term average streamflow values for each watershed: one “wet” classification, two “normal” classifications (above and below normal), and two “dry” classifications (dry and critical).

Water-year type classification systems “simplify complex hydrology into a single, numerical metric that can be used in rule-based decision making” (Null & Viers 2013), and have been applied to development of drought indices throughout the United States (Heim 2002; Quiring 2009), and to other uses, such as hydropower reservoir management in Chile (Olivares et al. 2015). Explicit linking of water system operations to a water-year type provides the opportunity for water system operations to better synchronize with the needs of aquatic ecosystems which depend on patterns of hydrologic variability for the integrity of their lifecycles (Richter et al. 1997).

The Sacramento and San Joaquin water-year type indices and their additive combination known as the “Eight River Index” determine water-year type for the State Water Project (SWP) and the Central Valley Project (CVP). Allocations for out-of-stream users, environmental flows, and limits to exports south of the Bay Delta are tied to water-year types (SWRCB 2000). Water-year types are therefore an integral part of water policy in the state and exert a significant effect on federal, state, and local agencies through the regulatory restrictions designed around them. The frequency distribution of Sacramento and San Joaquin water-year types is projected to change significantly with changes in hydroclimatic conditions (Null & Viers 2013), which will have effects on the Central Valley water system performance beyond the long-term persistent hydrologic shifts themselves.

The decision scaling platform uses water year typing to develop inputs for CalLite 3.0 which simulates the current regulatory framework built around water year types. This makes the platform capable of exploring how modifying water-year type thresholds or water-year index formula might alter the performance of the system. Adapting water-year type formulations and index thresholds to be based on a non-stationary climate is a potential strategy to ensure negative impacts caused by water scarcity are shared among water users in the way regulatory restrictions were originally designed to achieve.

Annex H: Groundwater Storage and Recovery

One potential solution to California's future water supply problem is enhanced groundwater storage and recovery. This activity proposes an exploration of the relative net benefits of various configurations of groundwater storage and recovery in the Central Valley System (CVS) using the suite of models presented in Figure 2. Due to the ease of simulating surface water flow and irrigation, most detailed modeling is carried out for surface-water processes, while the groundwater component is left based on approximations and gross simplifications. Groundwater models are computationally expensive and require a detailed examination of subsurface geology and flow in two dimensions.

The California Department of Water Resources (DWR) has developed detailed models for surface water allocation (CalSim) and groundwater movement (C2VSim). Unfortunately, the finely detailed groundwater modeling code causes long CalSim runs and is not amenable to testing non-natural major adjustments to the aquifer. There is promise in using CalLite 3.0, an aggregated version of CalSim-II with runtimes of around 10 minutes, as an environment for exploring how to better make use of groundwater resources. However, CalLite 3.0 may not be suitable for the representation of groundwater interactions. A first step to evaluating opportunities for North-of-Delta groundwater storage and South-of-Delta groundwater storage using the model workflow developed as part of this study is to fully explore opportunities for modifications to groundwater interactions using CalLite 3.0.

The prospect of using the simpler code and quicker runtimes of CalLite 3.0 to explore groundwater-focused model runs has previously been considered by DWR. The use of CalSim-II to experiment with non-natural groundwater scenarios would likely require a great deal of processing to rewrite the intensive coding to allow for modification, and even if reformatted, this model has slow runtimes. CalSim-III has a new feature that links to the C2VSim model via a collection of functions called the Dynamic Link Library (DLL) and thus allow CalSim-III to remotely simulate groundwater processes. Ideally, one could use the same concept to link C2VSim and CalLite 3.0, but there are two fundamental problems: different divisions of the Central Valley and different representations of surface-aquifer interactions.

The Central Valley is divided differently between these two models. The groundwater model, C2VSim, uses a fine-resolution finite element grid, seen in Figure 44, based on hydrologic considerations. CalSim-III is broken up into basins called *depletion study areas*, and the discrepancy between the two is represented in the DLL via a link-node representation of the groundwater system which makes the two conceptualizations coincident. The issue is that the basin units for CalLite 3.0 are different from CalSim-III, for which the DLL was made. This would require a reconceptualization of spatial units in CalLite 3.0.

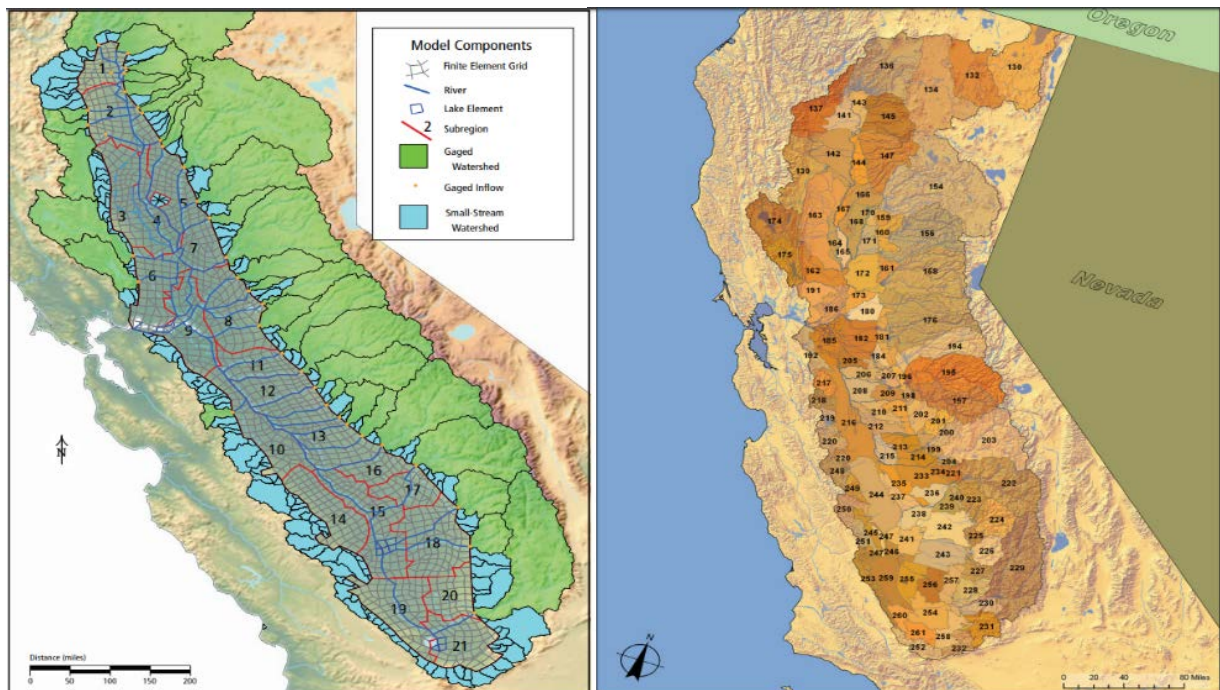
Discussions with DWR professionals have revealed that the bigger problems in their previous effort were inconsistencies in the way that C2VSim and CalLite 3.0 dictate stream networks interaction with the aquifer system. In both models, points of interaction occur at discrete points called stream-aquifer (SA) nodes. In C2VSim, these nodes are usually located at the origin, midpoint, junctures, and ends of streams. The CalLite 3.0 system does not consider this level of detail. In addition, the number of streams indexed into CalLite 3.0 is fewer than those in the C2VSim. This inconsistency is shown in Figure 45. It is for this reason that the original effort to introduce the C2VSim processes into CalLite 3.0 was originally dropped. The issue is that one would have to map and distribute the sparser nodes in CalLite 3.0 into the more detailed C2VSim layout.

While these issues seem difficult to rectify, the hope is that with creative processing in GIS, the issue of different basic spatial units and different SA node representation can be carried out without long periods of pre-processing and validating CalSim-II code. GIS could be used to help redefine the CalLite 3.0 land divisions based on the CalSim-III method. The larger challenge of the SA node issue would require GIS software to use its ability to delineate streamflow to trace the connections between node systems and break up the less-detailed node system in the CalLite 3.0 code.

Formatting CalSim-II code could take a prohibitory amount of time. If GIS can be used to resolve these differences, the coding and changes would take place within CalLite 3.0, which is a much simpler process. The result would be the ability to explore groundwater storage as an option with the same level of confidence in the results as surface water models.

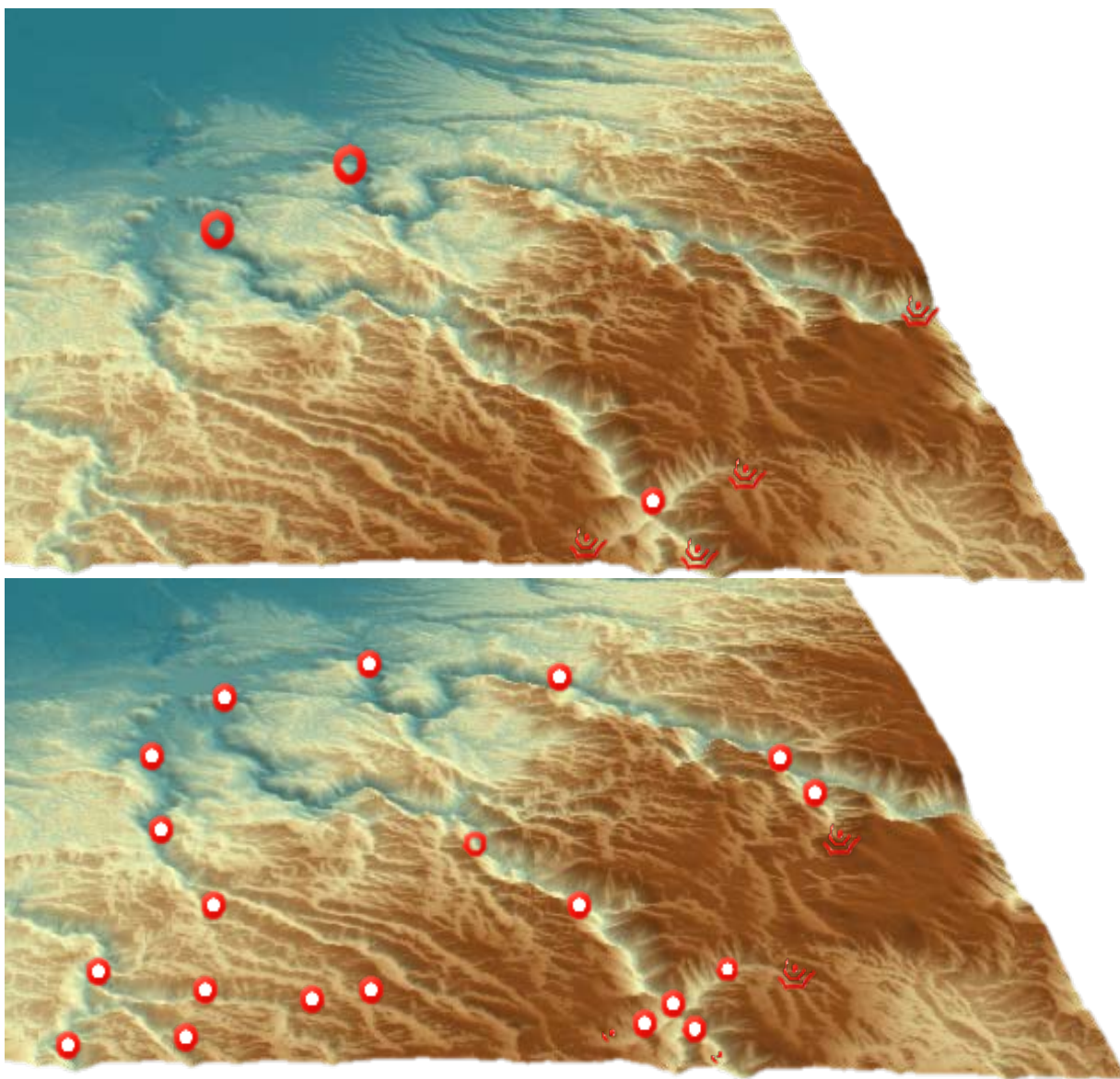
In the case that the simpler CalLite 3.0 approach described above proves infeasible, then the need to conduct experiments on augmented groundwater recharge would motivate a transition from CalLite 3.0 to CalSim-III in the fundamental model workflow developed for this study. In that case, groundwater augmentation analysis would feed into a substantially larger task involving embedding of CalSim-III into the model workflow in the place of CalLite 3.0.

Figure 44 Different Representations of the Central Valley



Note: The left-hand graphic shows the C2VSim representation and the right-hand graphic shows the CalSim/CalLite representation.

Figure 45 Representation of Stream-Aquifer Node Representation



Note: The top graphic shows the Callite representation and the bottom graphic shows the C2VSIM representation. Taken from a United States Geographic Survey (USGS) digital elevation model (DEM) of mid-San Joaquin Valley.

Annex I: Move From CalLite 3.0 to CalSim-III Operations Modeling

At the outset of DWR’s Vulnerability Assessment with decision scaling study, CalLite 3.0 was chosen as the operations model to use in the analysis. CalLite 3.0 provided several benefits over California Department of Water Resources’ (DWR’s) flagship operations model at the time, CalSim-II, and is free and publicly available. CalLite 3.0 has a run time of 7–12 minutes for an 86-year simulation and is documented to provide results that are within about 1 percent of CalSim-II results, the production of which requires a comparative run time of 12 hours. Moreover, CalLite 3.0 requires 796 inputs as compared with the CalSim-II requirement of over 2,000 inputs. Because the decision scaling framework requires many hundreds of operational runs and a climatologically consistent method of perturbing model inputs, CalLite 3.0 held a distinct advantage over CalSim-II and was chosen as the operational model to be used in this study and provide a proof of concept.

With the completion of DWR’s Vulnerability Assessment and progression to the evaluation of adaptation strategies, it is worth considering moving to DWR’s newest operations model, CalSim-III. CalSim-III was released to the public for review in December 2017. While not fully accepted by DWR as its operational model, the model is close to a finished product and only minor changes are expected to be incorporated after public review.

Moving to CalSim-III would require a substantial effort to evaluate all of the input data CalSim-III requires (over 3,000 inputs) and develop a method of synthetically generating and perturbing those data based on available climatologic and hydrologic data. This effort would closely follow the process undertaken with CalLite 3.0.

A decision scaling framework built on CalSim-III would provide several benefits. CalSim-III links to the C2VSim model via a collection of functions called the Dynamic Link Library (DLL) which allows remote simulation of integrated groundwater-surface water processes. CalSim-III has refined spatial-scale and representation of Central Valley water demand through its novel implementation of “demand units” that can be aggregated into “Water Budget Areas.” These two advancements, not available in CalLite 3.0, mean that CalSim-III simulations will more accurately account for climate change impacts on Central Valley groundwater and water demand and how those effects influence surface water conditions and deliveries. CalSim-III is fully supported and will continue to be improved and updated by DWR’s Bay Delta Office. Studies completed using CalSim-III would be more consistent with studies being done by DWR and would be considered as slightly more robust. Finally, CalLite’s simplifications add some level of error to results while CalSim-III’s more sophisticated hydrologic inputs and water demand calculations, including groundwater, would likely improve the accuracy of the results.

This page is intentionally left blank.